IntechOpen

Uranium

Safety, Resources, Separation and Thermodynamic Calculation

Edited by Nasser S. Awwad

URANIUM - SAFETY, RESOURCES, SEPARATION AND THERMODYNAMIC CALCULATION

Edited by **Nasser S. Awwad**

Uranium - Safety, Resources, Separation and Thermodynamic Calculation
http://dx.doi.org/10.5772/intechopen.69413
Edited by Nasser S. Awwad

Contributors

Yuji Fukaya, Katarzyna Kiegiel, Grazyna Zakrzewska-Koltuniewicz, Agnieszka Miskiewicz, Dorota Gajda, Sylwester Sommer, Stanislaw Wolkowicz, Miloš René, Gholamreza Shayeganrad, Valeri Smolenski, Alena Novoselova, Vladimir Volkovich, Yana Luk'yanova, Alexander Osipenko, Alexander Bychkov, Michael Aide

Notice

First published in London, United Kingdom, 2018 by IntechOpen
eBook (PDF) Published by IntechOpen, 2019
IntechOpen is the global imprint of INTECHOPEN LIMITED, registered in England and Wales, registration number: 11086078, The Shard, 25th floor, 32 London Bridge Street
London, SE19SG – United Kingdom
Printed in Croatia

British Library Cataloguing-in-Publication Data
A catalogue record for this book is available from the British Library

Additional hard and PDF copies can be obtained from orders@intechopen.com

Uranium - Safety, Resources, Separation and Thermodynamic Calculation
Edited by Nasser S. Awwad

p. cm.

Print ISBN 978-1-78923-118-2

Online ISBN 978-1-78923-119-9

eBook (PDF) ISBN 978-1-83881-387-1

Meet the editor

Dr. Nasser S. Awwad obtained his MSc degree in Inorganic and Radiochemistry in 1997 from Benha University, PhD degree in Inorganic and Radiochemistry in 2000 from Ain Shams University, and postdoctoral degree in 2004 at Sandia National Laboratories, New Mexico, USA. He was an associate professor of Radiochemistry in 2006 and a professor of Inorganic and Radiochemistry in 2011 at the Egyptian Atomic Energy Authority. He is a professor at King Khalid University, Abha, KSA, from 2011. Dr. Nasser S. Awwad has published two chapters in the following books: *Natural Gas - Extraction to End Use* and *Advances in Petrochemicals*. He edited three books about uranium, new trends in nuclear sciences, and lanthanides. In addition, he published 54 papers in ISI journals. He also supervised 4 PhD degree and 16 MSc degree students in the field of radioactive and wastewater treatment. He participated in 25 international conferences in South Korea, the USA, Lebanon, the KSA, and Egypt. He reviewed 2 PhD degree and 13 MSc degree research studies. He participated in six big projects with KACST in the KSA and Sandia National Laboratories in the USA about the conditioning of radioactive sources (wastewater treatment). He is a member of the Arab Society of Forensic Sciences and Forensic Medicine, a member of the Egyptian Society of Nuclear Sciences and Applications, an associate editorial board member of the *Arab Journal of Nuclear Sciences and Applications*, and a rapporteur of the Permanent Committee for Nuclear and Radiological Protection at King Khalid University. He is interested in utilizing the different techniques related to the treatment of radioactive nuclides using nanomaterials.

Contents

Preface

This book deals with the topics related to uranium through seven chapters, with the first five chapters covering the entirety and the formation of uranium and its composition in the raw materials and methods of mining and extraction and separation by different techniques such as solvent extraction, ion exchanges, precipitation, or membrane contactor. It also deals with the safety of nuclear reactors and fuel, as well as the uses of plutonium and uranium enrichment units and its physical and chemical properties. Chapters 6 and 7 deal with the calculations of electrochemical and thermodynamic properties of La, Nd, and U and the factors of separation of uranium from the fission products as well as calculations of the thermodynamics of uranium in the soil environment. This book contains must-read materials for students, engineers, chemists, physicists, and researchers working in the area of safety, monitoring, resources, mining, and recovery of uranium, in addition to thermodynamic calculation. This book provides valuable insights into the related safety of nuclear reactor and breeding, utilization of plutonium, uranium-enriched plants, energy security of uranium resources, geochemistry of uranium rocks, physical and chemical properties of UF_6, recovery of uranium by different techniques, thermodynamics and separation factor of uranium from fission products, uranium hydrolyses, uranium adsorption, complexation of uranium, and chemical thermodynamics of uranium in the soil environment.

Nasser S. Awwad, PhD
Professor of Inorganic and Radiochemistry
King Khalid University
Faculty of Science
Chemistry Department
Saudi Arabia

Chapter 1

History of Uranium Mining in Central Europe

Miloš René

Additional information is available at the end of the chapter

http://dx.doi.org/10.5772/intechopen.71962

Abstract

The Central European deposits were the first industrially mined uranium deposits in the world. Uranium minerals were noticed by miners in the Ore Mts. area (Saxony, Bohemia) for a long time prior the uranium discovery. The uranium mineral pitchblende was reported from this ore district as early as 1565. Pitchblende was firstly extracted for production of colouring agents used in the glassmaking industry. The German chemist Klaproth in 1789 detected uranium by analysing pitchblende. In 1896, A.H. Becquerel discovered the phenomenon of radioactivity. His student Marie Sklodowska-Curie recognized that pitchblende has higher radioactivity as pure uranium salts. Later, together with her husband P. Curie, they discovered two new elements: radium and polonium. Research by O. Hahn and its colleges led later to using of uranium as first nuclear weapons. The significant amount of uranium ores for producing of the Russian nuclear weapons and nuclear power plants in the former Eastern Bloc was mined in the East Germany (GDR) and Czechoslovakia. The total production of uranium ores in GDR from 1946 to 2012 was 219,626 t U. In Czechoslovakia, the total uranium production from 1945 to 2017 was 112,250 t U.

Keywords: pitchblende, uranium glass, radioactivity, radium, polonium, nuclear energy

1. Introduction

The Central European uranium deposits were the first industrially mined deposits in the world. Uranium minerals were noticed by miners in the Ore Mts. area (Saxony, Bohemia) for a long time prior the discovery of uranium by Klaproth in 1789. The uranium mineral pitchblende was reported from this ore district as early as 1565. Pitchblende was firstly extracted for production of colouring agents used in the glassmaking industry. Uranium glass became very popular in the mid-nineteenth century. The important glassworks on this time exist in North and South Bohemia (Jizera Mts., Krkonoše, and Bohemian Forest).

The German chemist Klaproth in 1789 detected a new element, uranium, by analysing pitchblende from the Johanngeorgenstadt silver deposit. Its name (uranit, later uranium) was derived from the planet Uranus, discovered in 1781 by F.W. Herschel. Later, A.H. Becquerel discovered the phenomenon of radioactivity. His student Marie Sklodowska-Curie by study of some pitchblende samples, including samples from the Jáchymov uranium deposit, recognised that pitchblende has higher radioactivity as pure uranium salts. Later, together with her husband P. Curie, in 1898, they discovered two new elements: radium and polonium. Radium was used in self-luminous paints and in medicine to produce radon gas. Research by O. Hahn, L. Meitner and F. Strassmann in 1934 led to using of uranium as a fuel in the nuclear power industry and first nuclear weapons.

2. Discovery of pitchblende and uranium

Uranium minerals were noticed by miners in some silver ore deposits from the Ore Mts. area (Krušné Hory/Erzgebirge) for a long time prior the uranium discovery. The uranium mineral pitchblende was reported from this ore district as early as 1565. However, the miners have found that in places with higher occurrence of uraninite silver and its minerals disappear. The first occurrence of pitchblende entails trouble (pitch). Along with silver ores, some cobalt-bearing minerals later were also mined, which were used for production of some enamels for glass and ceramic industry. In Jáchymov, main silver deposit on the Czech (Bohemian) side of the Ore Mts. area, the first enamel factory originated in 1780. After the discovery of organic ultramarine colours in 1828, the market for the more expensive cobalt colours was closed.

The German dispensing chemist Klaproth (1743–1817) had in his experimental laboratory in Berlin performed some experiments with pitchblende from the Johanngeorgenstadt uranium deposits in the Saxony. During these experiments in Berlin in 1789, Klaproth was able to precipitate a yellow compound (likely sodium diuranate) by dissolving pitchblende in nitric acid and neutralising the solution with sodium hydroxide. Klaproth assumed this yellow compound was the oxide of a yet-undiscovered element. By heating this substance with charcoal, he obtained a black powder, which he thought was the newly discovered element itself [1]. However, that powder was an oxide of uranium. Klaproth named the newly discovered element after the planet Uranus, which had been discovered eight years earlier by William Herschel. First sample of uranium metal was prepared in 1841 by Eugéne-Melchior Péligot, professor of analytical chemistry on the Central School of Arts and Manufactures in Paris, by heating uranium tetrachloride with potassium [2].

3. Use of pitchblende in glass and porcelain industries

Klaproth had later experimented with using some yellow uranium compounds as glass colours. Some other chemists from silver metallurgical work in the Jáchymov started also with experiments using these yellow components in glassmaking industry. The Ministry for

tillage of the Austrian-Hungary monarchy in Vienna recognised high interest for this new business and delegated the young chemist Adolf Patera (1819–1894) to discover a cheap technology for the production of yellow uranium colour. In the years 1851–1855, silver metallurgical work was reconstructed to factory for production of uranium yellow colours (k.k. Urangelbfabrik). Later, a new young chemist Arnošt Vysoký (1823–1872), who was named in 1866 as the director of this metallurgical and chemical works, developed some new uranium colours for the glassmaking industry (uranium orange yellow colour, uranium ammonium yellow, and high orange uranium colour) and the "black uranium colour" for the porcelain industry [3]. All these uranium colours from the Jáchymov factory were highly valued in the European market, especially in the Great Britain and France. According to high international interests for uranium colours from the Jáchymov, the original silver metallurgical work and factory for production of uranium colours in 1871 was quite reconstructed, and in 1879, this work was named as the biggest world factory for production of uranium colours. Original production of uranium colours in 1853 (84.6 kg) rose in 1886 to 12,776 kg of uranium colours. However, 10 years later, interest for uranium colours distinctly declined. After year 1896, the production of uranium colours in the Jáchymov highly declined and mining of uranium ore was almost stopped. After World War I, new competitive uranium colour factories originated in Belgium, Great Britain and Canada. The uranium colour factory in Jáchymov and factory in the Oolen, Belgium, closed in 1926 with a cartel agreement for the European market with 40% quotient for the Jáchymov factory. However, majority of glass and porcelain factories in the Czechoslovakia bayed the cheaper uranium colours from the British firms. After occupations of Jáchymov by Nazis (1938),the new Germany company (St. Joachimsthaler Bergbaugesellschaft) was established in 1939 (St. Joachimsthaler Bergbaugesellschaft), which have mined uranium ore for the German nuclear experiments. The chemical factory for producing of uranium colours and radium was closed and settled. Distinctly lower quantity of uranium colours was produced in some small factories in the German part of the Ore Mts. area (Krušné Hory/Erzgebirge), which used pitchblende mined in the Marienberg, Annaberg and Johanngeorgenstadt silver-cobalt-nickel-uranium deposits [2].

4. Uranium glass

Uranium glass became popular in the mid-nineteenth century, with its period of greatest popularity being from 1880s to the 1920s [2, 4]. The most typical colour of uranium glass is pale yellowish-green, which in the 1920s led to the nickname Vaseline glass based on a perceived resemblance to the appearance of petroleum jelly as formulated and commercially sold at that time. Vaseline glass is usually used for any uranium glass especially in the United States. The first major producer of uranium glass is commonly recognised as Franz Xaver Anton Riedel (1782–1844) from the Dolní Polubný (Unter-Polaun) in the Jizera Mountains, North Bohemia. This glassmaker had started with the production of uranium glass in 1841 and had developed yellow and green uranium glass named after his daughter Anna yellow (Anna gelb) and Anna green (Anna grünn). Some other uranium glassworks existed in this time in the Krkonoše Mts. (Riesengebirge), on the boundary between Bohemia and Poland

(Harrachov in the Czech Republic and Szklary in Poland) and in the South Bohemia (Lenora, Josefsthal near Zvonková). A glassmaker from the Nový Svět near Harrachov developed and on the fair in Prague (1831) presented new, partly opaque uranium "Chrysoprasglass" [5].

Production of uranium glass was popular also in the other European countries, especially in Great Britain, France and Germany. In the Great Britain, it was glassworks in London (White friars) and Sturbridge area (Thomas Webb glasswork). In France, the first uranium glass was produced in glasswork Choisy-le Roi in Paris in 1838. The uranium glass in France was later named as "Cristal Dichroide".

The highly different uranium glass products produced by glassworks in the North and South Bohemia mainly pressed glass cups and polished vases and were very popular souvenirs sold predominantly in the West Bohemian health resorts (Karlovy Vary, Mariánské Lázně, Františkovy Lázně) [2]. These glass products from the uranium glass were very important utility products of the Biedermeier and Art Nouveau periods.

5. Discovery of radioactivity, radium and polonium

In 1895, W.C. Röentgen discovered new rays, later named as the "Röentgen rays". One year later, in 1896, A.H. Becquerel (1852–1908) discovered the phenomenon of radioactivity by exposing a photographic plate to potassium uranyl sulphate. He determined that a form of invisible rays emitted by uranium salts had exposed the plate. His student, Maria Sklodowska-Curie (1867–1934), recognised that some samples of pitchblende, including pitchblende from the Jáchymov uranium deposit, have a higher radioactivity as pure uranium salts. Marie and Pierre Curie (1859–1906) discovered the new element radium, in the form of radium chloride, in 1898. They extracted the radium compound from residues originated by production of uranium colours in the Jáchymov factory. For first experiments of both researches in 1898, they obtained from the Jáchymov uranium colour factory 5 kg of these residues, later 100 kg of these residues. In these residues, Marie and Pierre Curie discovered along with radium a second new element, polonium [6, 7]. For isolation of both new elements, both researchers in 1899 obtained from the Jáchymov factory 1000 kg of residues. These residues were collaborated in bigger laboratories of the Société Centrale de Produits Chimiques in Paris [8]. In 1910, radium was isolated as a pure metal by M. Curie and A. L. Debirne thought a radium chloride electrolysis. Radium metal was first commercially produced in the beginning of the twentieth century by Biraco, a subsidiary company of Union Miniere du Haut Katanga in its Oolen plant in Belgium. In the Jáchymov uranium colour factory, radium chloride was produced from 1908. In the years 1909–1937, the Jáchymov factory produced 64.3 g of Ra. In years 1908–1933, radium chloride was produced for its use in medicine to produce radon gas, which in turn was used in cancer treatment. In 1934, the Jáchymov uranium factory started producing self-luminous paints for watches, aircraft switches, clocks and instrument dials. The total production of uranium ores from the Jáchymov ore deposit in years 1853–1945 was 469.5 t of U [9].

After the isolation of radium by Marie and Pierre Curie from pitchblende from Jáchymov, several other scientists started to isolate radium in small quantities. Later, some small companies

purchased mine tailings from the Jáchymov uranium deposit and started isolating radium. In 1904, the Austrian government nationalised all mines in the Jáchymov and stopped exporting raw uranium ore. The formation of an Austrian monopoly and the strong urge of other countries to have access to radium led to a worldwide search for uranium ores. New uranium ore deposits were found in United States, Belgian Congo and Canada.

6. Discovery of radon and origin of radon spas

Ernest Rutherford and Robert B. Owens discovered radon in 1899. In 1900, Friedrich Ernst Dorn in some experiments found that radium emanates a radioactive gas, which was named radium emanation. Later, similar emanations for thorium and actinium were found, which were named as radon, thoron and actinon [10, 11].

The danger of high exposure to radon in silver-uranium mines has long been known. Georg Agricola, physician in Jáchymov, recommended ventilation in mines to avoid this mountain sickness (Bergsucht). In 1879, this condition was identified as lung cancer by investigation of miners from the Schneeberg silver-uranium deposit in the Saxony [12]. The first major studies with radon and health were performed in the context of uranium mining in the Jáchymov ore deposit [13, 14]. Recently, a detailed study of the influence of radon on miners' health in the Czech uranium mines was published by Řeřicha et al. [15].

Exposure to radon, a process known as radiation hormesis, has been suggested to mitigate diseases of movement system such as rheumatoid arthritis, spondylitis, ankylosing spondylitis, condition after orthopaedic surgeries, diseases of peripheral nervous system and metabolic diseases. Radioactive water baths have been applied since 1906 in Jáchymov, since 1912 in Bad Brambach and since 1918 in Oberschlema, Saxony [16–18].

Radioactivity of the first radioactive water springs in the Jáchymov mine Werner was measured by Austrian physicists Heinrich Mache and Stefan Meyer in 1905. They found higher radioactivity (2.5 kBq/l) [19]. These results started Jáchymov spa history. The first spa house was opened in 1911 (recently spa centre Agricola). In year 1912, a luxury spa house Radium Palace was opened. During years 1908–1924, the Štěp springs from the Werner mine was used for radon bath therapy. In 1924, spring Curie at the 12th level of the Svornost mine (30 l/min, 29°C, 5 kBq/l) was found. After closing uranium mining in the Jáchymov area, in 1960–1962, new hydrogeological exploration of radioactive springs at the 12th level of the Svornost mine was performed. Two new radioactive water springs were found (H-1 and HG-1 – Běhounek, 300 l/min, up to 36°C, 10 kBq/l). More recently performed hydrogeological exploration was found in 2000 spring Agricola (10 l/min, 29°C, 20 kBq/l) [20–24].

In Bad Brambach, a new spring of radon water was found by Max Weiding in 1911. The high radioactive water spring was later named Wettinquele and was used for radiotherapy from 1915 and represented a mineral water spring with the highest radioactivity in the world (26 kBq/l). The radon spa in Bad Brambach from 1945 to 1948 was used as nursing home for the Soviet arms and since 1949 is used as a spa for all patients with diseases of movement system [16].

Today, the community of Bad Schlema is an amalgamation of the formerly separate communities of Niederschlema and Oberschlema. After rich radon springs were opened in the Marx-Semler gallery in Oberschlema between 1908 and 1912, the world's richest radium spa developed after 1918. Ten years later, it was counted among Germany's most important spas. Once the uranium mining was taken over by the Soviet occupation forces, the spa and the downtown of Oberschlema were utterly obliterated. After uranium mining came to an end in 1990, the mayor, Konrad Barth, organised Schema's revival as a spa town, which was realised in 1998 when the new "Spa house" (Kurhaus) was opened. The newly opened radon springs afforded ample bathing. In 2005, Saxony's state government bestowed upon the community official designation "Bad", after it had already been recognised as a radon spa since 2004 [18, 25].

7. Uranium as fuel in the nuclear weapons and in the nuclear power industry

Otto Hahn and Fritz Strassmann conducted the experiments leading to the discovery of uranium's ability to fission and release binding energy in 1934. Lise Meitner and Otto Robert Frisch published the physical explanation in February 1939 and named the process "nuclear fission". Further work found that U^{238} isotope could be transmuted into plutonium, which like U^{235} isotope is also fissile by thermal neutrons. These discoveries led to the United States, Great Britain and Soviet Union to begin work on the development of nuclear weapons and nuclear power. After World War II, following the Cold War between the Soviet Union and the United States, huge stockpiles of uranium were amassed and tens of thousands of nuclear weapons were created using enriched uranium and plutonium made from uranium ores. Uranium ore was, after 1949, a highly strategic mineral material. In Central Europe, the principal uranium ore deposits were discovered in the Czechoslovakia and the East Germany (GDR). Some small uranium ore deposits were also found in Poland. The uranium ore from these deposits was in the first place used for the Soviets' nuclear weapons, later also for nuclear power industry [9, 26–29].

8. Czechoslovak uranium mining after World War II

In 1945, the Soviet Union controlled all uranium resources in the Czechoslovakia and in the Soviet occupation zone in the Germany and later also in Poland. In East Germany and in Poland, the so-called stock companies for exploration and exploitation of uranium ore deposits were established in which the Soviet share represented fifty percent. In East Germany, the income from the uranium exploitation came on the account of war reparation up to 1953. In Czechoslovakia, talks between Czechoslovak Prime Minister Zdeněk Fierlinger and the Soviet diplomatic agent Ivan Bakulin about the uranium ore mining and exclusive export to Soviet Union from August 1945 were finished on 23 November 1945 when the "Memorandum of understanding between the governments of Soviet Union and Czechoslovakia about the

extension of exploitation of radium-bearing uranium and concentrates in Czechoslovakia and their delivery to the Soviet Union" was signed. The Memorandum contained also an attachment, which proclaimed this document to be highly confidential. According to the Memorandum, the Joachim Mines State Enterprise was founded. Leading posts in this enterprise were taken over by the Soviet experts. The Memorandum, however, did not specify the costs of exported uranium ores. This problem was progressively discussed between 1949 and 1952 [28]. In 1945, the Jáchymov ore deposit represented the only available uranium source on the territory of the Soviet block where uranium ores could be exploited immediately. In East Germany, the first exploitation of uranium ores started in 1947 and 1948.

From 1945 to 1949, in the Jáchymov uranium mines, the German war prisoners started to work, who were later replaced mainly by political and other Czechoslovak prisoners. The Jáchymov together with Horní Slavkov and Příbram became known as parts of the "Czech Gulag". In Jáchymov, 65,000 prisoners worked in concentration camps until 1961 [9]. For following exploration of uranium deposits on the Czechoslovak territory, in 1946, "Prospective geology group", which later evolved into the independent organisation, was established. Thirty Soviet geologists formed the nucleus of this group, and according to territorial responsibilities, the group was subdivided into seven subgroups. During 1948 and 1962, the Horní Slavkov uranium deposit was opened and exploited. In the Czech part of the Ore Mts. (Krušné Hory/Erzgebirge), some smaller ore occurrences and deposits (e.g., Potůčky, Abertamy) were exploited.

In the first stage of uranium exploration, the selected territories according to older geological studies and geological mapping were covered in 1958–1964 by emanometry, sampling from a depth of 1 m. Productivity of three-personnel groups was about 300–500 holes per day. Productivity of later used technique with 3 m holes was much lower, and with this technique, only limited areas were covered. Some other geophysical methods that were used for exploration of uranium deposits were ground and car-borne gamma-ray survey [30]. From 1946 to 1955, exploration for uranium ores was concentrated on the known vein deposits in the Ore Mts. area (Jáchymov and Horní Slavkov) and area of the known base-metal vein deposit Příbram. During systematic emanometry and gamma-ray surveys, a new type of hydrothermal uranium deposits evolved in mineralised shear zones (Rožná, Olší, Okrouhlá Radouň, Zadní Chodov and Vítkov II). The sandstone-hosted deposits in northern Bohemia (Hamr, Stráž, Břevniště, Osečná-Kotel and Hvězdov uranium deposits) were found after gamma logging of hydrogeological borehole [30]. In 1989, the decision was made to reduce all uranium-related activities. Following this decision, in 1990, expenditures decreased to about 7 million USD and have declined ever since. No field exploration has been carried out since the beginning of 1994 [31].

Most of the known uranium resources in the Czech part of the Bohemian Massif occurred in 32 ore deposits, of which 30 have been mined out or closed up to year 1993. Of two remaining deposits, the Rožná and Stráž were mined also from 1993 up to 1996 (Stráž) or up to 2017 (Rožná). The mining of the last Central European uranium deposit (Rožná) was stopped in April 2017. The very small recent production of uranium in the Stráž uranium deposit is part of remediation of the after-effects of the in-situ leaching that impacted a total 266 million m^3

groundwater and an enclosure of 650 ha surface area. In former Czechoslovakia, a total uranium production from 1945 to 2017 was 112,250 t U. However, majority of uranium ore was mined in the Czech Republic. In Slovakia, in this time, only 211.4 t U was mined. In the Czech Republic from 2004, no prospection activities on uranium ore deposits exist. Recently, only different environmental remediation projects exist. The biggest project in area of the Stráž uranium deposit is expected to continue until approximately 2040 [31].

The mined uranium deposits in the Czech Republic could be divided into the three main genetic types: vein deposits, shear-zone deposits and sedimentary deposits (**Table 1**). The production of the 12 main uranium deposits is listed in **Table 2**. The Příbram, Jáchymov and Horní Slavkov uranium deposits represent the vein deposits. The Rožná, Zadní Chodov, Vítkov II, Olší, Okrouhlá Radouň and Dyleň deposits represent the shear-zone uranium deposits. The sedimentary deposits are evolved mainly in the Upper Cretaceous Uranium Ore District (Stráž, Hamr and Břevniště) (**Figure 1**). Only some small uranium deposits and occurrences were evolved also in the Carboniferous-Permian and Tertiary continental coal-bearing sediments.

The Příbram uranium ore district extends along the northwestern contact of the Central Bohemian Plutonic complex (CBPC) with Neoproterozoic and Cambrian rocks of the Teplá-Barrandian Zone. The 3200 km^2 complex crops out between two contrasting crustal units, in the Teplá-Barrandian Zone to the NW and Moldanubian Zone to the SE, in the central part of the Bohemian Massif. The plutonic complex is made up of multiple individual plutons and smaller magmatic bodies that vary in age, petrographic and geochemical characteristics, shape, size, internal fabrics and relationships to the host rock structures, from older calc-alkaline to potassium-rich calc-alkaline and ultrapotassic magmas. In the NW margin of the CBPC, in area of the Příbram ore district crop out biotite and biotite-amphibole granodiorites of the Blatná suite, together with the Marginal, high-K calc-alkaline biotite granites. The Neoproterozoic, a slightly metamorphosed flysch sequence, up to 2000 m thick, is overlain by a Lower Cambrian sediments, containing thin layers of quartz-pebble conglomerate at its base and slates at a higher stratigraphic position. A volcano-sedimentary complex underlies the Neoproterozoic flysch sequence, comprising intercalated claystones, sillstones and conglomerates. Both the Lower Cambrian and Neoproterozoic rocks are contact metamorphosed by the CBPC within an aureole that extends 1000 to 1200 m from the intrusive contact. This

Genetic type of deposit	Production, t U
Vein and shear-zone deposits	82,128
Cretaceous sandstones	29,014
Carboniferous-Permian sediments	608
Tertiary sediments	289
Total	**112,039**

Table 1. Genetic types of uranium deposits in the Bohemian Massif [32].

Uranium deposit	Mining	Production, t U
Příbram	1950–1991	50200.8
Rožná	1657–2017	22220.0
Stráž	1967–1996	14674.1
Hamr	1972–1993	13263.8
Jáchymov	1946–1964	7950.0
Zadní Chodov	1952–1992	4150.7
Vítkov II	1961–1990	3972.6
Olší	1959–1989	2922.2
Horní Slavkov	1948–1962	2668.3
Okrouhlá Radouň	1972–1990	1339.5
Břevniště	1982–1990	1107.8
Dyleň	1965–1991	1100.5

Table 2. Production of uranium in the main uranium deposits of the Bohemian Massif [32].

aureole is also cut by aplite and lamprophyre dykes. The Neoproterozoic host rocks form a simple fold, the Příbram anticline, with NE-trending axis, roughly parallel to the CBPC contact. Brittle structures in the Příbram ore district may be classified relative to the axial plane of the Příbram anticline as: (i) the most prominent, longitudinal NE-striking faults, i.e. subparallel to boundary of Neoproterozoic metasediments with the CBPC, (ii) transverse NW-striking faults, and (iii) oblique, E- or N-striking faults. Ore veins in the ore district strike NW (44% of veins), N (43% veins), and NE (13% veins). The ore veins are from a few metres to several kilometres long, from a few centimetres to more than 10 metres wide and comprise three mineral assemblages (from older to younger): (1) sulphidic with Pb, Zn and Cu-Fe sulphides, (2) uraninite bearing and (3) sulphide-selenide-carbonate. The main U-bearing minerals are uraninite and U-anthraxolite, coffinite being far less abundant. Uranium minerals occurred as veinlets, coatings and pods in calcite gangues. The deposit has been mined to a depth exceeding 1500 m and total mined amount of U was 50200.8 t [32].

The Rožná and Olší uranium deposits occur in the uppermost Gföhl unit of the high-grade metasediment series of the Moldanubian Zone. The host rocks of the Rožná U deposit consist predominantly of biotite paragneisses with intercalations of amphibole-biotite gneisses, amphibolites and small bodies of calc-silicate rock, marble, serpentinite and pyroxenite. The disseminated uranium mineralisation is coupled in the longitudinal N-S to NNW-SSE ductile shear zones, dipping WSW at an angle of 70–90°. The main mineralised shear zones of the Rožná uranium deposit are designated as the Rožná 1 (R1) and Rožná 4 (R4). In the less strongly mineralised Rožná 2 (R2) and Rožná 3 (R3) shear zones, numerous carbonate veins occur. Mineralised shear zones are segmented by steep, ductile to brittle NW-SE and SW-NE striking faults with younger carbonate-quartz-sulphide mineralisation.

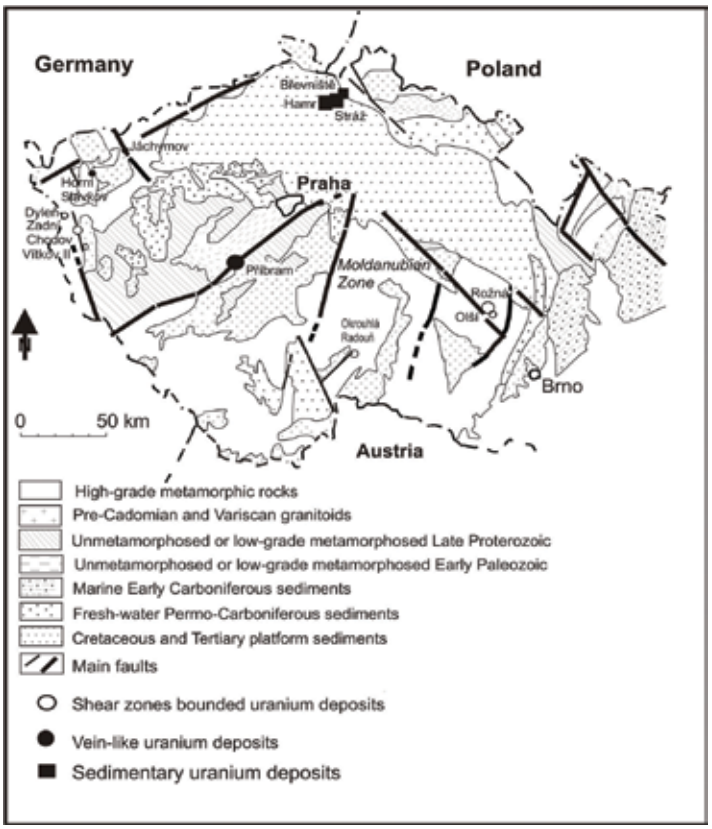

Figure 1. Main uranium deposits in the Czech part of the Bohemian Massif.

Ore mineralisation in the Rožná and Olší uranium deposits is formed by (i) disseminated coffinite > uraninite > U-Zr-silicate mineralisation evolved in chloritised, pyritised, carbonatised, and graphitised organic matter-enriched cataclastites of ductile shear zones, (ii) uraninite > coffinite mineralisation in carbonate veins, (iii) disseminated coffinite > uraninite in albitised and hematitised rock series (aceites) along ductile shear zones and (iv) mostly coffinite ore bound on the intersections of the ductile shear zones with younger NW-SE and SW-NE faults. Ore lenses of disseminated ore in fault zones R1 and R4 are 3.5 m thick on average, ore grade is around 0.5% U, up to 10% U locally. Ore bodies in ore zones R2 and R3 host a large number of carbonate veins up to 2 m thick with U-mineralisation of the average grade 0.6% U. Ore bodies in aceites with predominance of coffinite on uraninite and U-Zr silicate have U-mineralisation of a grade 0.1–0.15% U, exceptionally 0.3% U. Disseminated U-mineralisation bound to oblique fault zones is usually hosted by quartz-carbonate-sulphide breccias at intersections with diagonal and longitudinal structures. Compared to other types of mineralisation, the ore bodies are small but contain relatively high-grade ore of average grade 0.8% U and up to 20% U in some ore shoots. Total mine production of the Rožná-Olší ore district was 25,142 t U with an average grade of 0.24% U [32].

The North Bohemian Cretaceous uranium ore district (Stráž, Hamr, Břevniště ore deposits) is developed in the two Cenomanian formations, lower freshwater continental and upper marine sediments. The basement of the Upper Cretaceous sediments is formed in this area by low-grade metamorphic rock series (phyllites and quartzites) and small bodies of the Upper Proterozoic and Upper Devonian granitoids. The lower continental sediments are developed in the paleo relief depressions and are formed by conglomerates and pebbly to silty sandstones. All these sediments are usually enriched in organic matter. The sandstones of marine Cenomanian cover the whole area of uranium ore district. Its basal parts are formed by wash-out sediments, which are represented by silty sandstones. They are overlain by the sequence of Upper Cenomanian weakly cemented sandstones. Uranium mineralisation is developed in the basal part of the Cenomanian formation, and it is usually divided into four ore levels: A (freshwater sediments – stream and lacustrine sandstones), main B level is evolved at the base of marine Cenomanian in wash-out sediments; ore levels C and D are less extended and occur in the friable sandstones (C) and in the uppermost Cenomanian – fucoidal sandstone horizon (D). The mostly horizontal plates and lenses usually form the ore bodies. The thickness of these plates and bodies varies from decimetres to several metres. The mineralogical and geochemical composition of uranium mineralisation occurring in the North Bohemian Cretaceous uranium district is diversiform and unique [33–35].

Uraninite, complex U-containing gels, hydrozircon, baddeleyite and U-Th-Ca phosphates (ningyoite and brockite) are main carriers of uranium. For these uranium-enriched minerals (uraninite, hydrozircon, ningyoite and brockite) is highly significant enrichment in rare earth elements (REE) and Y. Uranium mineralisation is also coupled with occurrence of REE or Y minerals (crandallite, chernovite-(Y), rhabdophane and synchysite) [35, 36].

In 2012, in preparation of the new State Energy Concept of the Czech Republic, technical and economic re-evaluation of remaining uranium resources was undertaken. Total identified conventional resources in 2013 amounted to 119,256 t U. These resources are located in the North Bohemian Cretaceous basin (the Stráž, Hamr, Osečná-Kotel and Břevniště deposits). However, all these resources remain strictly protected due to environmental concerns (groundwater source protection zone) [31].

In Slovakia, from 1954 to 1990, small uranium deposit in the Slovak Ore Mts. (Novoveská Huta) was mined. The uranium ores were mined as by-product of copper mining. The uranium mineralisation in the Novoveská Huta ore deposit (Gemericum) occurs in two horizons of Permian volcano-sedimentary formation. The upper horizon is a part of volcano-sedimentary complex of volcanoclastic sandstones and conglomerates overlying rhyolites and their tuffs. Ore bodies form lenses mostly concordant to wall rocks. Their thickness reaches several metres. Uranium mineralisation is concentrated, however, largely in matrix of volcanoclastic rocks. The lower ore-bearing horizon occurs in breccias of the upper part of volcano-sedimentary complex with intermediate volcanic rocks. The length of the mineralised horizon is 4 km, the width varies from 200 to 600 m and the thickness reaches up to 80 m. Lenticular ore bodies are thick from several metres to tens of metres. Uranium mineralisation is disseminated or forms veinlets. Uraninite and molybdenite are dominant in uranium ore of both main horizons. U-Ti oxides, pyrite, chalcopyrite, tennantite, galena, sphalerite and arsenopyrite accompany them.

Hydrozircon also occurs in the lower ore-bearing horizon. Rich uranium mineralisation rarely occurs in faults cutting the U-Mo mineralised horizons in the western part of the Novoveská Huta deposit. Uranium and Mo mineralisation in these faults is represented by uraninite, coffinite and molybdenite.

Some small uranium deposits and occurrences were found also in the other West Carpathian geological units in Slovakia, namely in the Hronicum (Vikartovce, Kravany, Švábovce), Tatricum (Kálnice, Selec) and the Veporicum. All these geological units could be distinguished into two morphological types of uranium mineralisation, namely stratiform mineralisation in the Permian volcanoclastic complexes and vein mineralisation evolved in tectonic zones (quartz-carbonate, quartz-gold-bearing veins) [37].

In 2012–2014, new exploration licences for uranium ore were active in the Slovak Republic. The most perspective exploration licence covers uranium mineralisation in Kuriškova, near Košice in the Eastern Slovakia. In this area, conventional resources in amount of 15,830 t U were calculated and identified. In the Novoveská Huta, resources in amount of 3488 t U are recently registered [31]. However, mining of both uranium deposits is recently blocked by various environmental activities.

9. East Germany uranium mining after World War II

The uranium exploration and mining in East Germany (GDR) started in 1946 as the Soviet stock company, SAG Wismut. In the first stage of this mining activity, an old silver-uranium-cobalt-nickel ore deposit Johanngeorgenstadt was open. Later, the uranium ore deposits near Schneeberg and Oberschlema were found and mined. The second stage of uranium exploration had started in 1950 in the vicinity of the radium spa at Ronneburg. In both uranium ore districts, using a variety of ground-based and aerial techniques, the exploration activities covered an extensive area of about 55,000 km^2. About 36,000 boreholes in total were drilled in the area covering approximately 26,000 km^2. Total expenditures for uranium exploration were on the order of 5–6 billion of GDR mark [31].

In 1954, a new joint Soviet-German stock company was created (SDAG Wismut). Both governments held the joint company equally. At the end of the 1950s, uranium mining was concentrated in the region of Eastern Thuringia (Ronneburg ore district). From the beginning of the 1970s the Ronneburg ore district provided about two-thirds of uranium annual production in the GDR. In East Germany, in contradiction to Czechoslovakia, the prisoners were used in uranium mining in limited extent. The prisoners were used mainly in 1946–1947 and the total number of prisoners used in SAG Wismut from 1946 to 1949 was 59,492 [38].

Total production in East Germany in 1946–1990 was 219,517 t U, making it the third largest producer in history behind the United States and Canada. The uranium mining and processing of uranium ores in two processing plants were stopped in 1989. Decommissioning of uranium mines and production facilities started in 1990. Between 1991 and 2012, uranium recovery from mine water treatment and environmental restoration amounted to a total of

2540 t U. Since 1992, all production in former East Germany has been derived from clean-up operations at the Königstein mine. In 2007, the production in the Königstein mine has been 38 t U [31].

The uranium mining in East Germany was concentrated in two main regions: the Ore Mts. region in Saxony (Schneeberg, Niederschlema-Alberoda, Johanngeorgenstadt, Schwarzenberg and Pöhla-Tellerhäuser) and the Ronneburg district in Thuringia. Small uranium deposits were evolved in the Cretaceous sandstones near the Königstein in Saxony [39–41]. Uranium deposits in the Ore Mts. region are hydrothermal vein deposits. In these ore deposits, three uraniferous mineral associations were established (quartz-calcite-pitchblende, carbonate-pitchblende-fluorite and bismuth-cobalt-nickel-silver-uranium). Uranium in these associations is represented by pitchblende, sooty pitchblende and coffinite. In veins of the Niederschlema-Alberoda deposit, coffinite constitutes up to 5% of the uranium content. The main ore deposit in this region was Niederschlema-Alberoda and it was one of the largest vein uranium deposits in the world, which has produced 73,900 t U. Other uranium deposits in the Ore Mts. region produced distinctly lower amount of uranium (Oberschlema 6700 t U, Johanngeorgenstadt 3600 t U, Pöhla-Tellerhäuser 1240 t U, Schwarzenberg 670 t U and Schneeberg 160 t U).

The Niederschlema-Alberoda uranium ore district is located in the Western Ore Mountains, in Germany, near the state boundary to Czech Republic. This ore district is evolved in the intersection of the SW-NE striking Loessnitz-Zwoenitz syncline with NW-SE trending Gera-Jáchymov fault zone. The Loessnitz-Zwoenitz syncline is one from sectional tectonic structures, which are ingredients of the Erzgebirge-Fichtelgebirge anticlinorium in the fold framework of the Saxothuringian Zone. The most important and central tectonic element of the Gera-Jáchymov fault zone is the vein structure Red Ridge (Roter Kamm), also defining the border between the Niederschlema-Alberoda ore district in NE and the Schneeberg uranium deposit in SW. In the Loessnitz-Zwoenitz syncline, predominantly Upper Ordovician-Silurian-Middle Devonian "productive" rocks are folded into Lower Ordovician schists of the northern edge zone of the Erzgebirge-Fichtelgebirge anticlinorium. The rock series of the "productive unit" are phyllites with intercalations of metamorphosed black shales and metacarbonates. The uranium-bearing veins occur in the contact metamorphic zone of the syncline beneath the late-Variscan Aue granite pluton. This granite body, located within the Gera-Jáchymov fault zone, intruded early-Variscan metasediments, especially low-grade garnet phyllites and medium-grade mica schists. The Aue granite body comprises various biotite granites. The Aue granite should have served as a major source for U accumulated in post-granitic deposits of Schneeberg and Schlema-Alberoda ore districts.

The uranium ore veins have a common thickness from 0.1 to 0.3 m with a maximum of 1 m. However, some ore veins show a massive pitchblende mineralisation with a thickness up to 2 m, which were mined down to a depth of about 2000 m. The hydrothermal mineralisation is usually divided into three main stages. The most important is first pitchblende-quartz-calcite-fluorite-sulphide stage. The second, post-Variscan stage contains dolomite-selenide-pitchblende mineral association. For the third, Bi-Co-Ni stage, the predominance of arsenides

and sulphides Co and Ni and native Bi is significant. The main mined ores were uranium ores, and accompanying ores (Co, Ni, Ag, Bi, Se and/or Pb, Zn and Cu from older quartz-sulphide veins) have been extracted only temporarily and in small quantities [39, 40].

The second most significant area with uranium mineralisation in GDR was the Ronneburg district in Thuringia. This district is part of the Thüringisch-Fränkischen Schiefergebirge. The main geological structure of this district is the Berga anticlinorium. Uranium mineralisation occurs in the Upper Ordovician to Lower Devonian black schist series with total thickness about 250 m. The main part of uranium mineralisation is bounded on the Upper Ordovician Leder schists. In the Ronneburg ore district, three morphological types of uranium mineralisation, namely mineralisation in faults and shear zones, mineralisation in breccias and highly dispersed mineralisation in black schists, were distinguished. Uranium mineralisation was formed by two associations: carbonate-uraninite and uraninite-pyrite associations. The main mined association was uraninite-pyrite association containing uraninite, pyrite, coffinite, marcasite, chalcopyrite, arsenides, calcite, dolomite, hematite and hydrogoethite. The uranium deposits in the Ronneburg district were mined from 1951 to 1990 in three open pits (Ronneburg, Lichtenberg and Stolzenberg) and in seven shafts. Total open pit and mine production of the Ronneburg ore district was 112914.3 t U with average grade of 0.099% U [40].

Small occurrence of uranium mineralisation was also found in the Lower Permian hard coal-bearing sediments of the NW-SE Döhla basin near Dresden. The basin that evolved along the late Variscan Elbe lineament contains the Upper Carboniferous and Lower Permian freshwater sediments (conglomerates, breccias, schists and hard coal-bearing sediments). The Lower Permian hard coal sediments contain hydrothermal uranium mineralisation (uraninite and coffinite) together with sulphide (sphalerite, chalcopyrite and galena) and carbonate mineralisation. Main uranium mining area in the Döhla basin was by Dresden-Gittersee and Freital. Total mine production of the Freital ore deposit mined from 1968 to 1989 was 3691 t U with average grade of 0.11% U [40].

In the natural park Saxony Switzerland, near Pirna was from 1967 to 1990 mined uranium deposit Königstein. This deposit was developed in the local Cretaceous basin that is NW part of the North Bohemian Cretaceous basin. From this large basin, the local Pirna basin was separated by the NNW-SSE Elbe lineament. The uranium mineralisation is developed in the three Cenomanian formations: lower freshwater continental, middle lagoon sediments and upper marine sediments. Bodies of the Lower Cambrian granodiorites and Variscan granites of the Markersbach granite body form the basement. Freshwater sediments are developed in depressions of the paleo relief and consist of sandstones and clay-bearing schists. All these rocks are often rich in organic matter (coalified plant detritus). The sediments of marine Cenomanian contain different sandstone types. Mostly horizontal lenses form the ore bodies. The thickness of ore bodies was between 0.5 and 1.0 m, sometimes up to 2.5 m. Some part of uranium mineralisation occurs also in the younger faults. Uranium mineralisation is formed by uraninite, coffinite and fourmarietite. Total mine production of the Königstein ore deposit mined from 1967 to 1995 was 18526.9 t U with average grade of 0.03–0.08% U [40]. After closing all uranium deposits in 1990, various large-scale remediation activities were provided from 1991 to 2014 [31].

10. West Germany uranium mining after World War II

Starting in 1956, exploration for uranium ores in Federal Republic Germany (FRG) was carried out in several Variscan units, especially in Black Forest, Odenwald, Frankenwald, Oberpfalz, Bayerischer Wald and Harz. Three small uranium deposits were found: vein deposit near Menzenschwand in the southern Black Forest, sedimentary Müllenbach deposit in the northern Black Forest and the Grosschloppen deposit in the Fichtelgebirge. The total uranium production was about 700 t U [31].

11. Polish uranium mining after World War II

Exploration and exploitation of uranium ore deposits in Poland began in 1948 by opening of the vein uranium deposits in the Karkonosko-Izerski block of the Bohemian Massif (Wolnosc, Miedzianka, Podgorze, Rubezal, Mniszkow, Wiktoria, Majewo, Walowa Gora, Radoniów and Wojcieszyce). For processing of uranium ores from these mined deposits, in 1948, an industrial plant in Kowary (Lower Silesia) was established. Later, small occurrences and deposits of uranium mineralisation were founded in the Ladek and Snieznik Klodzki metamorphic complex of the Bohemian Massif (Kopaliny-Kletno). During the period 1948 and 1967, approximately 650 t of uranium was mined and all uranium ores were exported to the Soviet Union.

In 1956, exploration of uranium ore deposits by the Geological survey in areas of the Upper Silesian Coal Basin and the Polish lowlands began. During these exploration activities, small occurrences of uranium mineralisation were discovered in the Lower Ordovician sediments (Rajsk), in the Triassic sediments (Perybaltic Syneclize) and in the Sudetes area (Okrzeszyn, Grzmiaca and Wambierzyce). In May 2012, one concession for prospecting base metals and uranium deposit was granted in the Radoniów area. At present, research projects aimed at assessing the possibility of obtaining uranium from domestic low-grade uranium ores and waste rock piles left at historic uranium mining operations (Kowary) are being conducted. Special attention is being paid to the use of biological leaching. All these exploration activities concentrated on finding of potential uranium resources were provided from 2012 to 2014.

12. Hungarian uranium mining after World War II

The first prospecting for uranium ores started in 1952 with Soviet participation. During airborne and surface radiometry in the western part of the Mecsek Mts., the Mecsek deposit of sedimentary ore deposit was found in 1954. The first shafts in this area were placed in 1955 and 1956. In 1956, the Soviet-Hungarian uranium joint venture was dissolved and uranium production from this ore deposit became the sole responsibility of the Hungarian state. Uranium in the Mecsek deposit was mined from 1956 to 1997. Total production of uranium from this ore deposit was about 21,000 t U. The uranium ore in the Mecsek deposit occurs in Upper Permian sandstones that may be thick as 600 m. The sandstones were folded into the

Permian-Triassic anticline of the Mecsek Mts. The thickness of ore-bearing sandstone varies from 15 to 90 m. The ore minerals are represented by uraninite, coffinite, pyrite and marcasite.

Since 2006, four uranium exploration project areas were covered by seven exploration licences (Mecsek, Bátaszék, Dinnyeberki and Máriakéménd). Only the Mecsek project, where new geological model of the Mecsek uranium deposit was established, remains active. Following recent resource estimate re-evaluation, 17,946 t U is now reported as in situ high-cost inferred resources. Large-scale remediation activities in the area of the Mecsek uranium deposit were provided from 1998 to 2008 [31].

13. Conclusion

The Central European deposits were the first industrially mined uranium deposits in the world. Uranium minerals, especially uraninite (pitchblende), were noticed firstly by miners in the Ore Mts. area (Saxony, Bohemia) for a long time prior the uranium discovery. The uraninite was in this time found by miners in places with higher occurrence of uraninite, the silver and its minerals disapper. The first occurrence of pitchblende consequently entails trouble (pitch). The German chemist Klaproth in 1789 detected uranium by analysing pitchblende from the Johanngeorgenstadt uranium deposit in the German part of the Krušné Hory/Erzgebirge Mts. In the nineteenth century, some chemists from silver metallurgical works in the Ore Mountains area, especially in Jáchymov, started with experiments using the yellow uranium–bearing components originated by processing of silver-uranium ores in glassmaking industry. Uranium glass became popular in the mid-nineteenth century, with its period of greatest popularity being from 1880s to the 1920s.

In 1896, A.H. Becquerel discovered the phenomenon of radioactivity. His student Marie Sklodowska-Curie recognised that pitchblende has higher radioactivity as pure uranium salts. Later, together with her husband P. Curie, they discovered two new elements: radium and polonium. In years 1908–1933, radium chloride from various uranium deposits, especially from the Jáchymov deposit was produced, for its use in medicine to produce radon gas, which in turn was used in cancer treatment. Later, radium was used for radon production. Highly radioactive mineral waters occurred in some localities in the Ore Mts. (Krušné Hory/Erzgebirge) and were used to mitigate diseases of movement system such as rheumatoid arthritis, spondylitis, ankylosing spondylitis, condition after orthopaedic surgeries, diseases of peripheral nervous system and metabolic diseases. Radioactive water baths have been applied since 1906 in Jáchymov, since 1912 in Bad Brambach and since 1918 in Oberschlema, Saxony.

Otto Hahn and Fritz Strassmann conducted the experiments leading to the discovery of uranium's ability to fission and release binding energy in 1934. Lise Meitner and Otto Robert Frisch published the physical explanation in February 1939 and named the process "nuclear fission". The first use of nuclear fission in nuclear weapons applied at the end of World War II in Japan (Hiroshima, Nagasaki) started the first boom of exploration and exploitation of uranium ores in the whole world. The significant amount of uranium ores for producing the

Russian nuclear weapons and nuclear power plants in the former Eastern Bloc was mined in East Germany (GDR) and Czechoslovakia. The total production of uranium ores in GDR from 1946 to 2012 was 219,626 t U. In Czechoslovakia, total uranium production from 1945 to 2017 was 112,250 t U. Some small amount of uranium ores after World War II was mined also in Poland (650 t U) and Hungary (21,000 t).

In the Czech Republic and East Germany, the exploration activities for uranium mineralisation were stopped between 1990 and 2004. In the Slovak Republic, Poland and Hungary, some small exploration activities on uranium mineralisation were provided between 2012 and 2014. Potential possibility of future exploration and mining of uranium ores is in the Central European countries recently blocked by various environmental and civil activities.

Acknowledgements

This work was carried out thanks to the support of the long-term conceptual development research organisation RVO: 67985891.

Author details

Miloš René

Address all correspondence to: rene@irsm.cas.cz

Institute of Rock Structure and Mechanics, Academy of Sciences of the Czech Republic, Prague, Czech Republic

References

[1] Klaproth MH. Chemical investigation of uranium, some new metal material. Chemische Annalen. 1789;**2**:387-403 (in German)

[2] Kirchheimer F. Uranium and its History. Stuttgart: E Schweizerbart'sche Verlagsbuchhandlung; 1963. 380 p (in German)

[3] Vysoký A. About uranium, uranium minerals and uranium yellow's. Živa. 1860;**8**:25-30 (in Czech)

[4] Schwanker RJ, Eigenstetter M, Laubinger R, Schmidt M. Uranium as colour in glass and glaze. Physik in Unserer Zeit. 2005;**36**:160-167 (in German)

[5] von Philipsborn H, Geipel R. Uranium colours, uranium glass, uranium glaze, radiometrical, technical, historical. Schriftenreihe Bergbau und Idustriemuseums Ostbayern 2005;**46**:1-159

[6] Curie P, Curie M, Bémont G. On a new, strongly radioactive substance contained in pitchblende. Comptes rendus hebdomadaires des séances de l'Académie des sciences. 1898;**127**:1215-1217 (in French)

[7] Curie P, Curie M. About new radioactive material contained in pitchblende. Comptes rendus hebdomadaires des séances de l'Académie des sciences. 1898;**127**:175-178 (in French)

[8] Kolbe A. Why would be in the St.Joachimsthal pitchblende occurred chemical elements polonium and radium not before 1898 in Austria discovered. Montan Rdsch. 1961;**9**:356-359. (in German)

[9] Pluskal O. The post war history of Czechoslovak uranium from Jáchymov (Joachimsthal). Czech Geological Survey (Spec. paper) 1998;**9**:1-48. (in Czech)

[10] Perrin J. Radon. Annales de Physique. 1919;**11**:5 (in French)

[11] Adams EQ. The independent origin of actinium. Journal of the American Chemical Society. 1920;**42**:2205

[12] Schmidt R. History and beginning of uranium mining in Saxony. In: Karlsch R, Schröter H, editors. The Radiated Past. St. Katharinen: Scripta Mercaturae Verlag; 1996. pp. 77-96 (in German)

[13] Běhounek F, Santholzer V. About radioactivity of the rocks from the Jáchymov uranium ore district in bohemia. Gerlands Beitraege zur Geophysik. 1931;**33**:60-69 (in German)

[14] Santholzer V, Ulrich F. Radio-geological survey of Czechoslovakia. Nature. 1934;**1934**:961

[15] Řeřicha V, Kulich M, Řeřicha R, Shore DL, Sandler DP. Incidence of leukemia, lymphoma, and multiple myeloma in Czech uranium mines: A case-cohort study. Environmental Health Sciences. 2006;**114**:818-822. DOI: 10.1289/ehp.8476

[16] Watznauer A, Koch U. Geological and hydrogeological relations in spring area of bad Brambach. Abhandlungen der Sächsischen Akademie der Wissenschaften. 1989;**57**:49-58 (in German)

[17] Veselovský F, Ondruš P, Komínek J. History of the Jáchymov (Joachimsthal) ore district. Journal of the Czech Geological Society. 1997;**42**:127-132

[18] Titzmann O. Uranium mining in opposite to radium baths. Bad Schlema: Own Print. 2003. 464 p. (in German)

[19] Mache H, Meyer S. About radioactivity of springs of the bohemian baths group: Karlsbad, Marienbad, Teplitz-Schönau-dux, Franzensbad and St. Joachimsthal. Sitzungsberichte der Kaiserlichen Akademie der Wissenschaften. 1905;**64**:1-35 (in German)

[20] Laboutka M, Pačes T. The hydrogeology and geochemistry of water in the Jáchymov district. Sborník geologických Věd, Hydrogeologie a inženýrská geologie. 1966;**4**:59-112 (in Czech)

[21] Pačes T. Chemical equilibira and zoning of subsurface water from Jáchymov ore deposit. Geochimica et Cosmochimica Acta. 1969;**33**:591-609. DOI: 10.1016/0016-7037(69)90017-9

[22] Laboutka M, Vylita B. Mineral and thermal waters of western bohemia. Geographical Journal. 1983;**7**:403-411

[23] Möller P, Dulski P, Gerstenberger H, Morteani G, Fuganti A. Rare earth elements, yttrium an H, O, C, Sr, Nd and Pb isotope studies in mineral waters and corresponding rocks from NW-bohemia, Czech Republic. Applied Geochemistry. 1998;**13**:975-994. DOI: 10.1016/s0883-2927(98)00024-9

[24] Těšínská E. The beginning of the radon spa, Joachimsthal, bohemia. Part 1: Its organization impulses and connections. Dějiny vědy a techniky. 2008;**41**:205-232 (in Czech)

[25] Zoellner T. Uranium: War, Energy and the Rock that Shaped the World. London: Penguin Books; 2009. 352 p

[26] Halloway D. Stalin and the Bomb. The Soviet Union and Atomic Energy 1939-1956. New Haven, London: Yale University Press; 1994. 480 p

[27] Karlsch R. Uneven partner – Contractual and financial problems of the GDR uranium supply. In: Karlsch R, Schröter H, editors. The Radiated Past. St. Katharinen: Scripta Mercaturae Verlag; 1996. pp. 263-300 (in German)

[28] Zeman Z. Czechoslovak-soviet uranium contract. In: Karlsch R, Schröter H, editors. The Radiated Past. St. Katharinen: Scripta Mercaturae Verlag; 1996. pp. 60-76 (in German)

[29] Zeman Z, Karlsch R. Uranium Matters. Central European Uranium in International Politics 1900-1960. Budapest, New York: CEU Press; 2008. 303 p

[30] Matolín M, Pluskal O, René M. Uranium Mineralization in the Bohemian Massif and its Exploration. Uranium Exploration Case Histories. Vienna: IAEA; 1981. pp. 389-398

[31] Uranium 2014: Resources, Production and Demand. Paris: OECD; 2014. 508 p

[32] Kafka J, editor. Czech Ore and Uranium Mining Industry. Ostrava: Anagram; 2003. 647 p, (in Czech)

[33] Čadek J, Mirovský J, Novák F, Vavřín I. Association of uranium and zirconium in the sandstone type uranium deposits in northern bohemia. Časopis pro mineralogii a geologii. 1975;**20**:131-140

[34] Scharm B, Burda J, Hofreitr V, Sulovský P, Scharmová M. Remarkable mineral assemblage on uranium deposits in northern bohemia (the Stráž block). Časopis pro mineralogii a geologii. 1980;**25**:113-124

[35] Sulovský P. Sandstone-hosted U-Zr-REE Mineralization in North Bohemian Cretaceous Basin. Uranium Production and Raw Materials for the Nuclear Fuel Cycle. Vienna: IAEA; 2005. p. 91-95

[36] Scharmová M, Scharm B. Rhabdophane group minerals in the uranium ore district of northern bohemia (Czech Republic). Journal of the Czech Geological Society. 1994; **39**:267-280

[37] Rojkovič I. Uranium mineralization in Slovakia. Acta Geologica Universitatis Comenianae. Monographic Serie. 1997. 117 p

[38] Roeling R. Workers, hard labourer, atractive labour and sociales circumstances. In: Karlsch R, Schröter H, editors. The Radiated Past. St. Katharinen: Scripta Mercaturae Verlag; 1996. pp. 99-133 (in German)

[39] Schuppan W, Büder W, Lange G. On uranium mineralization in the vein deposits of the western Erzgebirge, Germany. Monograph Series on Mineral Deposits. 1994;**31**:191-207

[40] Runge W, editor. Chronicle of Wismut. CDROM. Wismut GmbH: Chemnitz; 1999. 2738 p (in German)

[41] Baumann L, Kuschka E, Seifert T. Deposits of the Ore Mts. Stuttgart: Georg Thieme Verlag; 2000. 300 p

Chapter 2

Safety and Economics of Uranium Utilization for Nuclear Power Generation

Yuji Fukaya

Additional information is available at the end of the chapter

http://dx.doi.org/10.5772/intechopen.72647

Abstract

Safety and economics of uranium utilization for nuclear power generation were investigated and discussed. In order to sustain energy supply with nuclear power generation, uranium resources should be abundant. From the viewpoint of depletion of the resources, fast breeder reactor (FBR), which is breeder reactor of plutonium, has been developed. In this context, the uranium utilization and plutonium utilization with breeding by FBR are compared and discussed from the viewpoint of safety, sustainability, and energy security. In addition, the significance of partitioning and transmutation (P&T), which is one of the advantages of FBR, was also discussed from the viewpoint of environmental burden from radioactive waste.

Keywords: uranium resources, safety, electricity generation cost, plutonium breeding

1. Introduction

Nuclear power is an attractive energy source of clean air and carbon-free electricity that produces no greenhouse gases or air pollutants unlike power generation with fossil fuel. Moreover, it is said that fossil fuels are in danger of running out. Especially for the petroleum resources, the duration period is about 40 years. In this context, nuclear power generation (NPG), whose fuel is uranium, has been installed as alternative energy. However, fast breeder reactor (FBR), which is breeder reactor of plutonium, has been developed from the viewpoint of depletion of uranium resources [1] but not deployed as a commercial reactor yet. Many researchers and engineers believe that sustainable energy supply can be established only with FBR fuel cycle. However, we should reconsider the problem of depletion of uranium resources before coming to a decision because safety of reactor depends on reactor types. Moreover, other problems, e.g., economics and environmental burden, should be considered. To this end, safety of nuclear reactor with uranium utilization and that with plutonium breeding is

discussed in Section 2. Sustainability of uranium resources and that with plutonium thermal use is discussed in Section 3. Economics of electricity generation with conventional uranium, sweater uranium, and plutonium multi-recycling by FBR is discussed in Section 4. Energy security for uranium and plutonium utilization is discussed in Section 5.

2. Safety of nuclear reactor and breeding

Passive safety features are preferred for advanced reactor design, such as Economic Simplified Boiling Water Reactor (ESBWR) [2], Advanced Passive 1000 (AP1000) [2], and European Pressurized water Reactor (EPR) [3], to enhance safety and reliability and to reduce human intervention. In Fukushima Daiichi accident on March 11, 2011, passive safety features were desired especially for isolation condenser (IC) systems in unit 1 [4].

In addition, high-temperature gas-cooled reactor (HTGR) attracts attention after the accident due to the inherent safety features for all safety functions of "shutdown," "cooling," and "containment" [5]. As a result, the development of HTGR was recommended in "strategic energy plan," which is formulated by the government of Japan on April 11, 2014 [6].

The fundamental safety features are composed of the three functions of control of reactivity (shutdown), removal of heat from the reactor (cooling), and confinement of radioactive material (containment). In the Fukushima Daiichi accident, the first function "shutdown" was successfully performed. However, the second function "cooling" failed even with the IC systems, which have enough heat removal function for 8 hours per IC system. For the IC systems, passive safety features were desired as described in the previous section. As a result, the final function of "containment" was lost as well.

The first feature of "shutdown" was performed as the automatic scram by detecting the earthquake. For light water reactor (LWR), if the scram would be failed, the reactor power settles down to zero power by moderator reactivity feedback due to the reduced density of the moderator and the Doppler effect due to the increased fuel temperature when heat removal from core is lost.

That is equivalent to inherent safety feature due to self-regulation of power of LWR for normal operation condition. The negative reactivity feedback is caused by expansion of moderator. The moderator temperature coefficient, void coefficient for boiling water reactor (BWR), is designed to be negative as it depends only on the degree of moderation and not on the core size. In other words, the LWR core is designed to be under-moderated [7] such that the neutron moderation is not sufficient to obtain a maximum multiplication factor. At the same time, the multiplication factor is reduced by a moderator density reduction.

For HTGR, the graphite structure is also employed as moderator. The volume ratio of fuel to the moderator, which is an indicator for degree of moderation, is determined by the integrity of core structure and a state of the art of fuel fabrication. Generally, for almost all nuclear reactors, as fuel assembly has more number of fuel pins, the fuel temperature can be reduced to lower because the power-sharing decreases per fuel pin. For HTGR with pin-in-block type fuel, the fuel pins are allocated into the coolant hole in graphite fuel block. The number of fuel pins is

restricted by the requirement for the fuel block strength against thermal stress. The fuel pins are composed of coated fuel particles (CFPs). The maximum volume fraction is determined by a state of the art of fuel fabrication to restrict initial failure fraction of the CFPs. To obtain high burnup for long life cycle, the volume fraction prefers the maximum value. Moreover, the moderating power and the absorption cross section of graphite are lower than those of light water. The optimized design for criticality is not preferable from the viewpoint of the long life cycle with considering burnup. According to the result, HTGR's design condition is in the undermoderated region when the core design is reasonable and realistic from the viewpoint of the heat removal, the integrity of structure, and the long life cycle. Moreover, the solid moderator of graphite is never voided. To realize a negative power reactivity coefficient, there are two factors, the Doppler effect of fuel temperature and reactivity feedback of moderator temperature due to neutron spectrum shift of Maxwellian distribution peak [8]. As a result, thermal reactor including LWR and HTGR has the inherent safety feature due to self-regulation of power.

On the contrary, many FBR designs allow a positive void reactivity coefficient because of the increase of threshold fission reaction of fertile material with high neutron energy over 1 MeV due to the hard spectrum. **Figure 1** shows the fission and capture cross sections and the ratio of fission cross section to absorption cross section. The ratio stands for the fission probability per neutron absorption reaction. The fission probability also rapidly increases over 1 MeV, and the probability is around unity. Then, when the coolant of sodium is voided, the neutron over 1 MeV increased, and positive reactivity is inserted.

Due to the positive void reactivity coefficient, the coolant is boiled, and the power burst, which melts the fuel pins, occurs upon unprotected loss of coolant flow (ULOF) accident [9]. To prevent the power burst, Integral Fast Reactor (IFR) [10] is designed with a large safety margin for heat removal to avoid coolant boiling instead of inherent safety features of neutronic characteristics for self-regulation due to negative coolant void coefficient. The concept

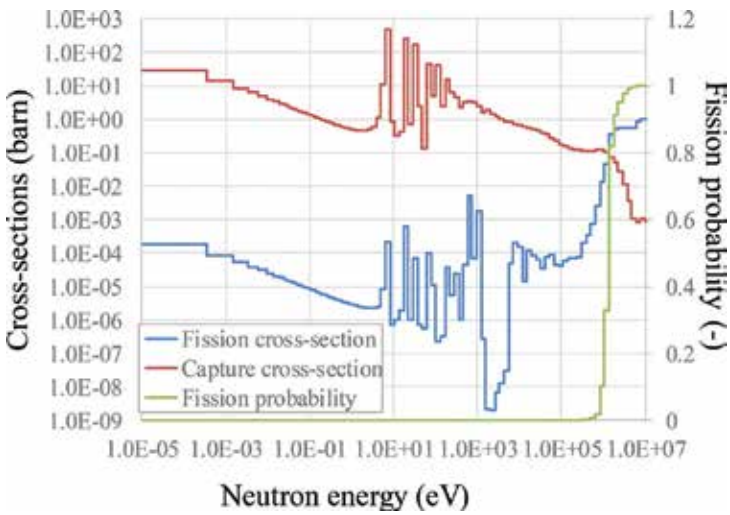

Figure 1. Cross section of ^{238}U and fission probability per neutron absorption.

of the inherent safety feature of IFR was demonstrated using an IFR prototype, Experimental Breeder Reactor No. 2 (EBR-2) [11]. Although IFR allows a positive void coefficient, it was demonstrated that, upon ULOF accident, a reactor operating at full power can be safely shut down using a negative reactivity feedback due to Doppler effect without the need of the scram, other safety systems, or operator actions.

However, the commercial FBRs, such as European fast reactor (EFR) [12], which is one of representative FBRs of Generation IV, have high economy and high breeding ability and cannot have the passive safety feature by the enhanced heat removal function because of its minimal safety margin to obtain high core performance. The safety is guaranteed with a reliable shutdown system in the event of coolant flow loss.

To obtain negative or small positive void coefficient, FBR with large core should be designed with pancake-type core to increase neutron leakage for axial direction when the coolant is voided [13]. However, sodium-cooled FBR cannot obtain the negative void coefficient only with the pancake-type core. Then, the concept of "sodium plenum" [14] was proposed to increase the axial neutron leakage. In this concept, upper axial blanket and upper side of fuel are removed to enhance the neutron leakage when the coolant is voided. Naturally, breeding ability will weaken.

Thus, safety and economy, or breeding ability, are related to the transactions for fast reactors (FRs) including FBR. If core performance is prioritized, the passive safety feature for "shutdown" will be abandoned.

3. Sustainability of energy resources

3.1. Duration period of uranium resources

Uranium resources should be abundant compared with requirement, and energy security is also necessity to ensure the energy sustainability. The duration period, which is defined as the ratio of available resources to the consumption rate, is employed as a measure of the abundance. The consumption rate is estimated to be approximately 60,000 tU/year (61,980 tU/year) by referring to the measured amount required in the world for electricity capacity of 372 GWe at the end of 2012 [15].

The available resources are categorized to identified resources and undiscovered resources. The identified resources stand for uranium deposits delineated through sufficient direct measurement. The undiscovered resources stand for expected existence on the basis of geological knowledge. Usually, only identified resources are employed to estimate the duration period. However, undiscovered resources and other resources described below also exist and will be available. In the present study, the duration periods except for the identified resources are also evaluated to measure the abundance.

The amount of total identified resources in 2013 is approximately 7.6 million tU (7,635,200 tU) [15]. This amount corresponds to a duration period of approximately 120 years (123.2 years). The resources increased by 7.6% from 2011 by new discoveries owing to the revitalization of investigations on resources with the recent soaring market price of uranium. **Figure 2** shows

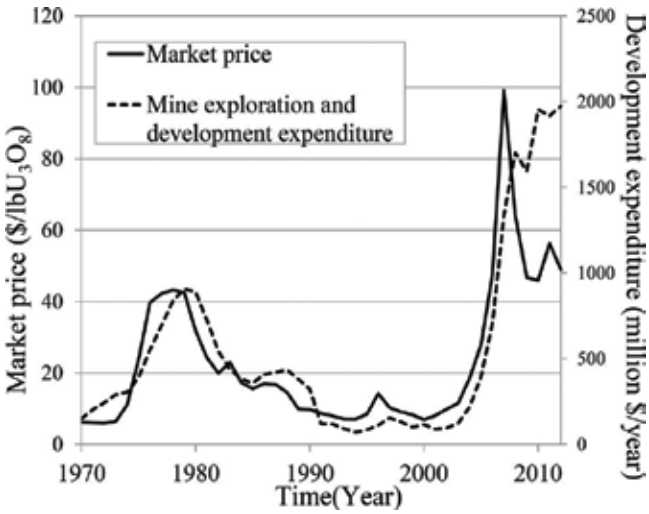

Figure 2. Market price of uranium and mine exploration and development expenditure.

the relation between the market price and the mine exploration and development expenditure [15, 16]. The investment for the exploration and development follows the market price. This trend is common for other resources, e.g., petroleum and coal.

The amount of total undiscovered resources in 2013 is approximately 7.7 million tU (7,697,800 tU), which is a marginal decrease from approximately 10 million tU (10,429,100 tU) reported in 2011 [15]. The reason why the resources decrease is that the USA did not report the amount in 2013. Then, I regard the amount of undiscovered resources as the value of 10,429,100 tU reported in 2011. This amount corresponds to approximately 170 years (168.3 years) of the duration period.

For the estimation of the amount of conventional uranium resources including the identified and undiscovered resources, the highest cost category, i.e., < 260 $/kgU, is used. Furthermore, there are other resources called unconventional resources recovered not from uranium mines as uranium ore. The unconventional resources are recovered as minor by-products such as uranium from phosphate rocks, nonferrous ores, carbonatite, black shale, and lignite. The recovery cost from these products is higher because of the low uranium concentration. In the future, these resources would become a viable source when market price of uranium exceeds 260 $/kgU [15]. The amount of these sources is 7.3–8.4 million tU [15], which corresponds to a duration period of approximately 130 years (117.8–135.5 years). The resources described above can maintain the energy sustainability for the present. However, more resources are needed to achieve the permanent energy sustainability.

Uranium from seawater, which is also categorized to unconventional resources, amounted to 4.5 billion tU [17] corresponding to a duration period of approximately 72,000 years (72,604 years). The uranium is dissolved in the seawater at a low concentration of 3.3 parts per billion (ppb) [17]. Moreover, the amount of uranium at the surface of the seafloor is approximately a thousand times more than the uranium dissolved in seawater, which is approximately 4.5 trillion tU [18]. The uranium solved in seawater is in an equilibrium state with the uranium contained in

the rock on surface of the seafloor [18]. The concentration of 3.3 ppb is remained because of the equilibrium state. This suggests that not only the amount of the uranium dissolved in seawater but also that in the rock on the surface of the seafloor corresponding to the duration period of approximately 72 million years can be recoverable. In other words, the uranium from seawater is almost an inexhaustible resource.

3.2. Utilization of plutonium

Plutonium is generated along with burnup of ^{235}U by conversion of ^{238}U. Suppress plutonium should be incinerated from the viewpoint of nuclear proliferation. Even when the plutonium is disposed, it is problematic and called a "plutonium mine." As time goes on, the plutonium becomes easy to use. Dose from accompanying fission products (FPs) decays, and a fraction of plutonium fissile (Puf) also increases as shown in **Figure 3**. **Figure 3** shows the change on the fraction of the plutonium fissile in spent fuel of LWR. The peak value of around 0.75 appears at 20,000 years near the half-life of ^{239}Pu of 24,000 years. In addition, the ability of conversion is measured by conversion ratio (CR). The conversion ratio is defined as follows [19]:

$$CR = \frac{Average\ rate\ of\ fissile\ atom\ production}{Average\ rate\ of\ fissile\ atom\ consumption} \quad (1)$$

The conversion ratio of LWR is around 0.6 [19]. If the actinoid nuclides are burned as same amount as fissile nuclides in fresh, the conversion ratio coincides with residual ratio (RR), which is defined as the ratio of fissile inventory in discharged fuel to that in fresh fuel. In many designs of LWRs, the fissile inventory and the inventory of burned nuclides are almost same, and conversion ratio can be regarded as residual ratio.

Plutonium can be also used as resources even in thermal reactor, that is, "plutonium thermal use." The duration period increased to 1.6 times, which is the sum of uranium resources of unity and generated plutonium of 0.6, when once-through utilization of plutonium. With considering necessity of reprocessing facility only for spent plutonium fuel, this option can be a realistic candidate.

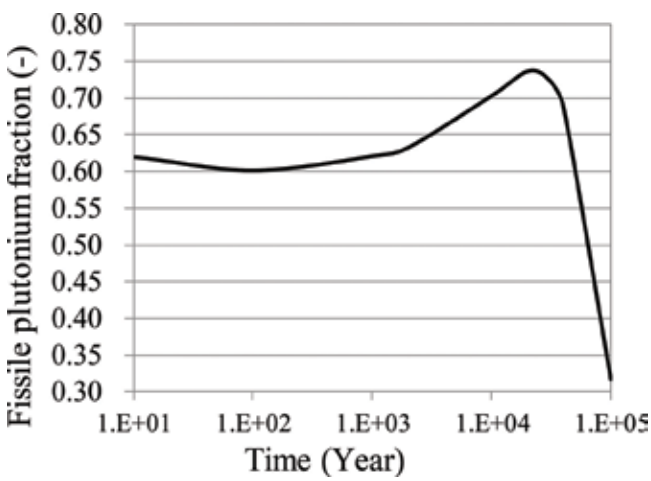

Figure 3. Change on a fraction of fissionable plutonium.

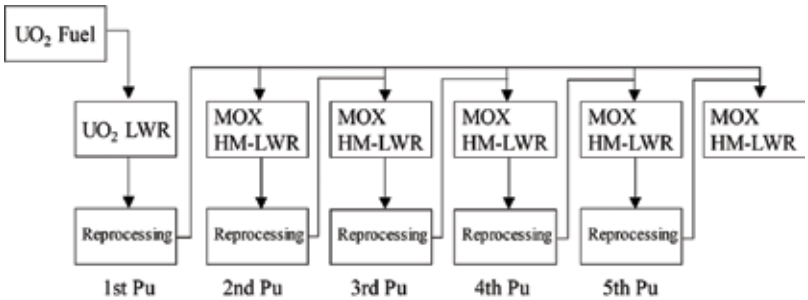

Figure 4. Plutonium multi-recycling scheme for HMLWR.

The residual plutonium can be also used by mixing fresh plutonium to recover the fraction of fissile plutonium. This concept can be realized by high moderation LWR (HMLWR) [20], which is the full mixed oxide (MOX) fuel reactor concept by using exiting advanced boiling water reactors (ABWRs) and advanced pressurized water reactors (APWRs) without changing the plant system. However, the fuel rod diameter is reduced to increase an atomic number ratio of hydrogen to heavy metal (H/HM) value. The H/HM value is changed from 4.9 to 7.0 for BWR concept and from 4.0 to 6.0 for PWR concept. This is the reason why the concept is named "high moderation." The design change concerning to "high moderation" is necessary because the plutonium fuel hardens neutron spectrum.

The concept of plutonium recycling is shown in **Figure 4**. In the recycling process, it has been assumed that UO_2 cores and MOX cores are coexisting and the reprocessing of both UO_2 LWR core and high moderation MOX core provides plutonium. Multi-recycling of Pu in high moderation MOX cores causes degradation of plutonium, while the degradation is prevented by mixing the first plutonium. While repeating this process five times, the plutonium composition is almost saturated and regarded approximately as almost equilibrium state. Using the five times recycled plutonium, the feasibility of reactors was confirmed including safety assessment [20]. This means that multi-recycling of plutonium can be established even in thermal reactor by feeding fresh plutonium from the outside of the cycle.

The Puf consumption rates were evaluated for equilibrium state 39 and 33%, respectively, for the BWR and PWR concept. Those correspond to conversion ratio and/or residual ratio of 0.61 and 0.67, respectively. Here, the conversion ratio is presented by 0.6. With the plutonium consumption of HMLWR, the duration period increases 2.5 times, which can be evaluated as the sum of the infinite geometric series with the ratio of 0.6.

4. Economics of electricity generation

4.1. Recovery cost of uranium resources

For the economic electricity generation, it is preferable that uranium recovery cost is cheaper. With the recent price increase in the market, the highest cost category of <260 $/kgU for conventional uranium resources is added to Red Book 2009 [21]. On the other hand, the recovery cost of unconventional uranium is higher than 260 $/kgU as mentioned in Section 3.1.

Therefore, the cost of 260 $/kgU is considered as a criterion to determine whether a resource can be recovered economically or not.

Figure 5 shows the market price of uranium in the past decade [22]. The price increased abruptly to over 300 $/kgU in June 2007. However, this is a spot price that was not directly employed in trading. Generally, uranium is traded at its forward price. The average price of uranium purchased by owners and operators of US civilian NPP was 120 $/kgU (46.16 $/lb$U_3O_8$) in 2014 [23]. As shown in **Figure 6** [23], the price increased slowly from 2004, and the sharp increase in 2007 was related to the spot market price. In the present study, the current trading price of 120 $/kgU is employed as representative uranium price of conventional resources.

In general, it is believed that unconventional uranium resources such as uranium from seawater are difficult to recover economically. However, an effective recovery method based on a new type of polymer braid has been developed at Japan Atomic Energy Agency (JAEA) [17]. The uranium concentration of 3.3 ppb in seawater is extremely low, but the economic recovery can be achieved with the advantage of efficient absorbents synthesized by radiation-induced graft polymerization and an ocean current. This method can compensate for the difficulty in recovery from low concentration solution. The economic recovery was proved by evaluation with a detailed system design based on the ability to recover confirmed by experiment.

About 1.5 gU/kg adsorbent of uranium was successfully recovered from seawater in Okinawa over a 30-day period. From these tests and trials, the potential cost of uranium recovery, considering a scaled-up annual recovery of approximately 1200 tU/year, was evaluated. The cost is composed of adsorbent production (69%), uranium recovery (29%), and elution and purification (2%). In this estimation, six repeated soaking cycles are assumed. To realize the economic recovery, the duration of absorbent is important because the cost mainly depends on adsorbent production. The realistically achievable cost with current technology using braids with 18 repeated soaking cycles is 208 $/kgU with the exchange rate of 120 yen/$ [17]. In the future, a more reasonable cost of 110 $/kgU [17] can be realized using braids with 60 repeated soaking cycles.

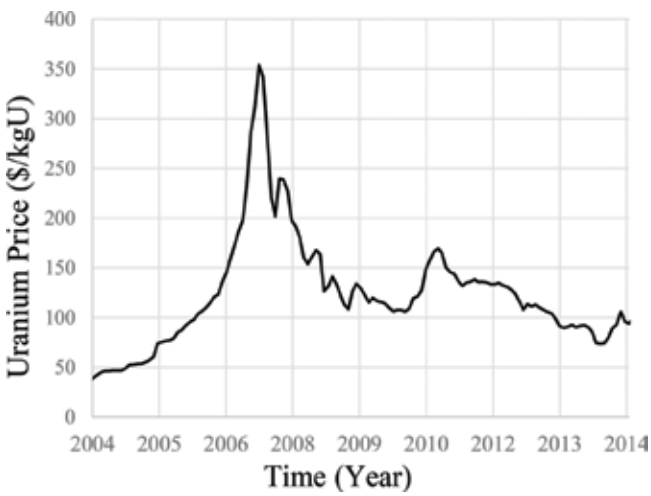

Figure 5. Spot market price of uranium.

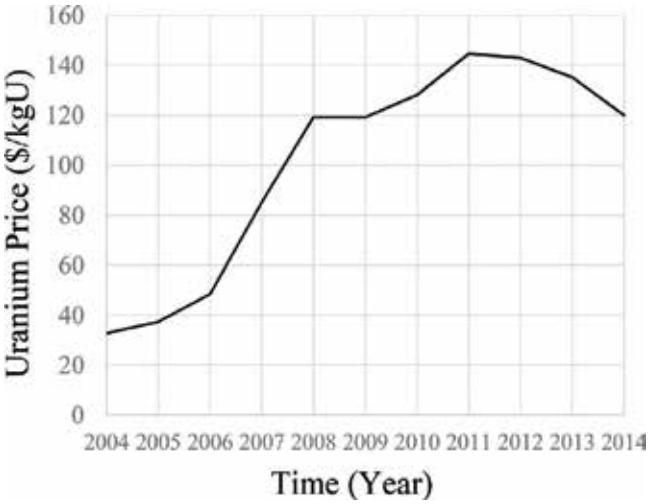

Figure 6. Weighed average price of uranium purchased by owners and operators of US civilian NPPs [23].

The seawater uranium can be extracted economically even by current technology with the cost of 208 $/kgU, which is lower than the criteria of 260 $/kgU. However, the cost is higher than the trading price of 120 $/kgU, even though the lower cost of 110 $/kgU can be achieved in the future. As a result, it is concluded that the cost of seawater uranium with current technology itself is not reasonable even though seawater uranium can be considered as economically recoverable resources.

4.2. Electricity generation cost using seawater uranium recovery cost of uranium resources

The cost of seawater uranium recovered with current technology is not sufficiently low. However, the economy of electricity generation should be assessed not for uranium purchase cost but for the entire cost. In this section, characteristics of electricity generation cost for NPG and the cost with seawater uranium are discussed.

The electricity generation costs of LWR were evaluated with conventional uranium and seawater uranium in Ref. [24] reflecting on the latest condition investigated by the cabinet of Japan [25]. The cost of LWR was evaluated assuming the PWR plant with electric power (gross) of 1300 MWe. In addition, the costs of HTGR were evaluated as well. That is evaluated based on a gas turbine high-temperature reactor 300 (GTHTR300) [26] designed by JAEA as a helium-cooled and graphite-moderated commercial scale HTGR with 600 MWt thermal power and 850°C outlet coolant temperature. The GTHTR300 is combined with four reactor units in a plant. Total thermal power of the plant is 2400 MWt, and gross electric power is 1100 MWe.

The cost of HTGR is cheaper than LWRs due to the cheaper construction cost and higher thermal efficiency of 45.6% [26] than LWRs of approximately 33%. The construction costs are compered in **Figure 7**. The cost of HTGR, only for the reactor component, is larger than that of LWR due to the lower power density design to offer higher levels of safety. Other parts of

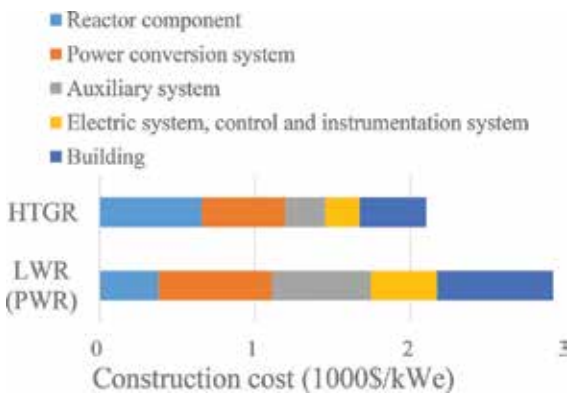

Figure 7. Construction cost of HTGR and LWR.

construction costs of HTGR are cheaper than those of LWR because of the simple direct gas turbine system and rationalization of auxiliary system by modularization. For power conversion system, the direct gas turbine system of HTGR is more compact than the water and steam systems of LWR. The auxiliary system is also more compact for direct gas turbine system. Therefore, the electric system, control and instrumentation system are also reduced for direct gas turbine system. Finally, the volume of buildings is also small for HTGR.

The electricity generation cost is composed of capital cost, operation cost, fuel cost, and social cost. For NPP, the capital cost consists of depreciation cost, interest cost, fixed property tax, and decommissioning cost. The operation cost consists of maintenance cost, miscellaneous cost, personnel cost, head office cost, and tax. The fuel cost consists of each part of the nuclear fuel cycle cost, which includes uranium purchase cost, conversion cost, enrichment cost, fuel fabrication cost, spent fuel storage cost, reprocessing cost, and waste disposal cost. These costs are the sum of yearly costs converted to present values and normalized by the electricity power generation. After the Fukushima Daiichi nuclear power plant disaster, social cost, which includes political cost, compensation cost, and environmental cost, is considered as a part of the electricity generation cost. Environmental cost is required only for the energy source that releases CO_2 gas.

To understand the characteristics, the cost fractions of the NPP are compared with those of a coal-fired power plant (CFPP), which has the largest electricity generation capacity in the world, as shown in **Figure 8**. As electricity generation cost for NPP, LWR cost with conventional uranium is employed. The CFPP cost is estimated by the Japanese cabinet secretariat by assuming a plant with electricity generation capacity of 750 MWe [25]. The cost for NPP consists of capital cost (25.8%), operation cost (32.2%), fuel cost (23.9%), and social cost (18.0%). The cost for CFPP consists of capital cost (15.2%), operation cost (13.5%), fuel cost (45.2%), and social cost (26.1%). The fraction of fuel cost of NPP is less than that of CFPP, which uses fossil fuel. Moreover, most of the fuel cost (38.5%) was spent on coal purchase. On the contrary, the uranium purchase cost for NPP is merely 4.0% of the entire cost because of the proportion of uranium purchase cost for NPP. The fuel cost in NPP consists of several categories from front-end to back-end as listed in **Table 1**, and the fraction of uranium purchase cost in the entire fuel cost is a small value of 16.9%. This is different from fossil fuel power generation, which directly obtains energy from the fuel without fabrication.

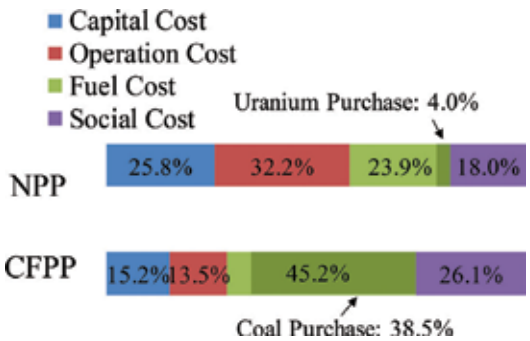

Figure 8. Fraction of electricity generation by NPP and CFPP.

The evaluated cost of the fuel and total electricity generation are listed in **Tables 2** and **3**. The fuel costs increase by approximately 10% by employing seawater uranium for both LWR and HTGR. For electricity generation cost, increases of approximately 3% are observed for LWR and HTGR due to the small fraction of uranium purchase cost as described above. The cost of LWR increases mere 0.21 cents/kWh, from 7.34 to 7.55 cents/kWh, by using seawater uranium. Even with seawater uranium, the cost of HTGR is cheaper than the existing LWR with conventional uranium.

4.3. Electricity generation cost for various fuel cycle schemes

To discuss electricity cost with plutonium utilization including FBR, the cost evaluated by partitioning and transmutation (P&T) working group of OECD/NEA [27] is summarized as follows. In addition, significance of P&T is discussed later because it is said that P&T is an advantage of FR including FBR and accelerator-driven system (ADS). In the report, seven fuel cycle schemes are compared. The schemes are listed as follows. Basically, LWRs mainly generate electricity by using uranium except for the seventh scheme. They are (1) LWR once-through, (2) plutonium burning by LWRMOX, (3) TRU burning in FR, (4) TRU burning in ADS, (5) TRU burning in LWRMOX and ADS, (6) double strata, and (7) closed cycle by FBR, respectively.

	Fraction (%)
Uranium purchase	16.9
Conversion	1.2
Enrichment	25.6
Fabrication	14.5
Storage	2.3
Reprocessing	26.2
Waste disposal	13.4

Table 1. Fraction of NPP fuel cost.

	LWR	LWR	HTGR	HTGR
		(S U*)		(S U)
Uranium purchase	0.29	0.51	0.29	0.50
Conversion	0.02	0.02	0.02	0.02
Enrichment	0.44	0.44	0.55	0.55
Fabrication	0.25	0.25	0.45	0.45
Storage	0.04	0.04	0.02	0.02
Reprocessing	0.45	0.45	0.34	0.34
Waste disposal	0.23	0.23	0.18	0.18
Total	1.71	1.93	1.85	2.06

*SU stands for seawater uranium.

Table 2. Fuel cost (cents/kWh).

	LWR LF*=80%	LWR LF =80%	HTGR LF = 80%	HTGR LF = 80%	HTGR LF = 90%	HTGR LF = 90%
		(SU**)		(SU)		(SU)
Capital cost	1.91	1.91	1.63	1.63	1.44	1.44
Operation cost	2.38	2.37	1.63	1.63	1.38	1.38
Fuel cost	1.71	1.93	1.85	2.06	1.85	2.06
Social cost	1.33	1.33	1.33	1.33	1.19	1.19
Total cost	7.34	7.55	6.43	6.64	5.86	6.07

*LF stands for load factor.

**SU stands for seawater uranium.

Table 3. Electricity generation cost (cents/kWh).

The electricity generation costs are listed in **Table 4**. The cheaper option is the once-through option of LWR. The cost of the second scheme of plutonium burning with MOX, where the FR is ignorable, is also cheap. Plutonium utilization in thermal reactor is not problematic from the viewpoint of electricity generation cost. The seventh scheme of multi-recycling by FBR shows the highest cost. That is increased by approximately 40% compared with the cost of LWR. The cost increase is mainly caused by fuel fabrication and reprocessing including MA.

Fuel cycle scheme	1	2	3	4	5	6	7
Electricity generation cost (cents/kWh)	3.80	4.07	4.24	5.35	4.94	4.42	5.69

Table 4. Electricity generation cost for each fuel cycle scheme.

http://dx.doi.org/10.5772/intechopen.72647

5. Energy security

5.1. Energy security of uranium resources

The accessibility is important from the viewpoint of energy security. Accessibility should be discussed from the viewpoint of geography and concession. The resources should be distributed widely from the viewpoint of geography, and the concession to obtain the resources should be also ensured from the viewpoint both of economy and politics.

Figure 9 shows distribution of identified resources of conventional uranium [15]. The top three countries Australia, Kazakhstan, and the Russian Federation occupy about half of the resources of the world. By the concentration of uranium resources, the risk of damage to sustainable energy supply increases owing to natural disasters, political instability, etc. In fact, uranium price in 2007 shown in **Figure 2** soared due to the catastrophic water inflow in Cigar Lake Mine in Canada [28], even though increase of uranium demand in China and India is also affected [15]. If the production of several mines in a certain region would be damaged simultaneously by large-scale disasters or political instability, the energy sustainability cannot be achieved. It is concluded that the conventional uranium resources have a problem of geography from the viewpoint of energy security.

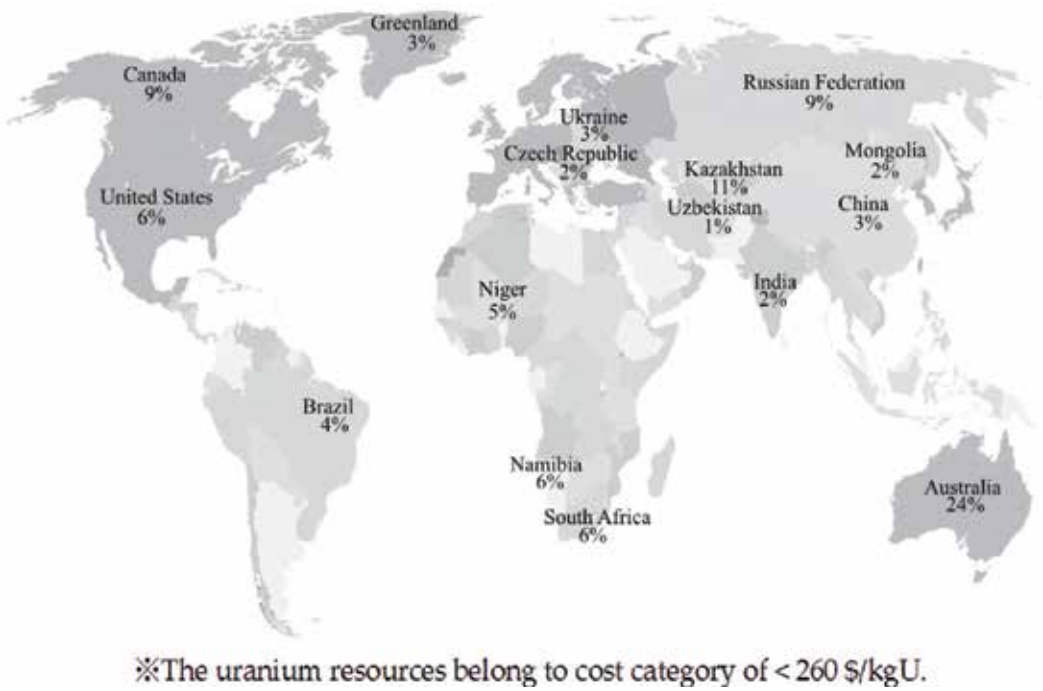

Figure 9. Global distribution of identified resources.

Moreover, the uranium requirement exceeds the production in the recent two decades as shown in **Figure 10** [15]. The mass balance has now been achieved by the stock until 1990. In addition, the 1993 US-Russia Federation highly enriched uranium (HEU) purchase agreement was terminated in 2014 [15]. According to this agreement, the Russian Federation converts the 500 t of HEU from nuclear warheads to low enriched uranium (LEU) over 20 years from 1993 to 2013. As early as June 2006, the Russian Federation indicated that the HEU agreement will not be renewed when the initial agreement expires in 2013.

In this context, to purchase the uranium securely, mining interest of uranium ore, that is, concession, should be obtained by investing in the exploration and development of the mine. Here, I discuss Japanese case as representative country, which is not uranium-producing countries and does not have enough concession to satisfy the request. Many countries can be applied the similar condition as Japan. In Japan, requirement of uranium is approximately 8000 tU (8091 tU), and the production from own concession is 663 tU in 2007 [29]. The fraction is only 8.2%. Not only companies but also governments invest in the exploration and development of the mine to obtain the uranium concession. **Table 5** [29] lists the uranium concession owned by Japanese companies for mine under operation and development in 2009. Even though all mines under development will start the operation, the production can fill only half of the requirement. It is difficult to obtain the concession corresponding to the entire requirement. It is concluded that conventional uranium resources also have a problem of concession.

To realize the ultimate energy security, the resources should be recovered within the country. Countries facing the sea can utilize seawater uranium as domestic resources. The recovery process of seawater uranium is simpler than mine uranium as shown in **Figure 11** [17]. The extraction process of the recovery system consists only of elution in acid. It can be easy to introduce without any innovative technology. The transportation of absorbent is also realistic because the concentration of uranium in the medium is on the same degree of that in uranium ore. Moreover, the radioactive tailings, which may pollute the environment, are never generated unlike the uranium from mine. The amount of the production is large enough to satisfy the requirement if the current of the sea exists in exclusive economic zone (EEZ). The seawater uranium is effectively recovered with ocean current. The recovery system with capacity of

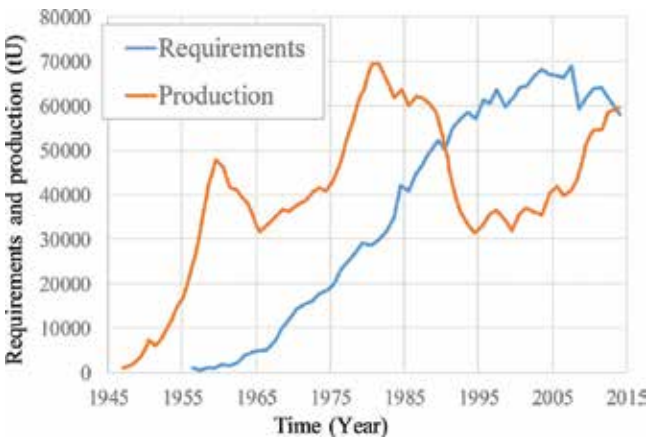

Figure 10. Annual world uranium requirements and production.

Country	Mine	Company	Concession (%)	Condition
Niger	Akouta	Overseas Uranium Resources Development Co.	25	Under operation
Canada	McClean Lake	Overseas Uranium Resources Development Co.	7.5	Under operation
Kazakhstan	West Mynkuduk	Kansai Electric Power Co.	10	Under operation
		Sumitomo Co.	25	Under operation
Canada	Cigar Lake	Tokyo Electric Power Co.	5	Under development
		Idemitsu Kosan Co.	7.9	
Kazakhstan	Kharasan 1–2	Marubeni Co.	13	Under development
		Tokyo Electric Power Co.	12	
		Toshiba Co.	9	
		Chubu Electric Power Co.	4	
		Tohoku Electric Power Co.	2	
Australia	Kintyre	Mitsubishi Co.	30	Under development
	Honeymoon	Mitsui & Co.	49	Under development

Table 5. Uranium concession owned by Japanese companies.

1200 tU/year requires the ocean area of 134 km^2 with a proper current. The Kuroshio Current is proper in Japan, and the ocean area of 6000 km^2 is available to recover the uranium without a conflict of the right of fishing. Annual uranium production of 53,731 tU/year is expected from this area. This is approximately 6.6 times as much as the requirement of 8091 tU in Japan, and it can occupy 87% of the requirement in the world.

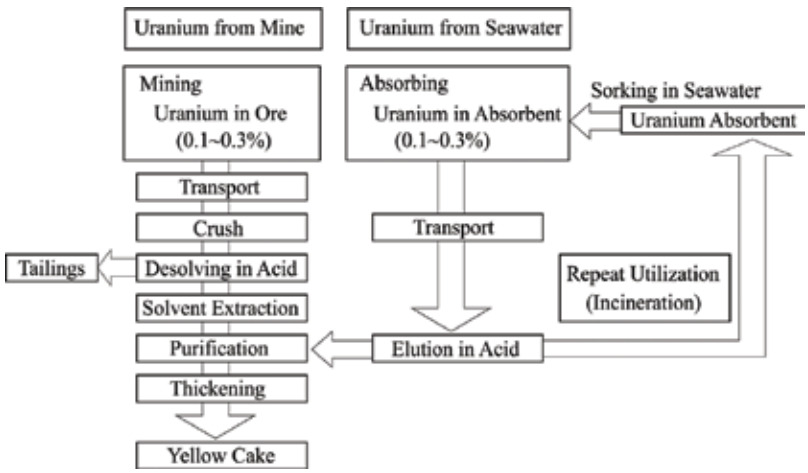

Figure 11. Process of uranium recovery.

Thus, the problems of geography and concession from the viewpoint of energy security can be solved by using seawater uranium. Then, the seawater uranium should be utilized regardless of the exhaustion of conventional uranium.

5.2. Energy security of plutonium utilization

Plutonium composition is depending on the condition of fresh fuel composition, burnup characteristics, and storage period before and after reprocessing. Plutonium composition is always fluctuated. Therefore, in Japan, fuel composition of FBR is managed by equivalent fissile coefficient [30]. The definition is as follows:

$$y = \nu\sigma_f - \sigma_{(n,\gamma)} \tag{2}$$

$$\eta_i = y_i / y_{^{239}Pu} \tag{3}$$

where y is the equivalent fissile value (cm^{-2}), $\nu\sigma_f$ is the microscopic production cross section (cm^{-2}), $\sigma_{(n,\gamma)}$ is the microscopic radioactive capture cross section (cm^{-2}), y_i is the equivalent fissile value of ith nuclide (cm^{-2}), $y_{^{239}Pu}$ is the equivalent fissile value of ^{239}Pu (cm^{-2}), and η_i is the equivalent fissile coefficient ith nuclide (−).

To reserve the product of fuel composition and the equivalent fissile coefficients, plutonium enrichment is determined. However, if fuel loading and/or operation of reactor would be significantly delayed, the fuel should be refabricated and reloaded because of the change on reactivity worth due to the decay of ^{241}Pu, whose half-life is 14.4 years, to ^{241}Am. In Monju, where sodium leakage accident occurred on December 1995 and start-up test is performed on May 2010, the depletion of criticality was observed [31] in the test. After the test, fuel reloading was performed on August 2010 to compensate the reactivity worth. The resilience of fuel cycle system with plutonium is weaker than that of uranium.

Moreover, there is a threat that the spent fuel would be seized in FBR cycle. In general, the Puf ratio of spent fuel is around 60% for LWR and FBR. However, that of FBR blanket is over 90%, that is, weapon-grade plutonium. In this context, the concept of protected plutonium production (PPP) [32] is proposed as an option. By addition of ^{237}Np and/or ^{241}Am, the Puf ratio can be reduced, and the dose rate of spent fuel can increase due to the converted ^{238}Pu in this concept. However, it should be noted that the doping MAs in fuel make working environment severe.

6. Environmental burden and significance of P&T

6.1. Geological disposal and safety

Along with electricity generation, radioactive wastes are generated. Especially, high-level radioactive wastes (HLWs) will be disposed in a deep geological repository. The HLWs, which are spent fuels for direct disposal and vitrified wastes for disposal with reprocessing, are contained into steel canisters and disposed by surrounding buffer material, which delays

http://dx.doi.org/10.5772/intechopen.72647

migration of radioactive nuclides and is made of bentonite. The waste package, canister, and buffer material are called engineered barrier system (EBS) from the viewpoint of containment and delayed function of radioactive nuclides.

The safety analysis of the geological repository [33] assumes the mechanism as shown in **Figure 12**:

- The canister and waste package failed by corrosion, and the radioactive nuclides dissolve in groundwater.
- The radioactive nuclides migrate through the host rock via groundwater.
- The radioactive nuclides migrate to aquifer through fault.
- The radioactive nuclides flow into river and diffuse into environment.
- The radioactive nuclides are exposed to the public.

Thus, host rock in repository works as barrier as well and is called natural geological barrier. The safety of geological repository is assessed by public exposure by assuming migration of radioactive nuclides due to the corrosion and failure of waste packages.

Moreover, transuranic (TRU) waste [34], which is categorized as low-level radioactive waste (LLW), is also generated when spent fuel is reprocessed and disposed. The dose of public exposure is evaluated for representative geological repository design for LWR wastes as shown in **Figures 13** and **14**, respectively, for HLW and TRU waste.

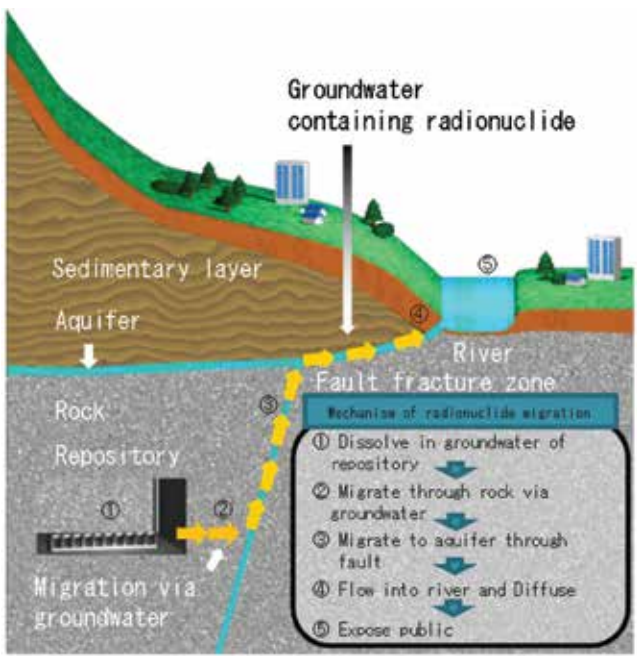

Figure 12. Process of public exposure.

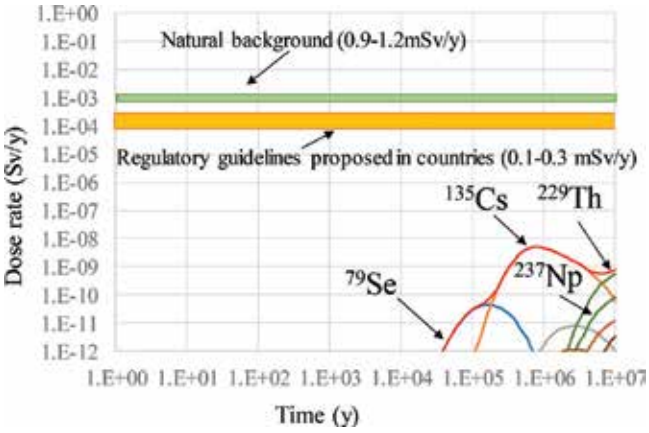

Figure 13. Public exposure from HLW [33].

Basically, the dose rate is limited by the guideline, which is deployed at approximately one order of magnitude lower than the level of natural background. The peak from HLW is composed of ^{135}Cs and four to five orders of magnitude lower than the guideline. The peak from TRU waste is composed of ^{129}I and two to three orders of magnitude lower than the guideline. In addition, the dose rate of HLW for direct disposal of LWR spent fuel was also reported [35]. The peak is composed of ^{14}C and one to two orders of magnitude lower than the guideline. The safety guideline is satisfied enough for exiting LWR waste disposal plans. Especially for HLW disposal with reprocessing, where MA transmutation has been often researched, the safety margin is huge.

With MA transmutation, the electricity generation cost increases as described in Section 4.2. "As low as reasonably achievable (ALARA) principal" [36], which was revised from as low as practical (ALAP), is known as radiation safety policy. Obviously, the necessity to reduce the public exposure is poor because of the huge safety margin. In this situation, the nuclear transmutation with significant cost increases against the ALARA principal. If the nuclear transmutation is plant, we should judge the "reasonability" by considering the benefit and cost.

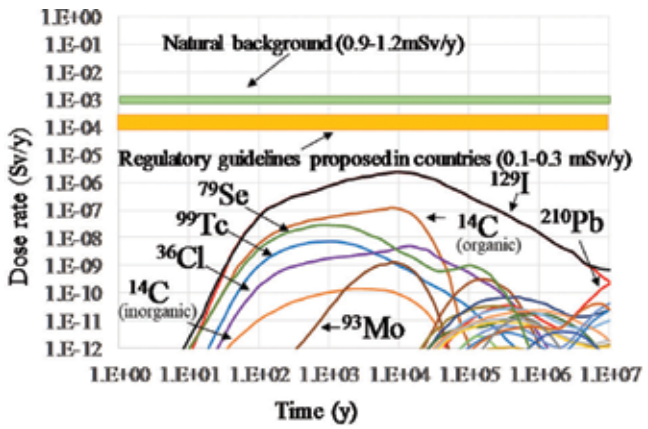

Figure 14. Public exposure from TRU waste [34].

6.2. Potential toxicity and significance of P&T

Potential toxicity is often used as a hazard index to assess environmental burden. Therefore, it is set up for the objective of nuclear transmutation to reduce the potential toxicity. The definition of potential toxicity is dose of internal exposure by ingestion when all radioactive nuclides are intaken. It is believed that the dose should be lower than that of natural uranium required for the fuel fabrication.

The potential toxicity of LWR spent fuel is shown in **Figure 15** for each element. The burnup is 45 GWd/t, and the enrichment is 4.5 wt%. To fabricate fuel of 1 t with the enrichment of 4.5 wt%, natural uranium of 9 t is necessary. The toxicity of uranium and plutonium, that is almost composed only of plutoniums, needs 100,000 years to decay to the natural uranium level. With reprocessing, uranium and plutonium are recovered, and the toxicity is not problematic. Next, americium needs 2000 years of cooling. If americium is converted by P&T, the cooling time can be reduced to 300 years, by which the dose of FPs decays lower than natural uranium.

From the viewpoint of the potential toxicity reduction under the natural uranium level, it is not necessary for neptunium and curium to convert to FPs. The FPs are composed of long-lived FPs (LLFPs) and other FPs. The toxicity of LLFPs around 1.0×10^3 Sv/tIHM is observed from 1 to 100,000 years. The toxicity of LLFPs is not problematic as well. In addition, the nuclides contributed to the toxicity are different from that contributed to the public exposure described in the previous section. From this comparison, it is found that the actual public exposure strongly depends on mobility characteristics of the nuclides compering with the inventory of the toxicity. Furthermore, the assumption of intaking all radioactive nuclides is not reasonable as a hazard index. In this context, an alternative index of "environmental impact" [37] is proposed by a specialist of geological disposal safety. That is defined as toxicity flowed out from the EBS.

The potential toxicity has also attracted a lot of attention after the Fukushima Daiichi accident in Japan to reconsider the significance of the utilization of nuclear technology. The graph of the potential toxicity is often shown even in television report. Then, nuclear conversion by

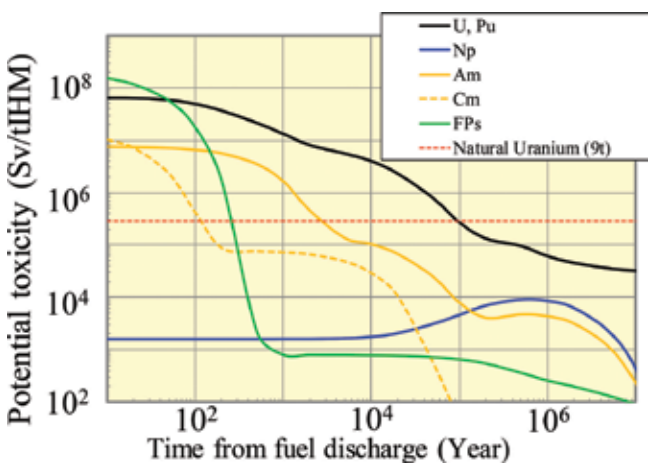

Figure 15. Potential toxicity of LWR spent fuel.

ADS also attracted a lot of attention. In this situation, an expert committee of Atomic Energy Society of Japan (AESJ) published the report for direct disposal [35]. In this report, the safety of geological disposal and public opinion were researched and discussed. It is emphasized that the potential toxicity cannot be the index directly to assess the safety, and the safety of geological disposal should be assessed by public exposure. The expert committee states its own view that the safety of geological disposal tends to be assessed by the potential toxicity in the recent society because it is easy to understand intuitively.

If the potential toxicity would be gotten public support as the hazard index and all MAs and LLFPs would be transmutated, the waste should be managed at least 300 years. Furthermore, if all radioactive nuclides would be transmutated to stable nuclides, the waste should be managed due to the toxicity of heavy metal.

6.3. Waste volume reduction and significance of P&T

P&T is expected to reduce waste volume and repository footprint [38]. However, partitioning and/or transmutation cannot reduce the inventory of waste nuclides itself. P&T reduces waste package volume by conquering the technical problem of vitrified waste fabrication [39].

For vitrified waste fabrication, there are limitations for heat generation (decay heat), waste content (FPs and MAs), platinum group metal (PGM) content, and molybdenum oxide content. The heat generation is limited to remain temperature of waste lower than 500°C during storage to prevent the phase transmutations such as crystallization and liquid-liquid phase separation at elevated temperatures. The waste content is limited to remain characteristics of glass for the confinement of the waste. The PGM content is limited not to shorten the lifetime of liquid-fed ceramic melter (LFCM). The molybdenum oxide content is limited to prevent the formation of molybdenum-rich phase, which is called yellow phase and degrades chemical durability of the vitrified form.

By partitioning [40], the PGM is recovered and used as resources. Strontium and cesium, whose decay heat is dominant, are partitioned and converted to Sr-Cs calcined waste. By employing high-waste-loading glass [41], high content of waste and molybdenum can be contained into the vitrified form.

To confirm the reduction of waste volume by P&T, numbers of waste package generation of four cycle schemes for LWR are compared as shown in **Figure 16**. The schemes are non-P&T, only transmutation, only partitioning, and P&T schemes. To reduce the number, partitioning is the most effective. The effect of high-waste-loading glass is dominant. The P&T scheme generates more waste packages than the partitioning scheme.

However, the partitioning is optimized to minimize the waste package generation and not optimized to minimize the repository footprint because the heat generation from Sr-Cs calcined waste is problematic to dispose. The repository footprint is mainly determined by heat generation from the waste. The buffer material of bentonite should be remained under the temperature of 100°C. The waste package pitches for disposal determined by the limitation of the buffer material temperature. In other words, the waste package with lower heat generation can realize lower footprint. Therefore, to dispose the Sr-Cs calcined waste, long cooling time is necessary.

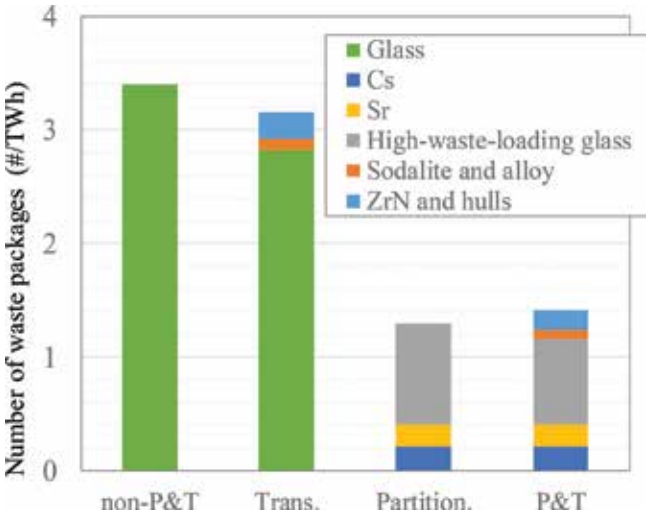

Figure 16. Number of waste packages per electricity generation [38].

There are two representative scenarios for P&T scheme [42]. Those are mainly optimized for the cooling time of Sr-Cs calcined waste. One hundred thirty and 300 years of cooling scenarios are employed. The specifications for LWR-SF (45 GWd/t) of 32,000 tIHM are listed in **Table 6**. Those are evaluated based on Ref. [38]. The P&T with 130 years of cooling can realize

	Cooling time (y)	Configuration	No. of package	Footprint (m^2)
Non-P&T				
Glass	50	V_0	40,000	1,776,000
P&T with 130 years of cooling				
HWL glass	5	V_1	8300	184,260
Sr-Cs	130	V_0	5100	226,440
Total			13,400	410,700
P&T with 300 years of cooling				
HWL glass	45	C	8300	7885
Sr-Cs	300	C	5100	4845
Total			13,400	12,730
Partitioning				
HWL glass	85	V_0	8300	368,520
Sr-Cs	150	V_1	5100	113,220
Total			13,400	481,740

Footprint of emplacement configuration V_0 is 44.4 m^2/cani., V_1 is 22.2 m^2/cani., and C is 0.95 m^2/cani [38].

Table 6. Specifications of disposal for LWR-SF (45 GWd/t) of 32,000 tIHM.

1/4 of footprint compared with that of non-P&T. With 300 years of cooling, 1/100 of footprint can be realized. However, only the partitioning can also realize 1/4 of footprint with 150 years of cooling for Sr-Cs calcined waste and 85 years of cooling for the high-waste-loading glass. The waste package including MAs needs the cooling time to decay ^{244}Cm, whose half-life is 18.1 years. For the rest decay heat, ^{241}Am, whose half-life is 433 years, is dominant and difficult to reduce by cooling. To realize more compact disposal, the transmutation is necessary.

The technology of partitioning is already demonstrated [40, 41]. On the other hand, transmutation should develop many innovative technologies concerning to neutron source by spallation reaction, Pb-Bi FR core, and pyro reprocessing for ADS and reactor core and advanced reprocessing for FBR. The partitioning technology without transmutation is preferable as early introduction option to suit uranium utilization.

6.4. Environmental burden with P&T

As described in the previous section, the safety of waste disposal should not be assessed by the potential toxicity. However, reduction of the potential toxicity is one of the objectives to develop fuel cycle system with FBR in Japan. All TRU nuclide is planned to recycled with the recovery ratio of 99.9% [43] to shorten the cooling time needs to decay the toxicity under the natural uranium level within 300 years.

However, with the recovery, the public dose from MAs would not be reduced. The MAs in 4N+1 decay series are problematic. ^{229}Th is the daughter of ^{237}Np, and other MAs in 4N+1 decay series, that is, ^{241}Pu, ^{241}Am, and ^{245}Cm, are decay to ^{237}Np. These nuclides should be recovered with high recovery ratio. It is said that the recovery ratio should be higher than 99.998% [44]. The relations of the recovery ratio to the molar flux of radioactive nuclide from EBS are shown in **Figure 17**. ^{135}Cs can be reduced with higher recovery ratio because that

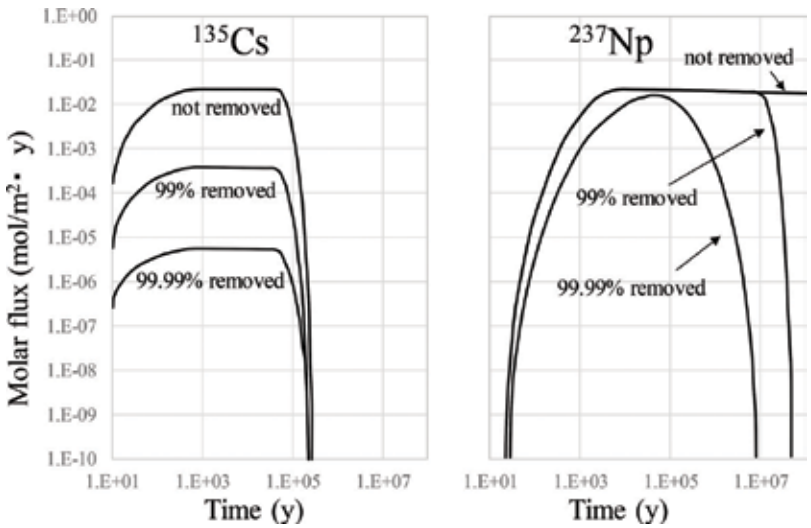

Figure 17. Relation of recovery ratio to the molar flux of radioactive nuclide from EBS [44].

			High decontamination				Low decontamination			
			MOX	MOX +Np	MOX +Np + Am	MOX +Np + Am + Cm	MOX	MOX +Np	MOX +Np + Am	MOX +Np + Am + Cm
FBR-MOX		Whole body	0.7	0.7	9	60	1000	1000	2000	2000
(114.9 GWd/t)		Hand	0.1	0.1	3	9	300	300	300	300
LWR-UOX	Standard burnup	Whole body	0.8	0.9	3	40	600	600	700	700
	(BWR 45 GWd/t)	Hand	0.2	0.2	3	7	100	100	100	100
	High burnup	Whole body	1	1	4	60	700	700	900	1000
	(PWR 60 GWd/t)	Hand	0.2	0.3	4	10	200	200	200	200
LWR-MOX	Standard burnup	Whole body	2	2	8	100	600	600	700	800
	(BWR 45 GWd/t)	Hand	0.3	0.43	8	20	100	100	100	200
	High burnup	Whole body	2	2	10	400	700	700	900	1000
	(PWR 60 GWd/t)	Hand	0.4	0.6	20	50	200	200	200	200

*The dose rates are normalized by the dose in representative fuel fabrication with spent fuel from Fugen [43].

**Dose rate lower than 1 for the whole body and hand: fabrication in GB is possible with the current technology.

Dose rate lower than two for the whole body and hand: fabrication in GB is possible with the current technology improving the process.

Dose rate lower than 10 for the whole body and hand: automation is necessary for fabrication in GB.

Dose rate higher than 10 for the whole body and hand: fabrication in GB is impossible [43].

Table 7. Feasibility of fuel fabrication in globe box [43].

http://dx.doi.org/10.5772/intechopen.72647

dissolved in groundwater congruently with glass form dissolution. On the other hand, the concentration of ^{237}Np is limited by solubility. Then, the inventory of ^{237}Np should be reduced lower than the amount corresponding to the solubility. The MA recycling may not contribute to reduce public dose with the recovery ratio of 99.9%.

Furthermore, MA recycling increases working environment burden like the concept of PPP. MA recycling makes difficulty not only for spent fuel but also for fuel fabrication. **Table 7** lists the feasibility of fuel fabrication in globe box (GB) [43]. MOX fuel and neptunium-doped MOX fuel with high decontamination can be fabricated in GB with the current technology. However, for americium- and/or curium-doped fuel, automation is necessary, or fuel fabrication in GB is impossible. Fuel with low decontamination cannot be fabricated in GB. In this context, there is the opinion that MA recycling should not be performed [45]. For nuclear proliferation, safeguard should be enhanced by increasing the transparency of society instead of MA recycling [45].

7. Summary

Safety and economics of uranium utilization for nuclear power generation were investigated and discussed. To compare the alternative candidate of plutonium breeding by FBRs, P&T technology, one of the advantages of FBRs, was also discussed.

For the safety of reactor, to remain inherent safety feature for "shutdown" function, uranium utilization in thermal reactor is necessary. The safety feature is lost in fast reactor. The core performance, breeding ability, and economy are related to a transaction in fast reactor.

The amount of conventional uranium corresponds to consumption of approximately 290 years, and it is not much enough to sustain the energy supply eternally. On the contrary, the amount of seawater uranium, which is 4.5 billion tU corresponding to 72,000 years and 4.5 trillion tU including the uranium at the surface of the seafloor corresponding to 72 million years, is almost inexhaustible.

Furthermore, by utilization plutonium in spent fuel in thermal reactor, the duration period of uranium can be increased. By once-through utilization, that can be increased to 1.6 times. By multi-recycling, which can by HMLWR, that can be increased to 2.5 times.

With seawater uranium, the electricity generation cost increases by mere 3%. With HTGR, the cost with seawater uranium is cheaper than the cost of existing LWR with conventional uranium. The cost of FBR with multi-recycling increases by 40% compared with the cost of LWR.

From the viewpoint of energy security, conventional uranium has problems, i.e., geology and concession. Therefore, seawater uranium should be recovered before exhaustion of conventional uranium from the viewpoint of energy security because the uranium mining concession, which is necessary to supply the uranium resources sustainably, is difficult to fulfill the entire requirement. Moreover, seawater uranium should be recovered by the countries facing ocean.

Plutonium utilization has problems of energy security due to the decay of ^{241}Pu. When fuel loading and/or reactor operation would significantly delay, the fuel should be refabricated and reloaded. Moreover, weapon-grade plutonium is generated in the blanket of FBR. There is a threat for the spent fuel to be seized.

For environmental burden, the safety of geologic disposal for existing LWR waste is secured by evaluating public dose with a sufficient margin. However, P&T is planned to reduce the potential toxicity, which the index should not be used for safety assessment. To reduce waste volume, P&T is effective. Only with partitioning, the repository footprint is reduced to 1/4 times. However, transmutation of MAs cannot reduce the public dose with the recovery ratio of 99.9% determined to reduce the potential toxicity. MA recycling with FBR increases the working environmental burden due to the increased dose.

As discussed above, uranium utilization in thermal reactor can achieve safe and sustainable energy supply with acceptable environmental burden.

Author details

Yuji Fukaya

*Address all correspondence to: fukaya.yuji@jaea.go.jp

Japan Atomic Energy Agency, Japan

References

[1] Walter A, Reynolds A. Fast Breeder Reactors. New York: Pergamon Press; 1981. 700 pp

[2] IAEA. Passive Safety Systems and Natural Circulation in Water Cooled Nuclear Power Plants. IAEA-TECDOC-1624, IAEA, Vienna; 2009

[3] Bouteille F, Azarian G, Bittermann D, et al. The EPR overall approach for severe accident mitigation. Nuclear Engineering and Design. 2006;**236**:1465-1470

[4] AESJ. The Fukushima Daiichi Nuclear Accident: Final Report of the AESJ Investigation Committee. Tokyo: Springer; 2015. 560 pp

[5] Ohashi H, Sato H, Tachibana Y, et al. Concept of an inherently-safe high temperature gas-cooled reactor. ICANSE 2011; 14-17 November 2011; Bali; 2011. pp. 50-58

[6] The Cabinet of Japan. Strategic Energy Plan [Internet]. 2014. Available from: http://www.enecho.meti.go.jp/en/category/others/basic_plan/pdf/4th_strategic_energy_plan.pdf [Accessed: 02-10-2017]

[7] Lewis E. Nuclear Power Reactor Safety. New York: John Wiley & Sons inc.; 1977. 648 pp

[8] Massimo L, Physics of High Temperature Reactors. New York: Pergamon Press; 1979. 220 pp

[9] Sun K. Analysis of Advanced Sodium cooled Fast Reactor Core Designs with Improved Safety Characteristics. Swiss Federal Institute of Technology Lausanne (EPFL) doctoral thesis; 2012. N5480

[10] Wade D, Chang Y. The integral fast reactor concept: Physics of operation and safety. Nuclear Science and Engineering. 1988;**100**:507-524

[11] Sackett J. Operation and test experience with EBR-II, the IFR prototype. Progress in Nuclear Energy. 1997;**31**:111-129

[12] Lefèvre JC, Mitchell CH, Hubert G. European fast reactor design. Nuclear Engineering and Design. 1996;**162**:133-143

[13] Fukaya Y, Nakano Y, Okubo T. Study on characteristics of void reactivity coefficients for high-conversion-type Core of FLWR for MA recycling. Journal of Nuclear Science and Technology. 2009;**46**(8):819-830

[14] Matveev VI, Chebeskov AN, Krivitsky IY. Core concept of fast power reactor with zero sodium void reactivity. Proceedings of the Specialists' Meeting on "Passive and Active Safety Features of LMFRs" IWGFR/85; 5-7 November 1991; Oarai; 1991. pp. 206-218

[15] OECD/NEA. Uranium 2014: Resources, Production and Demand: OECD/NEA; NEA No. 7059. 2015. p. 504

[16] OECD/NEA. Forty Years of Uranium Resources, Production and Demand in Perspective: OECD/NEA; NEA No. 6096. 2006. p. 276

[17] Tamada M, Seko N, Kasai N, et al. Cost estimation of uranium recovery from seawater with system of braid type adsorbent. Transactions of the Atomic Energy Society of Japan. 2006;**5**(4):358-363 [in Japanese]

[18] Tamada M, Seko N, Present state and future view of significant metals-recovery from seawater. Isotope News. April 2000;**551**:2-6 [in Japanese]

[19] Duderstadt JJ, Hamilton LJ. Nuclear Reactor Analysis. New York: John Wiley & Sons, Inc.; 1976. p. 650

[20] Kanda R, Yamamoto T, Iwata Y. Effective use of plutonium through its multi-recycling with high moderation LWRs. Proc. Int. Conf. on Advanced Nuclear Power Plants (ICAPP 2002); 9-13 June 2002; Hollywood; 2002. #1054

[21] OECD/NEA. Uranium 2009: Resources, Production and Demand: OECD/NEA; NEA No. 6891. 2010. p. 456

[22] International Monetary Fund. IMF Primary Commodity Prices [Internet]. 2017. Available from: http://www.imf.org/external/np/res/commod/index.aspx [Accessed: 02-10-2017]

[23] U.S. Energy Information Administration. 2014 Uranium Marketing Annual Report: U.S. Department of Energy; 2015. p. 61

[24] Fukaya Y, Goto M. Sustainable and safe energy supply with seawater uranium Fueled HTGR and its economy. Annals of Nuclear Energy. 2017;**99**:19-27

[25] Committee of Electricity Generation Cost Verification. Committee of Electricity Generation Cost Verification Report:19th. Cabinet Secretariat of Japan.; 2011 [in Japanese]

[26] Yan X, Kunitomi K, Nakata T, et al. GTHTR300 design and development. Nuclear Engineering and Design. 2003;**222**:247-262

[27] OECD/NEA. Accelerator Driven Systems (ADS) and Fast Reactors (FR) in Advanced Nuclear Fuel Cycles: OECD/NEA; Technical Report NEA/3109-ADS. 2002. p. 350

[28] Cameco.Co. Cameco 2013 Annual Report Cigar Lake [Internet]. 2013. Available from: https://www.cameco.com/annual_report/2013/mda/operations-development-projects/uranium/development-project/cigar-lake/ [Accessed: 02-10-2017]

[29] Advisory Committee for Natural Resources and Energy. The 3rd Conference on International Strategy Investigation Subcommittee. Ministry of Economy, Trade and Industry, Japan. 2009 [in Japanese]

[30] Nakae N, Ito M, Mishima T, et al. Control of Plutonium Content Using a Concept of Physical Accounting Method for Adjusted Fissile Enrichment. Dounen Gihou; 1986-Jun-70; 1986. pp. 77-81 [in Japanese]

[31] Hazama T, Kitano A, Kishimoto Y. Criticality evaluation for the Monju restart Core. Nuclear Technology. 2012;**179**(2):250-265

[32] Ohnishi T, Koyama S, Shiba T, et al. Protected plutonium production at fast breeder reactor blanket – Chemical analysis of Uranium-238 samples irradiated in the experimental fast reactor Joyo. Progress in Nuclear Energy. 2012;**57**:125-129

[33] JNC. Second Progress Report on Research and Development for the Geological Disposal of HLW in Japan; H12 Project to Establish the Scientific and Technical Basis for HLW Disposal in Japan; Project Overview Report. JNC; JNC TN1410 2000-001; 2000

[34] JAEA, Federation of Electric Power Companies. Second Progress Report on Research and Development for TRU Waste Disposal in Japan -Repository Design, Safety Assessment and Means of Implementation in the Generic Phase-. JAEA; JAEA-Review 2007-010. FEPC TRU-TR2-2007-01; 2007

[35] Atomic Energy Society of Japan. Interim Report of Expert Committee on Social Environment Concerning to Direct Disposal of Spent Fuel [Internet]. 2014. Available from: http://www.aesj.net/document/com-r_shiyouzuminenryou2014_m.pdf [Accessed: 02-10-2017] [in Japanese]

[36] ICRP. ICRP Publication 22, Implications of Commission Recommendations that Doses be kept as Low as Readily Achievable. New York: Pergamon Press; 1973. p. 18

[37] Ahn J. An environmental impact measure for nuclear fuel cycle evaluation. Journal of Nuclear Science and Technology. 2004;**41**(3):296-306

[38] Nishihara K, Nakayama S, Morita Y, et al. Impact of partitioning and transmutation on LWR high-level waste disposal. Journal of Nuclear Science and Technology. 2008;**45**(1):84-97

[39] Inagaki Y, Iwasaki T, Sato S, et al. LWR high burn-up operation and MOX introduction; fuel cycle performance from the viewpoint of waste management. Journal of Nuclear Science and Technology. 2009;**46**(7):677-689

[40] Kubota M, Morita Y. Preliminary assessment on four group partitioning process in JAERI. Proc. Int. Conf. Future Nuclear System (GLOBAL'97); 5-10 October; Yokohama; 1997. Vol. 1. pp. 458-462

[41] Yoneya M, Kawamura K, Igarashi H, et al.. Technical incentive to high-waste-loading process of HLLW. Proc. 5th Int. Conf. on Radioactive Waste Management and Environmental Remediation (ICEM'95); 3-7 September; Berlin; 1995. Vol. 1, pp. 389-393

[42] Oigawa H. Present status and Prospect of transmutation Technology for High-Level Radioactive Waste. Radioisotopes. 2012;**61**(11):571-586 [in Japanese]

[43] JAEA. Target Value of Decontamination Factor for Reprocessing System. Ministry of Economy, Trade and Industry. 2nd FaCT Evaluation Committee [Internet]. 2010. Available from: http://www.meti.go.jp/committee/kenkyukai/energy/fact/002_06_03_00.pdf [Accessed: 2017-10-2] [in Japanese]

[44] Nakayama S, Ahn J. Comments on contributions from partitioning-transmutation to environmental safety of geologic disposal of radioactive waste. Houshyaseihaikibutsukenkyu. 1996;**2**(1-2):27-34 [in Japanese]

[45] Kondo S. Kondo Atomic Energy Commission Chairperson's Overseas Business Trip Report. Atomic Energy Commission [Internet]. 2009. Available from: http://www.aec.go.jp/jicst/NC/iinkai/teirei/siryo2009/siryo36/siryo2-1.pdf [Accessed: 02-10-2017] [in Japanese]

Chapter 3

Shear Zone-Hosted Uranium Deposits of the Bohemian Massif (Central European Variscan Belt)

Miloš René

Additional information is available at the end of the chapter

http://dx.doi.org/10.5772/intechopen.71967

Abstract

The Bohemian Massif hosts a significant quantity of uranium deposits bound by brittle shear zones developed in high-grade metamorphic rocks (Rožná, Okrouhlá Radouň, Zadní Chodov and Dyleň) and/or granites (Vítkov II and Lhota). According to the international atomic energy agency (IAEA) uranium deposits classification, these deposits are classified as metamorphic deposits. For shear zone-hosted uranium mineralisation, the no direct relationship between ore mineralisation and granite bodies is significant. Ore lenses and/or disseminated ore mineralisation form the shear zone-hosted uranium deposits. The host rocks of these deposits are transformed in aceites. Aceites are defined as low-temperature alkaline metasomatic rocks, which are closely associated with uranium mineralisation. Complex coffinite-uraninite or coffinite-uraninite-brannerite assemblages form the shear zone mineralisation with predominance coffinite about uraninite.

Keywords: uranium, shear zone, aceite, coffinite, uraninite, brannerite, Bohemian Massif

1. Introduction

The Bohemian Massif as part of the Central European Variscan belt hosts a high quantity of uranium mineralisation [1, 2]. The shear zone-hosted uranium mineralisation is recently classified as metamorphic uranium deposits (e.g., Ace Fay, Canada) [3]. In the Bohemian Massif, the Rožná, Olší, Okrouhlá Radouň and Zadní Chodov ore deposits in the high-grade metamorphic rocks of the Moldanubian Zone and the Vítkov II and Lhota ore deposits in granitoids of the Bor pluton represent this group of uranium deposits. Apart from the predominant vein-type uranium deposits in the Ore Mts. (Niederschlema-Alberoda, Jáchymov) and the Příbram ore deposit, these deposits show no direct genetic relationship between mineralisation and granitic plutons (**Figure 1**).

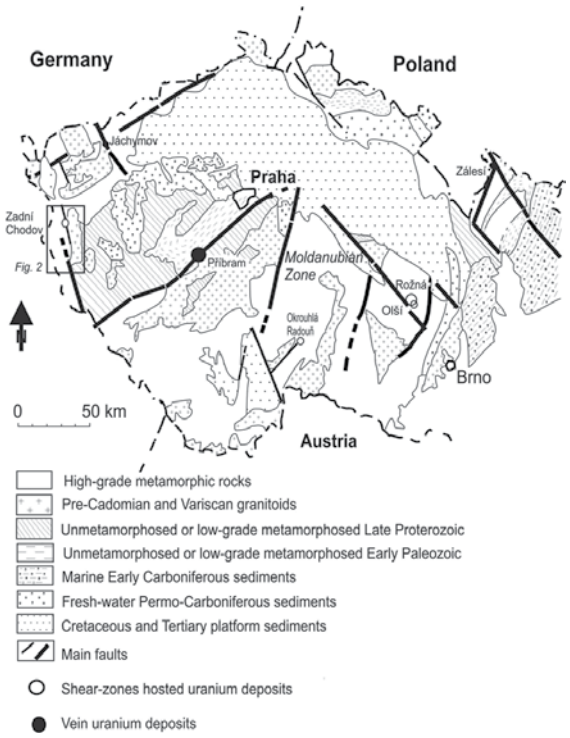

Figure 1. Simplified geological map of the Bohemian Massif with the most significant hydrothermal uranium deposits.

The shear zone-bounded uranium deposits consist of peneconcordant lenses or highly disseminated uranium mineralisation evolved in brecciaed shear zones and/or in fractures. The host rocks of these deposits are strongly altered in aceites, exhibiting extensive albitisation, chloritisation and hematitisation of the host rock series. In the recent classification of metamorphic and metasomatic rocks, these metasomatic rocks are named as aceites [4].

According to their mineral composition, the aceites are very similar to episyenites developed in uranium deposits of the Massif Central and the Armorican Massif in France, linked to leucogranitic plutons. Episyenites are defined as igneous-like rocks of syenite composition; displaying cavities produced by hydrothermal dissolution of quartz grains than can ultimately host uranium ore deposits [5]. Both rock types are products of low-temperature alkaline metasomatism associated with a significant input of Na_2O and the loss of SiO_2. Distinctly different mineral compositions have metasomatic deposits, which originated by high-temperature alkali metasomatism (e.g., Central Ukraine). Metasomatic facies in these uranium deposits include albitites, aegirinites and alkali-amphibole-rich rocks. In the recent international union of geological sciences (IUGS) classification of metamorphic rocks, these metasomatites are classified as fault-related metasomatites, which are common in the Precambrian shields [4]. The aim of this chapter is to present the detailed petrology, mineralogy and geochemistry of aceites and associated uranium mineralisation evolved in shear zone-hosted uranium ore deposits of the Bohemian Massif.

http://dx.doi.org/10.5772/intechopen.71967

2. Geological setting

In high-grade metamorphic rocks of the Moldanubian Zone are evolved the Rožná, Olší, Okrouhlá Radouň, Zadní Chodov and Dyleň uranium deposits. The high-grade metamorphic rocks are represented by biotite paragneisses with intercalations of amphibolites, calc-silicate rocks, marbles and lenses of partly serpentinised ultrabasic rocks (dunites).

The Vítkov II and Lhota uranium deposits occur in granitoids of the Bor pluton. An N-S trending, 35-km long magmatic body forms the Bor pluton, which is emplaced in the fault zone, which is a part of regional West Bohemian shear zone. The most voluminous rocks in the Bor pluton are coarse-grained biotite, usually porphyritic biotite granites. In the northern block, older amphibole-biotite granodiorites, tonalites and quartz diorites were also observed. Dykes of two-mica monzogranites, aplites, which predominates in the southern part of the Bor pluton, fill N-S faults. (**Figure 2**) [6].

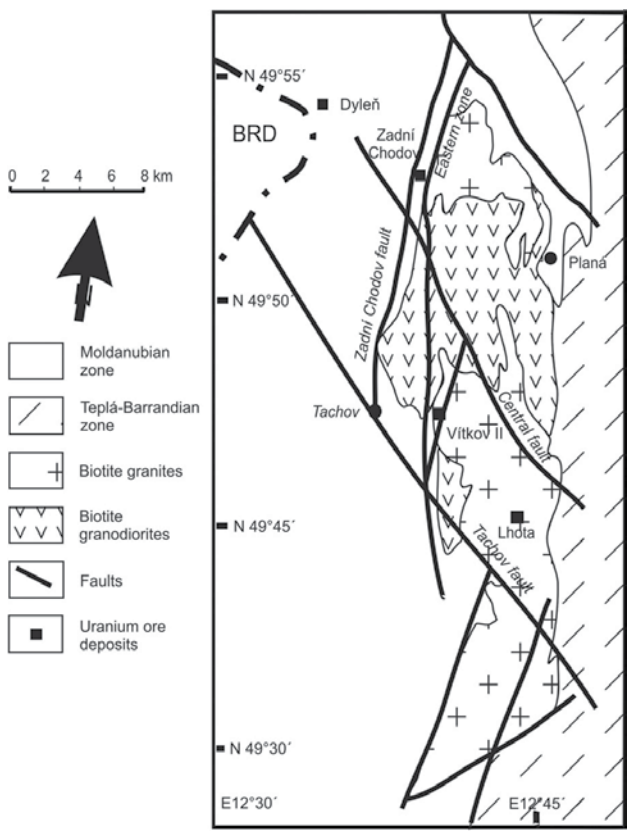

Figure 2. Geological map of the Bor pluton, modified from [6].

2.1. Rožná uranium deposit

The Rožná uranium deposit occurs in the uppermost Gföhl unit of the Moldanubian Zone. The host rocks of this ore deposit are formed predominantly by biotite paragneisses, amphibolites and small bodies of calc-silicate rocks, marbles, serpentinites and pyroxenites. The uranium mineralisation is bounded on the longitudinal shear zones (R1–R4). The main part of disseminated uranium mineralisation hosts the Rožná 1 (R1) and Rožná 4 (R4) shear zones. In the less strongly mineralised Rožná 2 (R2) and Rožná 3 (R3) shear zones, numerous pinnate carbonate veins occur. Longitudinal shear zones are segmented by NW-SE and SW-NE faults, which host post-uranium carbonate-quartz-sulphide mineralisation (**Figure 3**) [1].

Uranium mineralisation could be divided into (1) disseminated coffinite > uraninite > U-Zr-mineralisation evolved in altered rocks (aceites) of the mineralised shear zones (R1–R4), (2) uraninite > coffinite mineralisation in carbonate veins, (3) disseminated coffinite > uraninite in aceites adjacent to main shear zones (R1, R4) and (4) mostly coffinite mineralisation bound to the intersection of shear zones with an younger NW-SE and SW-NE faults. Ore lenses of disseminated uranium mineralisation in fault zones R1 and R4 are 3.5-m thick on average, ore grade is around 0.5% U, up to 10% U locally. Ore bodies in ore zones R2 and R3 host a large number of carbonate veins up to 2-m thick with U-mineralisation of the average grade 0.6% U. Ore bodies in aceites with predominance of coffinite on uraninite and U-Zr silicate have U-mineralisation of

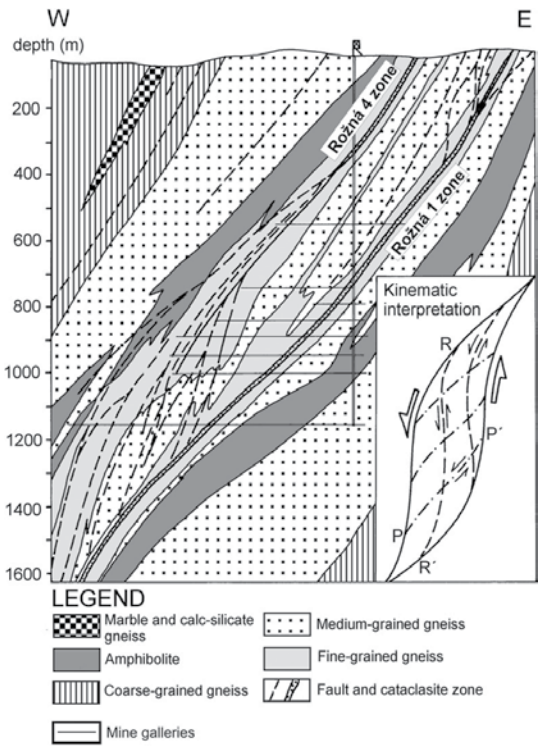

Figure 3. Schematic cross section of the Rožná uranium deposit, modified from [1].

a grade 0.1–0.15% U, exceptionally 0.3% U. Disseminated U-mineralisation bound to oblique fault zones is usually hosted by quartz-carbonate-sulphide breccias at intersections with diagonal and longitudinal structures. Compared to other types of mineralisation, the ore bodies are small but contain relatively high-grade ore of average grade 0.8 and up to 20% U in some ore shoots. Total mine production of the Rožná ore deposit was 22,220 tons U with average grade of 0.24% U, mined from 1957 to April 2017 [7]. The Rožná uranium deposit was the last mined uranium deposit in the Central Europe.

2.2. Olší uranium deposit

The Olší uranium deposit is also evolved in the NE part of the Moldanubian Zone. The host rocks of this uranium deposit consist mainly of plagioclase-biotite and amphibole-bearing paragneisses with small lenses of K-rich granitoids and serpentinites. Longitudinal N-S and NNW-SSE striking ductile shear zones (O1, O2 and O3) dip to W at an angle of 45–70°. Longitudinal shear zones are crosscut by ductile to brittle NW-SE and SW-NE striking fault zones that host lenses of contrasted uranium mineralisation. The main uranium ore bodies are evolved on the N-S longitudinal shear zones. The Variscan calcite-chlorite-uraninite association and the Mesozoic albite-chlorite-coffinite association represent the uranium mineralisation. Total mine production of the Olší ore deposit was 2922.2 tons U with average grade of 0.10% U, mined from 1959 to 1989 [7].

2.3. Okrouhlá Radouň uranium deposit

The Okrouhlá Radouň uranium deposit is situated in a NNW-SSE striking shear zone on the NE margin of the Klenov pluton, which is a part of the Moldanubian plutonic complex. The host rock series comprises partly migmatised biotite paragneisses and sillimanite-biotite paragneisses of the Moldanubian Zone and two-mica leucogranites of the Klenov pluton. Granites that formed a series of the NE-SW to NNE-SSW elongated sheets or larger irregular bodies with sheeted margins intruded into the high-grade metasediments. The sheets are mostly parallel to the foliation in the metasediments.

The most significant mineralised structure in this area, the Radouň shear zone, was explored along a strike length of approximately 3 km and to a depth of 650 m. The highest grade uranium mineralisation was developed at depths of 250–400 m beneath the present surface. The thickness of the mineralised shear zone is highly variable, ranking from 30 cm to approximately 7 m. The thickest portion of this zone was observed in the southern part of the uranium deposit, where a shear zone was developed in altered two-mica leucogranites and in highly hydrothermally altered, partly migmatised biotite paragneisses. The shear zone is infilled with cataclasites formed by host rock breccias, which were altered to clay-mineral-rich and chlorite-rich assemblages containing a disseminated uranium mineralisation comprising mainly coffinite and lesser amounts of uraninite. Total mine production of the Okrouhlá Radouň uranium deposit was 1339.5 tons U with average grade of 0.084% U, mined from 1972 to 1990 [7].

2.4. Zadní Chodov uranium deposit

The Zadní Chodov uranium deposit, which is located in the northern tectonic block of the Bor pluton, was developed by mine workings down to a level of 1250 m with a length of over 2.5 km. The host rock series are formed by migmatised biotite paragneisses of the Moldanubian Varied

Group with intercalations of quartzites, amphibolites, calc-silicate rocks and crystalline limestones. Uranium mineralisation is associated with N-S trending zones of the Zadní Chodov fault in areas of their intersection with NW-SE trending fault structures. The shear zones are infilled by highly chloritised and arigilitised host rocks.

The thickness of main mineralised shear zones (CH-1, CH-4 and CH-11) ranges from 30 cm to approximately 1–2.5 m. Their total thickness is about 50–150 m (**Figure 4**). The high-grade uranium mineralisation was developed at the depths of 440–960 m beneath the present surface. The most common uranium minerals are coffinite (65 vol.%), uraninite (25 vol.%) and brannerite (10 vol.%). Total mine production of the Zadní Chodov uranium deposit was 4150.7 tons U with average grade of 0.195% U, mined from 1952 to 1992 [8].

2.5. Dyleň uranium deposit

The Dyleň uranium deposit was located in high-grade metasediments of the Moldanubian Zone (migmatised biotite, biotite-sillimanite and quartzitic paragneisses with intercalations of quartzites). The main tectonic zone in the area of the Dyleň ore deposit is N-S trending zone of the Dyleň fault, dip to W at an angle of 60–70°. However, the uranium mineralisation is associated with NW-SE trending shear zones, dip to SW at an angle of 70–90°. The W-E striking faults crosscut both shear zone structures. All these shear zones and faults are infilled by chlorite-enriched aceites. Highly disseminated apatite-brannerite-coffinite association with up to 90 vol.% of coffinite represents the Variscan uranium mineralisation. Main part of uranium mineralisation is bounded on highly altered biotite paragneisses. Total mine production of the Dyleň uranium deposit was 1100.5 tons U with average grade of 0.14% U, mined from 1965 to 1991 [7].

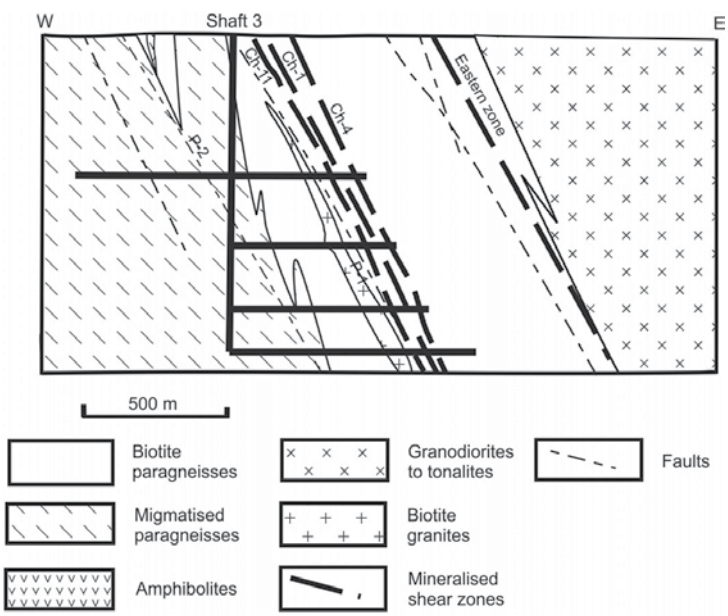

Figure 4. Schematic cross section of the Zadní Chodov uranium deposit, modified from [8].

2.6. Vítkov II uranium deposit

The Vítkov II uranium deposit occurs in the central part of the Bor pluton. Its main mineralised shear zones are zone 0–30 in the east and the Vítkov zone in the west. The thickness of the shear zones varies from 5 to 7 m to several tens of metres. Both the shear zones are infilled by crushed altered rocks, quartz and carbonates. Rich accumulations of U-minerals often occur in their vicinity. The pennate NW-SE faults evolved between both shear zones are infilled by dykes of biotite and two-mica granites and aplites. Granites of the Bor pluton in the area of the Vítkov II uranium deposit are usually intensely altered to aceites. The ore bodies comprise coffinite, uraninite and brannerite finely disseminated in the surrounding altered granites. The ore bodies are grouped into four ore pipes, which are accumulated in environs of the shear zone 0–30. Total mine production of the Vítkov II uranium deposit was 3972.6 tons U with average grade of 0.124% U, mined from 1961 to 1990 [7].

2.7. Lhota uranium deposit

The Lhota uranium deposit is situated in the central block of the Bor pluton. Uranium mineralisation is evolved in altered coarse-grained biotite granites, accompanied by smaller bodies of amphibole-biotite granodiorites and tonalites. All these granitoids are overlain by remnants of the Moldanubian high-grade metasediments. The NW-SE, partly also N-S trending aplite dykes, pierces this rock complex. The two ore bearing shear zones (Os-2 and Os-17) strike NW-SE and dip steeply NE. The thickness of these mineralised shear zones are 5–18 m. The mineralised shear zones comprise coffinite and brannerite.

This uranium deposit has been verified between 1953–1967 and 1975–1989 by five exploration shafts down a depth of 250 m and by numerous boreholes down to levels of 300–600 m. During these two exploration stages, uranium mineralisation with the total amount of 158 t U and average grade of 0.120% U was identified [7].

3. Analytical methods

The rock-forming (chlorite, plagioclase) and uranium minerals were analysed in polished thin sections using CAMECA SX-100 electron probe micro-analyser (EPMA) operated in WDX mode. The contents of selected elements were determined using an accelerating voltage and beam current of 15 keV and 20 or 40 nA, respectively, with a beam diameter of 2–5 μm. The raw data were converted into concentrations using appropriate PAP-matrix corrections [9]. The detection limits were approximately 400–500 ppm for Y, 600 ppm for Zr, 500–800 ppm for REE and 600–700 ppm for U and Th. Back-scattered electron (BSE) images were acquired to study the internal structure of mineral aggregates.

The whole-rock composition of the selected, unaltered and altered high-grade metasediments and granitic rocks from investigated uranium deposits is based on analyses of 50 samples. The selected trace elements (U, Th, REE, Y and Zr) were determined by ICP-MS (a Perkin Elmer Sciex ELAN 6100 ICP mass spectrometer) at Activation Laboratories, Ltd., Ancaster, Canada.

The decomposition of the rock samples for ICP-MS analysis involved lithium metaborate/ tetraborate fusion.

4. Results

4.1. Petrography of altered rocks

In altered high-grade metasediments and granitic rocks of above-mentioned uranium deposits (Rožná, Okrouhlá Radouň, Zadní Chodov, Lhota and Vítkov II), four major stages of hydrothermal alteration can be distinguished, namely pre-ore, ore and two post ore-ore stages. During pre-ore alteration, when main part aceites originated, original biotite from biotite paragneisses (Rožná, Okrouhlá Radouň and Zadní Chodov) and two-mica leucogranites (Okrouhlá Radouň) and/or biotite granites (Vítkov II and Lhota) were altered to chlorite I enriched in Fe. Transformation of biotite was sometimes accompanied by origin of rutile. Original plagioclases were altered into albite I ($An_{0–9}$). Albitisation is sometimes accompanied by K-feldspatisation, which was found at the Vítkov II uranium deposit in highly altered parts of original biotite granites. The albitisation and K-feldspatisation precede the quartz removal. The transitional zones between unaltered and altered high-grade metasediments and granitic rocks are usually gradational, spanning a few tens of centimetres to 1 m. Commonly, the transitional zone displays a weak red colouring due to the presence of fine-grained hematite laths distributed irregularly in originally albitised plagioclase (albite I). Hydrothermally altered rocks have medium porosities due to the hydrothermal leaching of original quartz (typically 10–15 vol.%). In highly altered high-grade metasediments and granitic rocks, the authigenic generations of albite II occur as epitactic overgrowths on pseudomorphs of albite II. The voids resulted through leaching of quartz were later filled by younger generations of albite (albite III) and chlorite (chlorite III). The newly originated albites II and III have near-end-member composition ($An_{0–0.8}$). The authigenic chlorites II and III are Mg-enriched (chlorite II Fe/Fe + Mg = 0.12–0.54, chlorite III Fe/Fe + Mg = 0.47–0.50). However, the original metamorphic and/or magmatic textures in the altered high-grade metasediments and/or granitic rocks are usually preserved.

During the ore stage, chlorite II, albite II, III, apatite and uranium minerals (uraninite, coffinite, brannerite) were originated. Uranium mineralisation usually comprises three different morphologic-mineralogical types. The highly altered granitoids of the Okrouhlá Radouň and Vítkov II ore deposits are marked by metasomatic coffinite and/or coffinite-uranium mineralisation. The metasomatic mineralisation is usually coupled with highly intensive albitisation and carbonatisation of granitic rocks. The lenticular-shaped uraninite and uraninite-coffinite mineralisation (Vítkov II and Lhota in the Bor pluton) occurs usually on boundary of granitic rocks with metamorphites. The disseminated uranium mineralisation occurs in the xenoliths of metamorphic rocks (Lhota) and in mineralised shear zones (Rožná, Zadní Chodov and Dyleň). In these uranium deposits, coffinite and brannerite occur predominantly in highly chloritised metamorphites. The suitable sources of Ti in brannerites were probably altered high-grade metasediments and/or amphibolites.

Albite and carbonates are the main constituents of the aceites formed through hydrothermal alteration of granites and high-grade metasediments and occupy 65–85 vol.% of the bulk rocks. The quartz post-ore stage is characterised by filling of voids, created by removal of magmatic and/or metamorphic quartz, by quartz II, origin of quartz veinlets (quartz III), veinlets of chlorite III and origin of younger hematite laths (hematite II).

The carbonate bearing post-ore stage is connected with the origin of calcite and relatively rarely sulphides, selenides and zeolites. Carbonates fill cavities in the altered rocks and/or form fine veinlets in highly altered granitic rocks. Occasionally, dolomite and siderite were found.

4.2. Geochemistry of altered rocks

In previous papers about shear zone-hosted uranium deposits in the Bohemian Massif [1, 10, 11], chemical composition of unaltered and altered host rocks was described in detail. Also, in those papers, detailed investigations of losses and gains during hydrothermal alteration of host rock series were performed using isocon method [12]. This chapter discusses about geochemistry of unaltered and altered rocks series concentrated on behaviour of selected trace elements, especially REE, Y and Zr.

The chloritised high-grade metasediments from the Rožná and Okrouhlá Radouň uranium deposits without uranium mineralisation are depleted in REE. This depletion is also displayed by lower ΣREE (Rožná 69–98 ppm, Okrouhlá Radouň 106–196 ppm) and high LREE/HREE ratios (4.0–17.6) relative to the unaltered metasediments. In contrast to chloritised high-grade metasediments without uranium mineralisation, mineralised metasediments from the Rožná and Zadní Chodov uranium deposits are enriched in REE (ΣREE = 108–390 ppm), especially in HREE (LREE/HREE 1.2–4.7) (**Figures 5** and **6**).

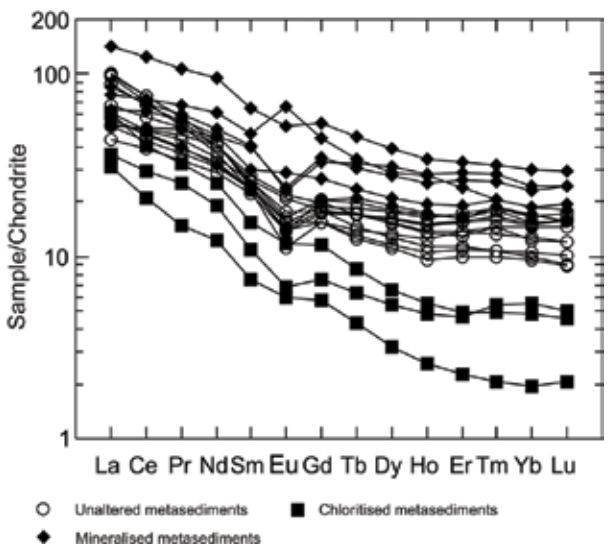

Figure 5. REE patterns of the high-grade metasediments and their hydrothermally altered equivalents from the Rožná uranium deposit. Original data normalised to chondrite according to [13].

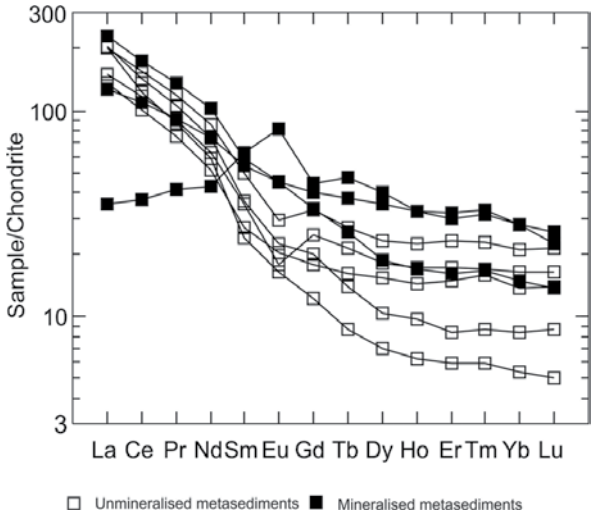

Figure 6. REE patterns of the high-grade metasediments and their hydrothermally altered equivalents from the Zadní Chodov uranium deposit. Original data normalised to chondrite according to [13].

The behaviour of Y and Zr in mineralised aceites from shear zone-hosted uranium deposits in the Bohemian Massif is variable. Yttrium is enriched in mineralised aceites from the Rožná and Okrouhlá Radouň ore deposits and its behaviour is close to behaviour of HREE in these rocks. Yttrium in these rocks occurs usually in coffinite (up to 3.4 wt.% Y_2O_3). In altered biotite granites from the Bor pluton, the concentrations of Y are similar to their concentrations in unaltered granitic rocks (**Figure 7**).

The concentrations of Zr in unaltered and altered rocks from all above-mentioned uranium deposits are similar. In unaltered host rocks from these ore deposits, Zr is concentrated in zircons. However, during hydrothermal alterations of these rocks, zircon is often highly altered and Zr is concentrated in uranium minerals, especially in coffinite.

4.3. Mineralogy

Coffinite in shear zone-hosted uranium deposits occurred in the Bohemian Massif usually prevails uranium mineral. In the Rožná and Zadní Chodov ore deposits, coffinite is concentrated in the deepest part of these deposits. The coffinite occurring in these shear zone-hosted ore deposits is commonly intimately associated with flakes of newly originated chlorite II. A majority of analysed coffinites from the Rožná, Okrouhlá Radouň and Lhota uranium deposits are enriched in Y_2O_3 (up to 3.4 wt.%) and ZrO_2 (up to 13.8 wt.%).

Uraninite in shear zone-hosted uranium deposits from the Bohemian Massif usually occurs as colloform aggregates in highly heterogeneous aggregates together with coffinite. In mineralised aceites, both minerals often form rims around chlorite flakes (**Figure 8**). In the Rožná ore deposit, the SiO_2 and UO_2 contents vary from UO_{2+x} to $USiO_4$, indicating the variable coffinitisation of uraninite (**Figure 9**). Almost all uraninite grains and aggregates were replaced by coffinite to a variable degree.

http://dx.doi.org/10.5772/intechopen.71967

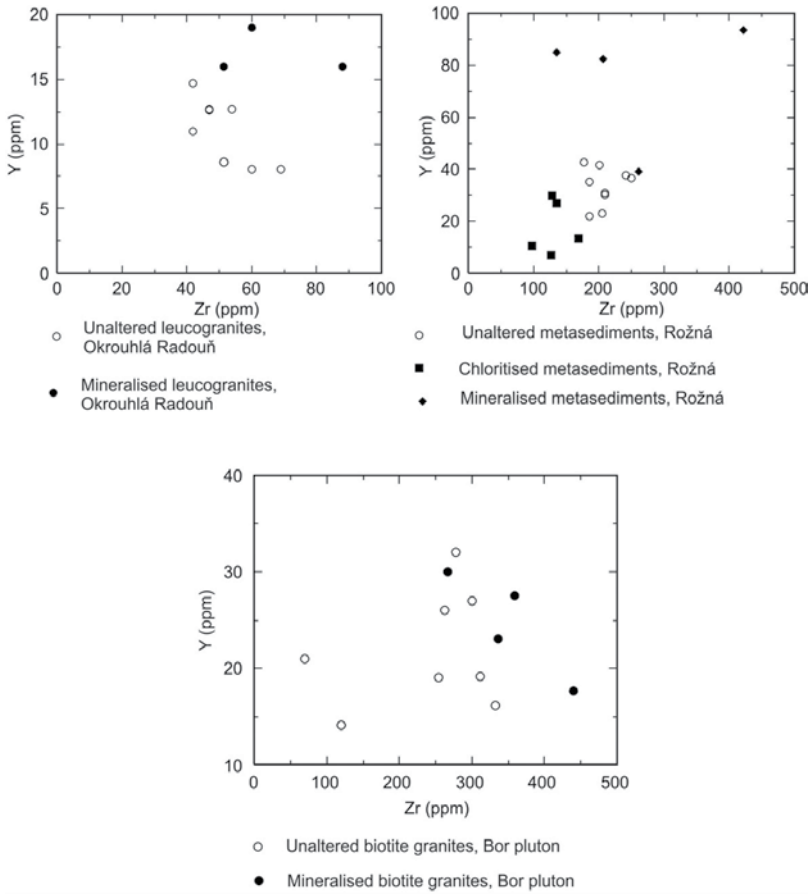

Figure 7. Plot Y versus Zr for unaltered and mineralised rocks from the Okrouhlá Radouň, Rožná and Zadní Chodov uranium deposits.

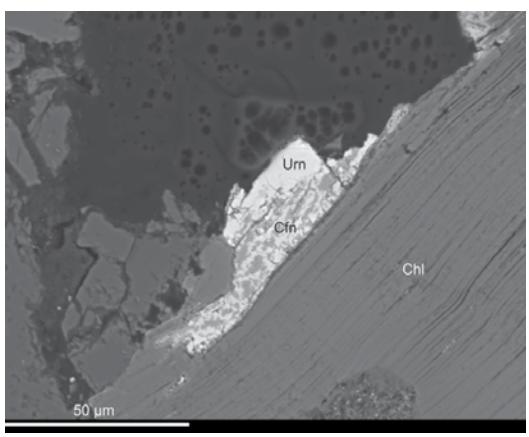

Figure 8. BSE image of uraninite (urn) and coffinite (Cfn) around chlorite flakes, Rožná uranium deposit.

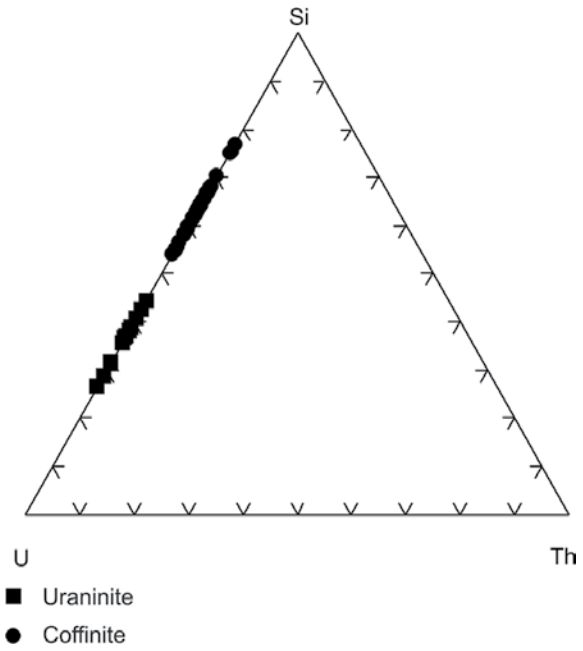

Figure 9. Chemical composition of coffinite and uraninite from the Rožná uranium deposit (wt.%).

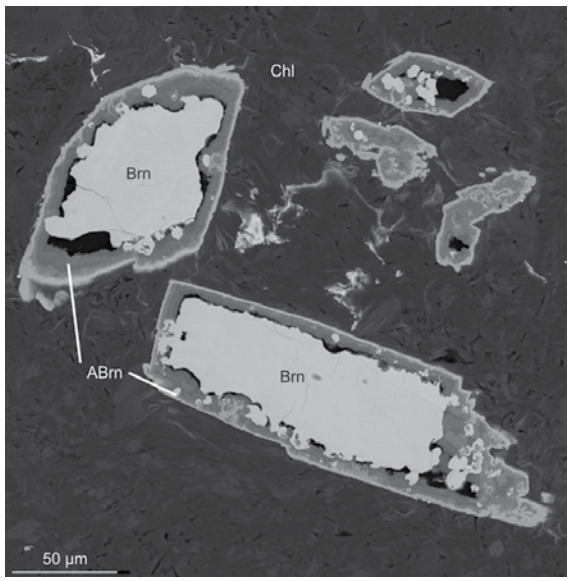

Figure 10. BSE image of brannerite (Brn) and altered brannerite (Abrn) enclosed in finely grained chlorite (Chl) from the Zadní Chodov uranium deposit.

Brannerite was found in the Rožná uranium deposit and in uranium deposits from the Bor pluton (Zadní Chodov, Dyleň and Lhota). In mineralized aceites brannerite occurs in form of acicular aggregates and/or irregular grains. Larger brannerite grains are usually

heterogeneous and on their rims altered to Ti-enriched brannerite and rutile (**Figure 10**). Brannerite from the Rožná uranium deposit is enriched in ZrO_2 (up to 4.82 wt. %). Brannerites from the Rožná uranium deposit were sometimes decomposed in complex non-stoichiometric U-Ti-Si-Zr phases.

5. Discussion

5.1. Origin of aceites

The differences in mineralogical composition of aceites in the studied shear zone-hosted uranium deposits from the Bohemian Massif are expressed by different composition of original host rock series (high-grade metasediments vs. granitic rocks) and different tectonic movements on shear zones of individual ore deposits. For altered metasediments (Rožná and Zadní Chodov), high concentrations of chlorite I and clay minerals (illite, kaolinite and smectite) as fillings of shear zones are significant. The clay minerals filling in these uranium deposits differ in composition of the assemblage of these minerals. The Fe-illite predominates at the Rožná ore deposit and in the shear zones at Zadní Chodov chlorite predominates over illite. For aceites evolved in altered granitic rocks (Okrouhlá Radouň, Vítkov II and Lhota), the rock matrix composed of chlorite I, albite I and hematite framework is characteristic.

Uranium in the host high-grade metasediments and granitic rocks of all investigated uranium deposits is essentially hosted in monazite and zircon, in leucocratic granites from the Okrouhlá Radouň ore deposit, and also in xenotime. In barren aceites, monazite and xenotime are usually missing and zircon is often highly altered. Therefore, the source of uranium may be found in the decomposition of uranium-bearing accessories, as is also proposed for the inconformity-type uranium deposits in Canada [14]. The titanium necessary for the origin of brannerite was probably released during chloritisation of Ti-enriched biotite and hydrothermal alteration of the Ti-rich accessory minerals (titanite and allanite).

A prominent hematitisation occurred in aceites from the Okrouhlá Radouň, Vítkov II and Lhota uranium deposits, and deeper parts of the Rožná uranium deposit indicates deep infiltration of oxidised, surface-derived fluids to the crystalline basement during the pre-ore stage. The deep circulation of fluids gave rise to desilification, hematitisation and albitisation of host rock complexes along shear zones. The fluids responsible for origin of aceites differ from earlier low-salinity metamorphic fluids in their generally higher but highly variable salinities (0–25 wt.% $NaCl_{eq.}$). Differences in the salinity of these fluids probably reflect the mixing of chemically heterogeneous basinal brines with meteoric water [1, 15].

5.2. Behaviour of REE, Zr and Y in aceites

Rare earth elements, Zr and Y, are usually considered as the immobile elements by hydrothermal alteration of host rock series [16]. However, hydrothermal experiments and some mineralogical research of nature rock series have demonstrated that these elements could be mobile during hydrothermal alterations, especially if the fluids contained strong complexation agents (e.g., fluoride or phosphate anions) [17–19]. The mobility of REE, especially HREE in aceites in the all studied uranium deposits, is suggested by enrichment of HREE in aceites from Rožná,

Okrouhlá Radouň and Lhota uranium deposits. The mobility of Zr and Y in the studied aceites is suggested by the occurrence of Zr- and Y-enriched coffinite from the Rožná, Okrouhlá Radouň and Lhota uranium deposits.

Enrichment in HREE during origin of uranium deposits in shear zone-hosted uranium mineralisation was found in unconformity uranium deposits from Australia and Canada [20–24]. Coffinites enriched in Zr and Y were found only in the uranium sedimentary deposits in New Mexico, United States [25] and in the natural fission reactor environment of the Oklo uranium deposit, Gabon [26].

6. Conclusion

The Bohemian Massif hosts a significant quantity of uranium deposits bound by brittle shear zones developed in high-grade metamorphic rocks (Rožná, Okrouhlá Radouň, Zadní Chodov and Dyleň) and/or granites of the Klenov and Bor plutons (Okrouhlá Radouň, Vítkov II and Lhota). The shear zone-hosted uranium deposits consist of peneconcordant lenses or highly disseminated uranium mineralisation evolved in brecciaed shear zones. The host rocks of these deposits are strongly altered, exhibiting extensive albitisation, chloritisation, hematitisation, and desilification in pre-ore stages. By hydrothermal alteration, aceites are products of low-temperature alkaline metasomatism associated with a significant input of Na_2O and the loss of SiO_2. Complex coffinite-uraninite or coffinite-uraninite-brannerite assemblages form the shear zone mineralisation with predominance coffinite about uraninite. Mineralisation evolved in shear zone-hosted uranium deposits of the Bohemian Massif displays enrichment of HREE, Y and Zr in examined uranium minerals, especially in coffinite. For analysed coffinites and brannerites, enrichment of Y (up to 3.4 wt.% Y_2O_3) and Zr (up to 13.8 wt.% ZrO_2) is significant.

Acknowledgements

This work was carried out, thanks to the support of the long-term conceptual development research organisation RVO: 67985891. The author is grateful to R. Škoda, Š. Benedová and P. Gadas from the Institute of Geological Sciences of the Masaryk University (Brno) for technical assistance with microprobe analysis of selected rock-forming and uranium minerals.

Author details

Miloš René

Address all correspondence to: rene@irsm.cas.cz

Institute of Rock Structure and Mechanics, Academy of Sciences of the Czech Republic, Prague, Czech Republic

References

[1] Kříbek B, Žák K, Dobeš P, Leichmann J, Pudilová M, René M, Scharm B, Scharmová M, Hájek A, Holeczy D, Hein UF, Lehmann B. The Rožná uranium deposit (Bohemian Massif, Czech Republic): Shear-zone hosted, late Variscan and post-Variscan hydrothermal mineralization. Mineralium Deposita. 2009;**44**:99-128. DOI: 10.1007/s00126-008

[2] René M. Uranium hydrothermal deposits. In: Vasiliev AY, Sidorov M, editors. Uranium, Characteristics, Occurrence and Human Exposure. New York: Nova Science Publishers, Inc.; 2012. pp. 211-244

[3] Uranium 2014: Resources, Production and Demand. Paris: OECD; 2014. p. 508

[4] Fetes D, Desmons J, editors. Metamorphic Rocks. A Classification and Glossary of Terms. Recommendations of the International Union of Geological Sciences Subcommission on the Systematics of Metamorphic Rocks. Cambridge: Cambridge University Press; 2007. p. 244

[5] Cathelineau M. The hydrothermal alkali metasomatism effects on granitic rocks: Quartz dissolution and related subsolidus changes. Journal of Petrology. 1986;**27**:945-965. DOI: 10.1093/petrology/27.4.945

[6] Holovka D, Hnízdo E. Final Report about Exploration on Uranium. Bor massif. Příbram: DIAMO; 1992. Unpublished report. p. 280 (In Czech)

[7] Kafka J, editor. Czech Ore and Uranium Mining Industry. Ostrava: Anagram; 2003. p. 647 (in Czech)

[8] Novák J, Paška R. Final Report about Exploration of the Eastern Shear-zone on the Zadní Chodov-Eastern Uranium Deposit. Příbram: Uranium industry; 1983. Unpublished report. p. 56 (in Czech)

[9] Pouchou JL, Pichoir F. "PAP" (φ-ρ-Z) procedure for improved quantitative microanalysis. In: Armstrong JT, editor. Microbeam Analysis. San Francisco: San Francisco Press; 1985. pp. 104-106

[10] René M. Rare-earth, yttrium and zirconium mobility associated with the uranium mineralisation at Okrouhlá Radouň, Bohemian Massif, Czech Republic. European Journal of Mineralogy. 2015;**27**:57-70. DOI: 10.1127/ejm/2015/0027-2422

[11] René M. Alteration of granitoids and crystalline rocks and uranium mineralisation in the Bor pluton area, Bohemian Massif, Czech Republic. Ore Geology Reviews. 2017;**81**:188-200. DOI: 10.1016/j.oregeorev.2016.09.033

[12] Grant JA. The isocon diagram–A simple solution to Gresens equation for metasomatic alteration. Economic Geology. 1986;**81**:1976-1982. DOI: 10.2013/gsrcongeo.81.8.1976

[13] Taylor SR, McLennan SM. The Continental Crust: Its Composition and Evolution. Oxford: Blackwell; 1985. p. 312

[14] Hecht L, Cuney M. Hydrothermal alteration of monazite in the Precambrian crystalline basement of the Athabasca Basin (Saskatchewan, Canada): Implications for the formation of unconformity-related uranium deposits. Mineralium Deposita. 2000;**35**:791-795. DOI: 10.1007/s001260050280

[15] Dolníček Z, René M, Hermannová S, Prochaska W. Origin of the Okrouhlá Radouň episyenite-hosted uranium deposit, Bohemian Massif, Czech Republic: Fluid inclusion and stable isotope constraints. Mineralium Deposita. 2014;**49**:409-425. DOI: 10.1007/s00126-013-0500-5

[16] Bau M. Controls on the fractionation of isovalent trace elements in magmatic and aqueous systems: Evidence from Y/Ho, Zr/Hf, and lanthanide tetrad effect. Contributions to Mineralogy and Petrology. 1996;**123**:323-333. DOI: 10.1007/s004100050159

[17] Giére R. Transport and deposition of REE in H_2S-rich fluids: Evidence from accessory mineral assemblages. Chemical Geology. 1993;**110**:251-268. DOI: 10.1016/0009-2541(93)90257-J

[18] Rubin JN, Henry CD, Price JG. The mobility of zirconium and other "immobile" elements during hydrothermal alteration. Chemical Geology. 1993;**110**:29-47. DOI: 10.1016/0009-2541(93)90246-F

[19] Hecht L, Thuro K, Plinninger R, Cuney M. Mineralogical and episyenitisation in the Königshain granites, northern Bohemian Massif, Germany. International Journal of Earth Sciences. 1999;**88**:236-252. DOI: 10.1007/s005310050262

[20] McLennan SM, Taylor SR. Rare earth element mobility associated with uranium mineralisation. Nature. 1979;**282**:247-249. DOI: 10.1038/282247a0

[21] Fayek M, Kyser TK. Characterization of multiple fluid-flow events and rare-earth-element mobility associated with formation of unconformity-type uranium deposits in the Athabasca basin, Saskatchewan. The Canadian Mineralogist. 1997;**35**:627-658

[22] Mercadier J, Cuney M, Cathelineau M, Lacorde MU. Redox-fronts and kaolinisation in basement-related U-ores of the Athabasca Basin (Canada): Late U remobilisation by meteoritic fluids. Mineralium Deposita. 2011;**46**:105-135. DOI: 10.1007/s0126-010-0314-7

[23] Mercadier J, Cuney M, Lach P, Boiron MC, Bonhoure J, Richard A, Leisen M, Kister P. Origin of uranium deposits revealed by their rare earth element signature. Terra Nova. 2011;**23**:264-269. DOI: 10.1111/j.1365-3121.2011.01008.x

[24] Frimmel HE, Schedel S, Brätz H. Uraninite chemistry as forensic tool for provenance analysis. Applied Geochemistry. 2014;**48**:104-121. DOI: 10.1016/j.apgeochem.2014.07.013

[25] Hansley PL, Fitzpatrick JJ. Compositional and crystallographic data on REE-bearing coffinite from the grants uranium region, northwestern New Mexico. American Mineralogist. 1989;**74**:263-270

[26] Jensen KA, Ewing RC. The Okélobondo natural fission reactor, southeast Gabon: Geology, mineralogy and retardation of nuclear-reaction products. Geological Society of America Bulletin. 2001;**113**:32-62. DOI: 10.1130/0016-7606(2001)113

Chapter 4

Uranium in Poland: Resources and Recovery from Low-Grade Ores

Katarzyna Kiegiel, Agnieszka Miskiewicz,
Dorota Gajda, Sylwester Sommer,
Stanislaw Wolkowicz and
Grazyna Zakrzewska-Koltuniewicz

Additional information is available at the end of the chapter

http://dx.doi.org/10.5772/intechopen.72754

Abstract

The presented studies deal with an assessment of the possibility of uranium recovery from the low-grade uranium resources in Poland. Uranium was leached from the ground uranium ores with efficiencies in 81–100% range that depend on the type of ore and leaching solution used. In the next step, the post-leaching solution was treated by the solvent extraction or ion exchange chromatography to separate uranium from other metals present in the ore. The novel routes of leaching by using membrane methods were examined. The final product, "yellow cake," was obtained in precipitation step. The studies of precipitation of uranium as ammonium diuranate or uranium peroxide from diluted uranium solutions are presented in this chapter. The work was completed with tentative economic analysis and environmental impact assessment along with radiation protection issues connected to uranium production.

Keywords: uranium ores, leaching, extraction, ion exchange chromatography, precipitation

1. Introduction

Continued interest in nuclear power and uranium industry revival is leading to the inevitable growing uranium demand. New sources of primary uranium will be derived from exploration and exploitation of lower grade ore bodies and also secondary resources as potential raw materials. In Poland, there are only low-grade uranium ores. The knowledge about a composition of a bedrock, uranium speciation and its composition with rock constituents is important for the design of the effective technology of extraction of uranium from low-grade

ores. The significant resources of uranium are also in unconventional raw materials, e.g. phosphates, nonferrous metal ores, carbonates, monazite sands, black shales, hard coal and brown coal, as well as sea water, from which it can be obtained as a minor by-product. In Polish ores, uranium usually is accompanied by other valuable metals, e.g. V, Mo and lanthanides that can be obtained simultaneously in the technological process to improve the economics of elaborated technology.

2. Uranium resources in Poland

Prospection of uranium deposits in Poland started in the late 1940s of the last century. In the years 1948–1963, Sudetes were the main region of exploration and exploitation of uranium resources [1]. Although more than 100 occurrences of uranium mineralization have been found in the Sudetes, only a few were exploited because of sufficient content of this metal. Uranium was also found and exploited as a by-product from iron sulfide deposit in Rudki ("Staszic" mine) in the Holy Cross Mountains. In this time, approximately 650–700 Mg of uranium was extracted from Polish ores and exported to Soviet Union [1, 2] (**Table 1**).

Polish uranium vein-type deposits in the Sudetes are related to metamorphic rocks. Moreover, uranium mineralization occurs in the sedimentary formation of Inter-Sudetic Depression:

Name of mine	Resources [Mg]	Exploited [Mg]	Main U minerals	Deposit type	U content [%wt]
Radoniów	375	214	Uraninite, pitchblende, metauranocircite, autunite, torbernite, uranopilite	Vein	0.17
Podgórze	280	199	Pitchblende, uranophane, autunite	Vein	0.2
Rubezal	0.5	0.5	Pitchblende	Vein	0.24
Wolność	118	94	Pitchblende, secondary minerals	Vein	0.1–0.2
Miedzianka	14.7	14.7	Pitchblende, secondary minerals	Vein	0.61
Mniszków	4.5	4.5	Pitchblende, secondary minerals	Vein	0.42
Wiktoria	0.28	0.28	Pitchblende, secondary minerals	Vein	n.d.
Wołowa Góra	2.5	2.5	Brannerite, secondary minerals	Vein	n.d.
Wojcieszyce	14.4	12.3	Pitchblende, asselbornite, autunite	Vein	n.d.
Okrzeszyn	938	3	Pitchblende, organometallic compounds	U-rich hard coal	0.05–0.11
Grzmiąca	792	3	Pitchblende, secondary minerals	Sandstone	0.054
Wambierzyce	217.5	0	Organometallic compounds	Black shale	0.01–0.03
Kletno-Kopaliny	20.71	20.7	Pitchblende, Torbernite	Vein	0.26–1

n.d. - no data.

Table 1. Uranium exploitation of Sudetes deposits [1–4].

Grzmiąca deposit related to Upper Carboniferous Sandstones, Okrzeszyn deposit related to uranium-rich Upper Carboniferous hard coal seams and Wambierzyce related to Lower Permian Walchia Shales.

In 1956, Polish Geological Institute (PGI) has initiated a new phase of prospecting of uranium. Additionally, parallel studies, based on all available geological and geophysical borehole data from the whole area of Poland, were conducted. The studies have led to the description of uranium mineralization in the Oligocene Menillite Shales of the Carpathians, the Carboniferous of the Upper Silesian Coal Basin and Zechstein copper-bearing shale [3]. Nevertheless, these uranium occurrences have no economic importance due to very low content of uranium, very small resources and close relationship with clay minerals and organic matter.

During prospection conducted by PGI, uranium mineralization in the Ordovician dictyonema Shales (Podlasie Depression) and the more perspective Lower and Middle Triassic sediments in the Peribaltic Syneclise (Vistula Spit area) were discovered and explored (**Table 2**).

Uranium mineralization of Ordovician dictyonema Shales was found in rock layers of thickness from several centimeters up to 4 m (average thickness is about 2.7 m). In vertical profile black shale series was found passing upward brown shales, replaced above by the light beige shales and phosphates. Uranium occurs mainly in black shales. Apart from uranium, higher concentration of other trace metals was observed. For black shales, concentration (geometric mean) of chosen metals was: U 38 [mg/kg]; Th 16 [mg/kg], Cu 236 [mg/kg], La 43 [mg/kg] and V 1508 [mg/kg]. For brown shales, concentration geometric mean was three times lower for most metals, and it was U 38 [mg/kg], Th 18 [mg/kg], Cu 169 [mg/kg], La 45 [mg/kg] and V 678 [mg/kg]. In the black dictyonema shales, uranium showed the strongest correlation with molybdenum (0.83), lead (0.57) antimony (0.52), cadmium (0.50), silver (0.36), lithium (0.28) and beryllium, while in brown dictyonema shales with vanadium (0.69), selenium (0.87), molybdenum (0.78), antimony (0.89), copper (0.34), cobalt (0.66), nickel (0.75) and REE (0.41) [7].

The highest uranium-rich Triassic rocks have been found in the middle part of Peribaltic Syneclise, in the rocks of Upper Bunter. The richest uranium mineralization is related to fine-grained, grey and green-grey sandstones, which occurs on the Vistula Spit area. It was found that uranium concentration in the sandstones is very variable and ranges from 4.2 mg/kg even up to 1.5%$_{wt}$. Higher concentration of some trace metals were also found in these rocks

	Ordovician dictyonema Shales	**Triassic Peribaltic sandstones**
Deposit type	Rock types with elevated uranium contents (black shales)	Sandstones
Speculative resources [Mg]	88,850	20,000
Depth of U retention [m]	400–1200	750–1170
Uranium minerals	Organometallic compounds	Coffinite, pitchblende, (inclusion in pyrite, galena and clausthalite)

Table 2. Ordovician dictyonema Shales and Triassic Peribaltic sandstones characteristics [5, 6].

(geometric mean): Th 6 [mg/kg], Cu 24 [mg/kg], La 31 [mg/kg] and V 195 [mg/kg]. Uranium related to Triassic sandstones showed the strongest correlation with lead (0.92), yttrium (0.92), silver (0.76), copper (0.75), antimony (0.7) and cobalt (0.44) [8].

3. Uranium extraction from low-grade and secondary resources: From ore to yellow cake

Uranium, more common element in the Earth's crust occurring in rocks, soil, rivers and ocean waters, has to be extracted from the raw material in a complex hydrometallurgical process [2]. The effect of ore mineralogy and mineral liberation of solid materials on the leaching behavior of uranium is not well defined. Uranium usually is accompanied by other valuable metals, e.g. V, Mo, Ag, Co and lanthanides that can be recovered in the technological process to improve the economics of the whole venture [9]. The procedure of uranium extraction must be designed to fit specific characteristics of the source material; however, the general procedure is similar for most of the ores and involves many separation steps. The basic stages are crushing and grinding, leaching, solid–liquid separation, ion exchange or solvent extraction and finally precipitation of the product, yellow cake – U_3O_8 (**Figure 1**) [10, 11]. In the beginning, the mined ores must be crushed and ground to make the uranium ores more susceptible to uranium extraction by leaching. The optimal particle size in leaching process is 0–0.2 mm. So small particles can be readily suspended to expose the uranium minerals on the action of lixiviant. Such a pre-prepared material could be leached with acidic (sulfuric acid, hydrochloric acid, etc.) or alkaline (carbonate) solutions [6, 12]. Tetravalent uranium has low solubility in both types of solutions. For this reason, the first step in uranium leaching process is oxidation of uranium(IV) to uranium(VI) form. The use of oxidants, e.g. manganese oxide, potassium permanganate, sodium chlorate or hydrogen peroxide, increases the leaching ability of uranium in water. In acidic leaching, uranium oxidation requires the presence of ferric ion, regardless of used oxidizing agents [10]. The oxidizing agent oxidizes ferrous ion to ferric ion that is oxidant for the uranium as shown in Eqs. 1, 2 and 3.

$$UO_{2(s)} + 2Fe^{3+} \rightleftarrows UO^{2+}_{2(aq)} + 2Fe^{2+} \tag{1}$$

$$2Fe^{2+} + MnO_2 + 4H^+ \rightleftarrows 2Fe^{3+} + Mn^{2+} + 2H_2O \tag{2}$$

$$UO_{2(s)} + 2Fe^{3+} \rightleftarrows UO^{2+}_{2(aq)} + 2Fe^{2+} \tag{3}$$

In alkaline leaching, the oxidizing agent oxidizes directly uranium as shown in Eq. 4.

$$UO_{2(s)} + H_2O_2 + 3CO^{2-}_3 \rightleftarrows UO_2\left(CO_3\right)^{4-}_{3(aq)} + 2OH^- \tag{4}$$

If uranium is closely associated with the organic compounds, the efficiency of leaching is low. The ores that contain the organic matter, e.g. dictyonema shales, have to be pre-treated by calcination. The samples of sandstones that contained less organic matter (below 0.1%) are

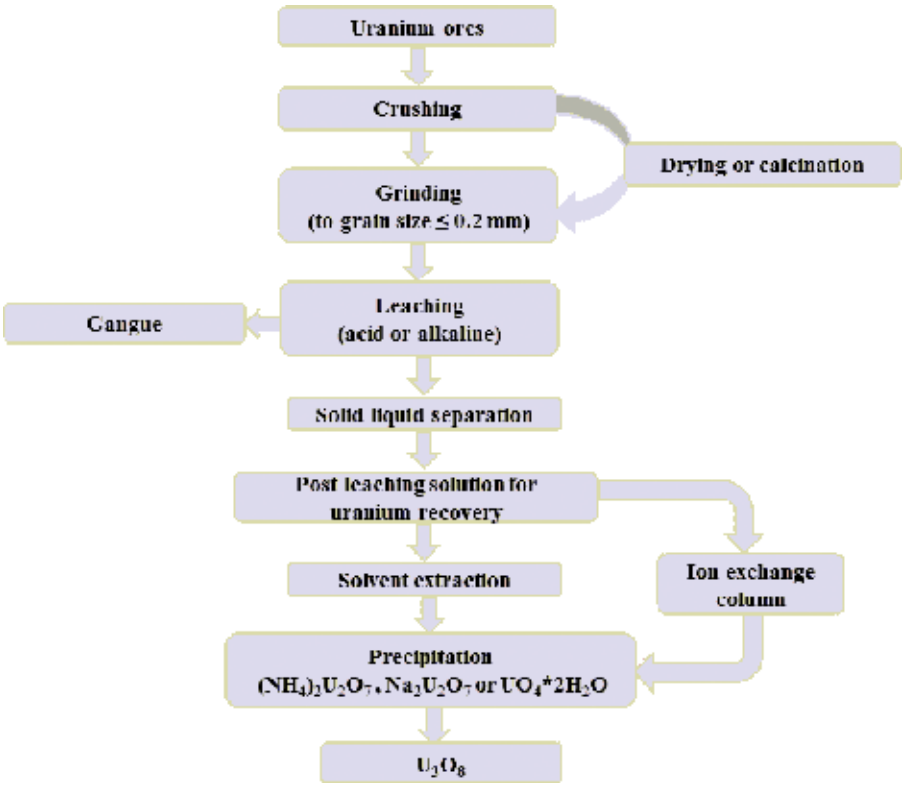

Figure 1. Treatment of uranium ores.

not calcinated in the oven. The post-leaching solution is separated from the ores residue by filtration. The concentration of uranium and other elements in post-leaching solution may be determined using ICP-MS analyses [13]. The leaching efficiency is defined as the ratio of the amount of the metal in post-leaching solution to the amount of the metal in the ore sample according to the formula (Eq.5):

$$E = \left(\frac{m}{m_0}\right) \cdot 100\% \tag{5}$$

where m is the total mass of the metal recovered in post-leaching solution and m_o is the total mass of the metal in the ore sample.

Many factors influence the leaching process among others, the kind and concentration of leaching medium, size of ore particles, liquid to solid ratio, temperature, pressure and the type of oxidizing agent.

The predominant process for recovery of uranium from rocks is the leaching with sulfuric acid [14–16]. The efficiencies of leaching in sulfuric acid environment reach 85–95%. However, this method is not appropriate for the leaching of uranium from carbonate rocks due to high acid consumption [17, 18]. It is worth to note that the alkaline leaching is more selective for uranium in comparison with acid processing. Uranium was selectively leached by the mixture of

sodium carbonate, sodium hydroxide and hydrogen peroxide from hydrous oxide Egyptian monazite [19] and from Polish ores [6, 12]. The leaching test using deionized water as a leaching solution (pH = 5.7) was also performed on Jordania carbonate rocks [20]. The leaching efficiency was 9% using deionized water as a leaching solution.

3.1. The leaching of Polish domestic ores

In Poland, as it was said earlier, there are occurred mainly two types of uranium ores: dictyonema shales and sandstones. The content of metals in post-leaching solution is very depending on the initial composition of the ore and the used procedure of extraction. The effect of ore mineralogy and mineral liberation on the leaching behavior of uranium and other metals is not well defined. For this reason, the prediction of results of the treatment of ores is not possible and it was necessary to make an experimental work. It showed that sandstones were more readily leachable in comparison with the dictyonema shales. In the leaching by acid, all metals accompanying uranium in the ores were also present in acid post-leaching solutions [6]. The best results of acid leaching of dictyonema shales were obtained in the leaching with 10% H_2SO_4 during 8 hours at 80°C. The efficiencies of uranium leaching from different ore materials were in the range of 64–81%. Other metals were leached with the following efficiencies: Th 67–80%, V 25–52%, Mo 33–78%, Cu 28–52% and La 31–66%. The leaching of sandstones with 10% sulfuric acid was carried out at 60°C. Uranium was leached with efficiency 71–100%; efficiencies of leaching other metals were: Th: 13–62%, Cu: 10–67%, Co: 8–57%, La: 24–60%, V: 28–58%, Yb: 26–67% and Fe: 11–47%.

In the case of alkaline leaching, only three or two metallic components of the ores were detected in post-leaching solution: U, Mo and V (dictyonema shales) or U and small amounts of V (sandstones). U from calcinated samples of dictyonema shales was extracted with 42% efficiency, molybdenum with 24% and vanadium with ca. 8% efficiency. In the case of sandstones, 57–92% of uranium and 2–22% of vanadium were leached with a mixture of sodium carbonate and bicarbonate. The comparison of uranium leaching efficiencies depending on lixiviant and leaching method is presented in **Figures 2** and **3**.

3.2. Recovery of uranium from the post-leaching solution

The above-described process, the solid–liquid extraction, is a very important stage in the technology of uranium production from the uranium ores. The separation of solid residue from liquid leaves the post-leaching solution that is a mixture of different metal ions. Uranium and other metals can be recovered from post-leaching solutions by solvent extraction [21–24] followed by stripping to aqueous phase [25, 26] or by ion exchange [27, 28].

3.2.1. Recovery of uranium by solvent-solvent extraction

Solvent extraction is a comprehensive technique for separation of ionic solutes. The uranyl ion (UO_2^{2+}) forms complexes with various extracting agents, among them tributylphosphate (TBP), di(2-ethylhexyl)phosphoric acid (DEHPA), triethylamine (TEA), tri-n-octylamine (TnOA), trioctylphosphine oxide (TOPO) and calixarenes, e.g. hexasodium 37,38,39,40,41,42-hexa(carboxymethoxy)calix[6]arene-7-5,11,17,23,29,35-hexasulfonate (**Figure 4**, calix[6]arene: $R^1 = SO_3Na$,

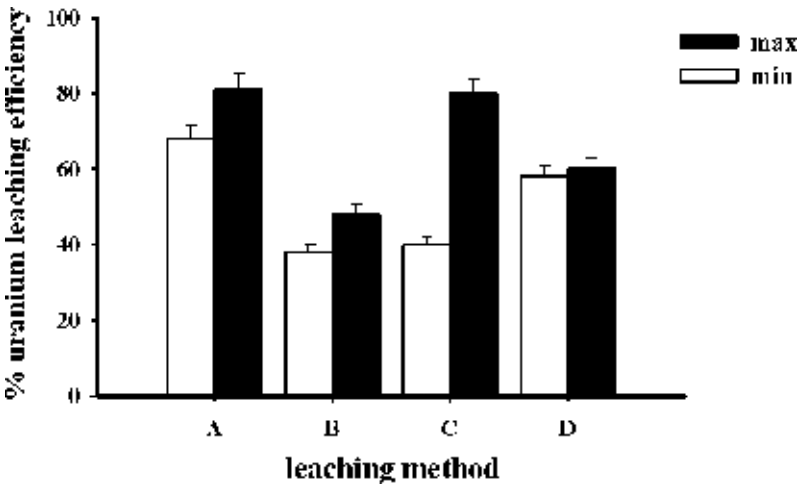

Figure 2. Efficiency of leaching uranium from dictyonema Shales using different methods. (A) Calcinated sample, lixiviant: 10% H_2SO_4, liquid/solid ratio of 8:1 (vol./wt. basis), oxidizing agent: MnO_2, 80°C, 8 h. (B) Calcinated sample, lixiviant: 5%Na_2CO_3/5%$NaHCO_3$, liquid/solid ratio of 8:1 (vol./wt. basis), oxidizing agent: MnO_2, 80°C, 8 h. (C) "acid-cure": 2 g of ground uranium ores were treated with 95% H_2SO_4 for 18 days, 25°C, 8 h. (D) Sintered sample with addition of 10% NaCl at 840°C during 3 h than leaching with 5% H_2SO_4, MnO_2, 80°C, 8 h.

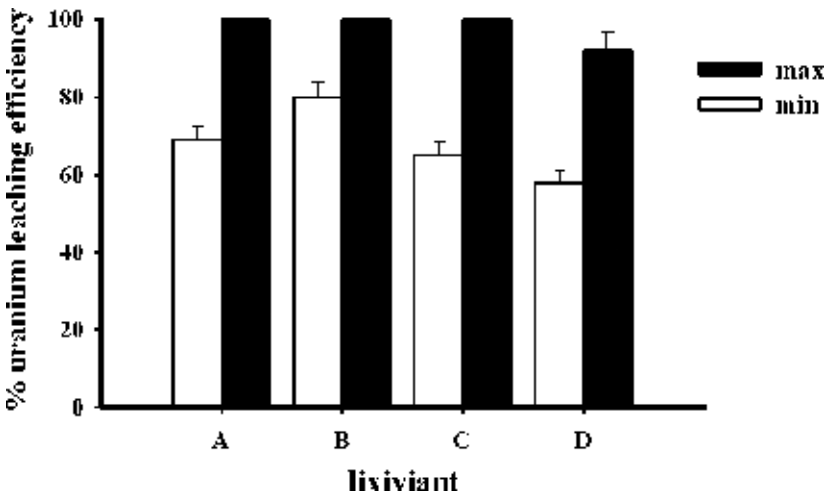

Figure 3. Efficiency of leaching uranium from sandstones by various lixiviants, liquid/solid ratio of 8:1 (vol./wt. basis). (**A**) 10% H_2SO_4, oxidizing agent: MnO_2, 60°C, 1 h. (**B**) 10% HCl, oxidizing agent: 30% H_2O_2, 60°C, 1 h. (**C**). 8% NaOH/18% Na_2CO_3, oxidizing agent: 30% H_2O_2, 60°C, 1 h. (**D**) 5% Na_2CO_3/5% $NaHCO_3$, oxidizing agent: $KMnO_4$, 60°C, 1 h.

R^2 = CH_2COOH). Calixarenes are a well-known family of macrocyclic molecules with broad field of potential applications in chemical, analytical and engineering materials area [29]. The reason of growing interest in these macrocycles is not only their easy synthesis through well-established and simple methods but also the possibility of shaping through functionalization with the appropriate groups R^1 and R^2. The calixarenes are applied for UO_2^{2+} complexation with high efficient results in terms of stability and selectivity [30].

TBP, neutral organophosphorus extractant, is probably the most known chelating agent. It was used on the commercial scale for the recovery of uranium (VI) not only from its ores but also from the spent nuclear fuel [31]. The selectivity of TBP is not high, similarly as its radiolytic stability. For this reason, other organophosphorus extractants, among them DEHPA, are applied in the technology of uranium production. DEHPA saponifies in stripping phase and wherefore the third phase is formed between the organic solvent and the aqueous phase. It can be prevented with a modifying agent, a suitable non-ionic surface active substance. The modifying agent like long-chain alcohols, alkyl phosphonates, alkyl phosphates and alkyl phosphine oxides have also a beneficial synergistic effect on the distribution ratio of uranium. One of such agents is TBP. The very good results were obtained in the extraction of uranium from the solutions resulting from leaching Polish uranium ores by using the mixture of DEHPA and TBP (0.2 M: 0.2 M) [32]. Before the solvent extraction, the post-leaching solutions were acidified to pH 1. This especially applied to the liquors from carbonate leaching. However, sometimes it was also necessary to adjust appropriate pH of the solution from acidic leaching. During the extraction process, uranium passes from the aqueous solution to the organic solution by using an extracting agent. The metal ions that have been extracted by the organic phase should be stripped by an aqueous phase in the stripping (re-extraction) process. A number of reagents are known in the literature to strip uranium from loaded extracting agents such as carbonates, acids, nitrates, chlorides, sulfates and hydroxides. In this study, the best results were obtained when stripping experiments were carried out with sodium carbonate or ammonium carbonate solutions. The extraction efficiency (%E) was calculated by the Formula (6):

$$\%E = \frac{100\,\% \cdot D_c}{D_c + \frac{V_{aq}}{V_{org}}} \tag{6}$$

where Dc is the distribution ratio, defined as the ratio of concentration of metal in organic phase over its concentration in aqueous phase, V_{aq} is the aqueous phase volume, and V_{org} is the organic phase volume [33].

The stripping percentage, %S was determined by the relationship (7):

$$\%S = \frac{100\,\% \cdot D_s}{D_s + \frac{V_{aq}}{V_{org}}} \tag{7}$$

where Ds is the distribution ratio of metal in stripping phase over its concentration in organic phase [33].

%R percent of the recovery of uranium in extraction/stripping process was determined by the relationship (8):

$$\%R = \frac{metal\ in\ the\ stripping\ phase}{metal\ in\ post-leaching\ liquor} \cdot 100\% \tag{8}$$

The obtained results were satisfying; the overall recovery (%R), extraction efficiency (%E) and stripping (%S) reached even 98%. Apart from uranium, the other elements were also analyzed. The results of extraction/stripping processes of alkaline and acidic post-leaching solutions are reported in **Tables 3** and **4**, respectively. The purification of uranium from accompanying metals from acid leaching solution was only in part. The efficiency of recovery of uranium

http://dx.doi.org/10.5772/intechopen.72754

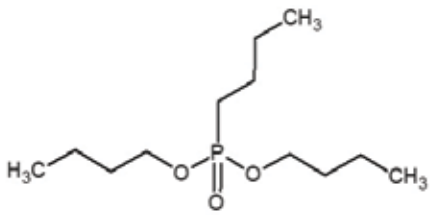

TRIBUTYLPHOSPHATE (TBP) TRIETHYLAMINE (TEA)

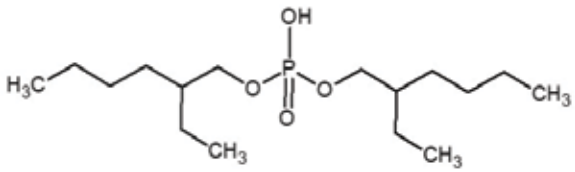

DI(2-ETHYLHEXYL)PHOSPHORIC ACID (DEHPA)

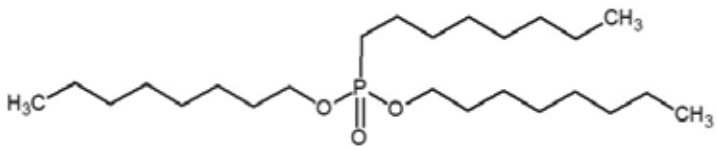

TRIOCTYLPHOSPHINE OXIDE (TOPO)

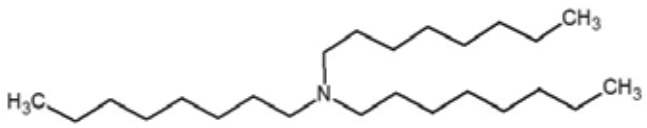

TRI-N-OCTYLAMINE (TnOA)

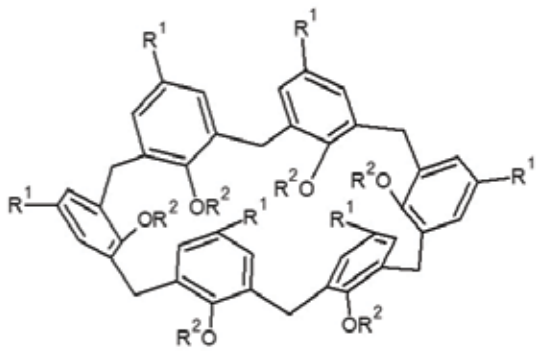

CALIX[6]ARENE

Figure 4. The extracting agents using for the separation of uranium from the solution.

Post-leaching solution		Extracting phase		Stripping phase 0.5 M $(NH_4)_2CO_3$			Stripping phase 0.5 M Na_2CO_3		
Metal	C_a [ppm][a]	C_b [ppm][b]	%E	C_c [ppm][c]	%S	%R	C_d [ppm][c]	%S	%R
U	25 ± 1.25	25 ± 1.25	100	24.7 ± 1.2	99	99	24.7 ± 1.2	99	99
Th	<0.1	—	—	—	—	—	—	—	—
Cu	14 ± 1.4	0	0	—	—	—	—	—	—
Co	0.5 ± 0.05	0	0	—	—	—	—	—	—
Mn	27 ± 2.7	0	0	—	—	—	—	—	—
La	0.2 ± 0.02	<0.001	<0.5	—	—	—	—	—	—
V	3 ± 0.3	0.75 ± 0.08	25	0.23 ± 0.02	31	8	0.23 ± 0.02	31	8
Mo	0.8 ± 0.08	0	0	—	—	—	—	—	—
Yb	0.2 ± 0.03	0.2 ± 0.03	100	0.19 ± 0.03	99	99	0.17 ± 0.03	85	85
Fe	230 ± 23	74 ± 7.4	32	21 ± 2.1	28	9	24 ± 2.4	32	10

[a] C_a—concentrations of metals in post leaching solution,
[b] C_b—concentrations of metals in organic phase from extraction process,
[c] C_c, C_d—concentrations of metals in stripping phase.

Table 3. Extraction and stripping efficiencies of metals from acidic post-leaching solution, [DEHP]:[TBP] 0.2 M:0.2 M, temperature: 22°C, pH 1, phase ratio (*organic/aqueous*) 1:1.

was high, but the final solution was contaminated by iron and small amounts of other metals: vanadium and ytterbium. On the other hand, the purification of uranium from alkaline post-leaching solution was almost complete (**Table 4**). The extraction, followed by stripping step gave pure uranium solution. It is worthy to mention that the single, one-stage extraction of uranium from acidic post-leaching liquors is not sufficient to separate pure uranium. Further purification and separation of uranium from accompanying metals could be performed by ion exchange chromatography or a sequence of ion exchange/extraction treatments.

3.2.2. Recovery of uranium by ion exchange

The ion exchange is a very efficient method that can be used for separation of uranium from other metals. The separation of uranium from acid pregnant leach solution obtained from Polish uranium ores, using commercially available, strongly basic anion exchanger, Dowex 1 was investigated [28]. The feed solution was introduced into the column. The complexes of uranium, vanadium and molybdenum were adsorbed on Dowex 1 and then they were eluted with 0.15 M H_2SO_4, followed by 1 M sulfuric acid. The first eluent removed the vanadium complex from the column. The second eluent allowed to obtain fraction of uranium complexes. The molybdenum complexes are very strongly fixed in anion exchange resin. They can be eluted only in part by 1 M H_2SO_4. Wherefore the uranium fraction can be contamined with molybdenum. It is worth to note that the purification of the acid pregnant solution from leaching of sandstones that does not contain the molybdenum gave a pure uranium fraction. In this work, there was also considered the recovery of other valuable metals present in uranium

Post-leaching solution		Extracting phase		Stripping phase 0.5 M $(NH_4)_2CO_3$			Stripping phase 0.5 M Na_2CO_3		
Metal	C_a [ppm][a]	C_b [ppm][b]	%E	C_c [ppm][c]	%S	%R	C_d [ppm][c]	%S	%R
U	20 ± 1	20 ± 1	100	19.8 ± 1	99	99	19.8 ± 1	99	99
V	0.63 ± 0.06	<0.01	—	—	—	—	—	—	—
Mo	0.72 ± 0.07	0	0	—	—	—	—	—	—

[a] C_a—concentrations of metals in post leaching solution,
[b] C_b—concentrations of metals in organic phase from extraction process,
[c] C_c, C_d—concentrations of metals in stripping phase.

Table 4. Extraction and stripping efficiencies of metals from alkaline post-leaching solution, [DEHP]:[TBP] 0.2 M:0.2 M, temperature: 22°C, pH 1, phase ratio (*organic*/*aqueous*) 1:1.

ores, especially the lanthanides. They can be separated from the effluent from anion exchange column by using the second column filled with strongly acidic cation exchanger (DOWEX50 WX8) (**Figure 5**) [5]. The efficiencies of recovery of metals were almost quantitative: 93% for uranium and 99% for lanthanides were recovered. The other metals accompanying uranium in their ores were not separated and were present in the effluent from columns.

3.3. Precipitation of uranium yellow cake

The solvent extraction and ion exchange processes were a part of the research on the possibility of uranium extraction from domestic resources in Poland. The next step was the precipitation of precursors of yellow cake - U_3O_8. From acidic solutions, uranium is precipitated in the form of ammonium or sodium diuranate, uranium peroxide and uranium trioxide by the addition of neutralizers such as sodium hydroxide, magnesium oxide or aqueous ammonia (**Figure 6**) [34, 35]. In all cases, the final product is yellow uranium salt, commonly known as yellow cake.

The studies of precipitation of uranium as two different salts: $(NH_4)_2U_2O_7$ and $UO_4{\cdot}2H_2O$ from the model uranium solution ($UO_2(NO_3)_2$ in 2 M H_2SO_4) were performed (respectively, Eqs. 9 and 10). As was proved, the influence of temperature and concentration of uranyl ions in the solution was significant. The precipitation of ammonium diuranate was carried out in the temperature range of 40–90°C, at pH 9–11. The concentration of uranium was between 0.3 and 0.7 mg/L. The obtained yield was really high 83–98% [36]. It is significant that this salt was precipitated from solutions containing a low concentration of uranium (0.3–0.5 mg/mL). The precipitation step was followed by calcination step at temperature 750°C, in which U_3O_8 was formed.

$$UO_2^{2+} + 6NH_{3(aq)} \rightarrow (NH_4)_2U_2O_7\downarrow + 4NH_4^+ + 3H_2O \quad (9)$$

This procedure was used for obtaining "yellow cake" from the effluent from anion exchanger, Dowex 1, that was described above. The yield was ca. 92% [28].

Uranium peroxide hydrates can be synthesized by dropping hydrogen peroxide to the acidic solution of uranyl ions, as it is shown in Eq. 8. Uranium peroxide can be precipitated from

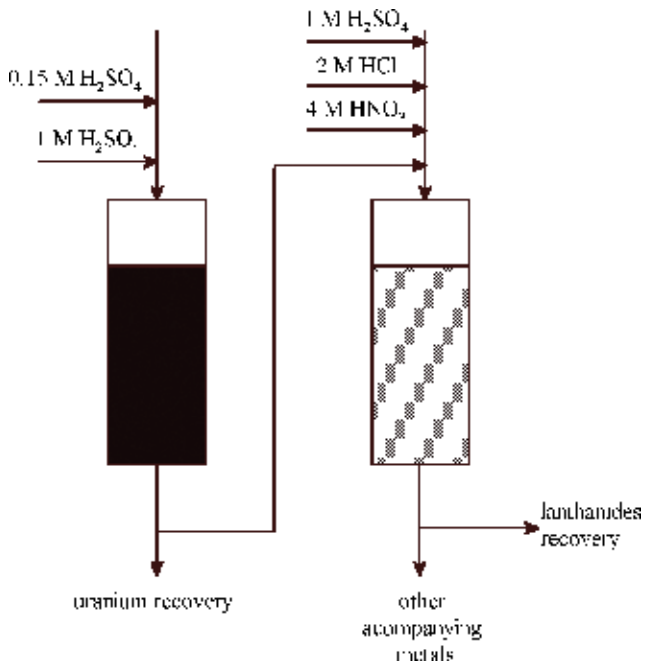

Figure 5. Set of two columns with strongly basic anion exchanger (DOWEX1 X8) and strongly acidic cation exchanger (DOWEX50 WX8).

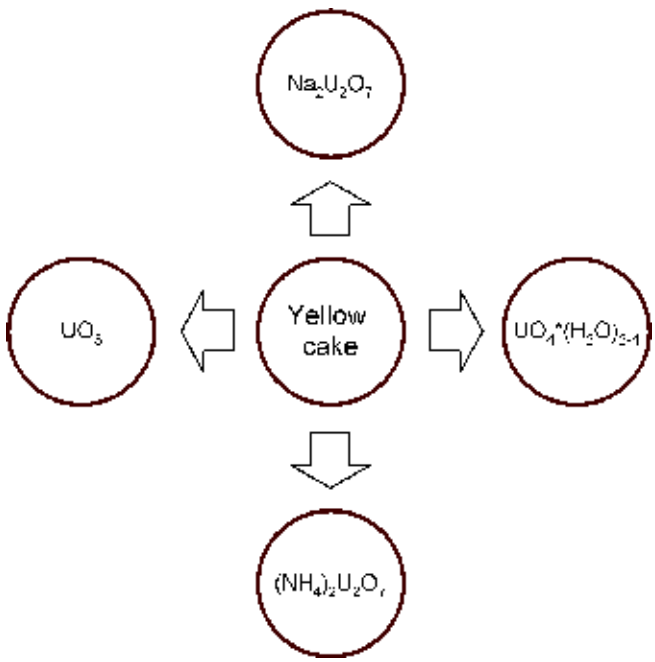

Figure 6. Precipitation of precursors of yellow cake.

eluted solution with concentration of uranium 0.5–0.9 g/L with high yield, almost quantitatively. It was found that optimal pH of the solution was between 9 and 11. The yield of the process provided at temperature 60°C was rather low, 17% for the solution with 0.5 g/L of uranium and 63% for the solution with 0.9 g/L of uranium. Increasing the temperature up to 90°C definitely improved efficiency, 93 and 99%, respectively.

$$UO_2^{2+} + H_2O_2 + 4\,H_2O \;\rightarrow\; UO_4 \cdot 2\,H_2O\downarrow + 2\,H_3O^+ \tag{10}$$

4. Novel methods of uranium extraction by using membrane methods

Membrane processes and effective separation techniques can be applied in uranium technology. The first of proposed applications of membrane techniques was leaching of uranium from the ores with separation of solid and liquid phases in a helical membrane contactor equipped with rotor. [37]. The second one was recovering of uranium from post-leaching solutions by using solvent extraction with application of the membrane contactors with polypropylene porous membranes [38].

4.1. Leaching of uranium using membrane contactor

As an alternative method of uranium leaching from the ores, the membrane contactor was proposed. The main advantage of using the membrane contactor is a possibility of combining two processes: leaching and separation of the solid phase from post-leaching solutions in one apparatus. Such an approach results in the reduction of total cost of operation with no consequences to the separation efficiency. Another advantage of using the membrane contactor is the possibility of conducting the leaching process at room temperature, which results in less energy consumption.

In the experiments, the membrane module with helical flow generated by rotating part, equipped with a tubular metallic membrane with the pore size of 0.1 μm, was applied. The scheme of the experimental set-up is presented in **Figure 7**. The sample of uranium ore with manganese dioxide, and a solution of 5% sulfuric acid, was placed in the stirred feed tank. Then, the suspension of uranium ore (feed) was transferred with a gear pump to the membrane contactor where the process of leaching was proceeded. The leaching process was conducted in a closed system, which means that permeate and retentate streams were recycled to the feed tank. The process parameters were as follows: velocity of the feed flow (Q_S) was changed in the range of 1.1×10^{-5}–2.2×10^{-5} m^3/s and rotation frequency of the rotor (Ω) from 0 to 2500 rpm.

The results of uranium leaching conducted in the membrane contactor were compared with those obtained in experiments carried out using mixer-settler system. Leaching process using mixer-settler system was described in detail elsewhere [12]. The process was conducted in the stirred tank at 80°C for 8 h, using 10% sulfuric acid. The results of the experiments are collected in **Table 5**. As can be observed results of experiments conducted in the membrane contactor were comparable to those obtained by leaching process conducted in the mixer-settler

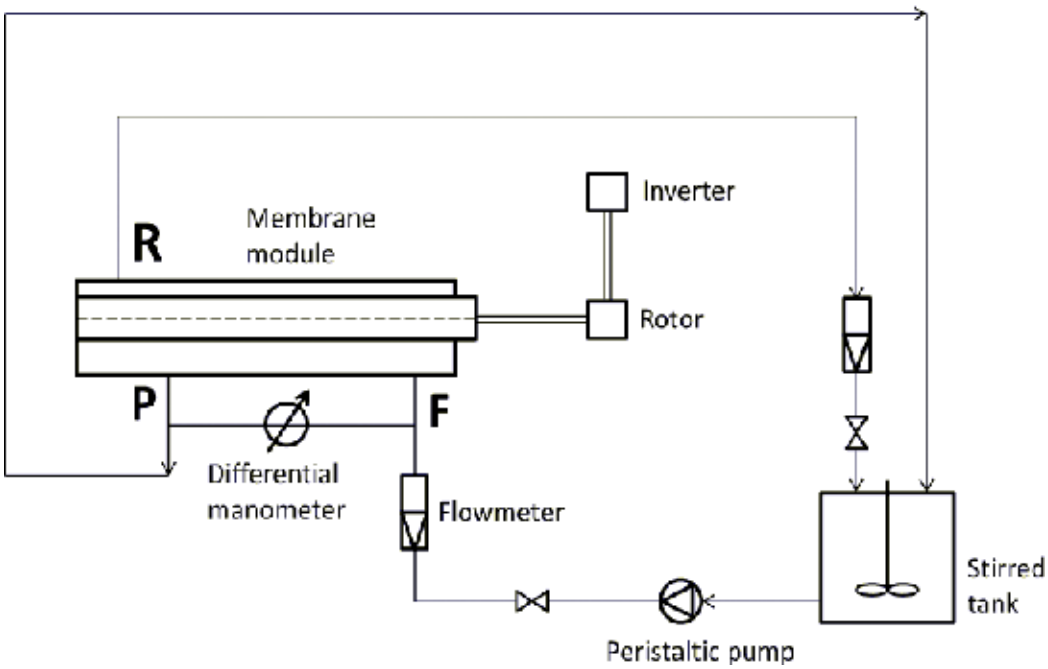

Figure 7. Experimental set-up for uranium leaching using membrane contactor.

system. The conducted experiments also have shown that both considered process parameters: velocity of the feed flow (QS) and a rotation frequency of the rotor (Ω) had an influence on the leaching efficiency of uranium and associated metals. When the velocity of the feed flow is considered, it can be noticed that an increase of this parameter results in an increase in the leaching efficiency of all analyzed metal ions. The increase in the rotation frequency of the rotor led to an increase in the leaching efficiency. However, this relation is clear only for the lower velocity of the feed flow (QS = 1.1× 10–5 m^3/s). In case of higher feed velocity, a visible improvement in leaching efficiency with increasing the rotation frequency was not observed.

4.2. Extraction of uranium using membrane contactor

The new approach for the liquid–liquid extraction of uranium involves the membrane contactor which enables effective contact of two phases engaged in the process. The two phases are separated by the membrane and species are transferred from one phase to the other by the diffusion mechanism. During the extraction in the membrane contactor, ions are received by the organic phase from the feed (aqueous phase) until thermodynamic equilibrium is reached.

In the experiments, an installation for extraction of uranium equipped with the membrane Liqui-Cel® Extra-Flow contactor produced by CELGARD was used. The scheme of the installation is presented in **Figure 8**.

The module contains microporous hollow fiber membranes made of a polypropylene (PP). The experimental set-up consists also of thermostat, two micropumps, flow meter and temperature sensor. The first stage of the work was a selection of process conditions. Appropriate selection of

Leaching in the membrane contactor					
Process parameters		**Leaching efficiency, %**			
Q_s, [m^3/s]	Ω, [rpm]	U	La	Th	V
1.1×10^{-5}	0	49.2	21.2	57.9	14.2
1.1×10^{-5}	1000	54.6	64.9	57.4	16.9
1.1×10^{-5}	1500	53.9	67.0	62.5	18.2
2.2×10^{-5}	0	67.5	75.9	75.9	21.8
2.2×10^{-5}	1000	68.9	77.9	64.6	25.6
2.2×10^{-5}	1500	56.7	65.5	65.5	18.0
2.2×10^{-5}	2000	45.7	61.0	59.7	16.7
2.2×10^{-5}	2500	63.9	94.1	25.8	25.1
Leaching in the mixer and settler system					
Process conditions			Uranium leaching efficiency, %		
80°C, 8 h			73.0		

Table 5. Leaching efficiency of uranium and accompanied metals obtained by two different methods of leaching.

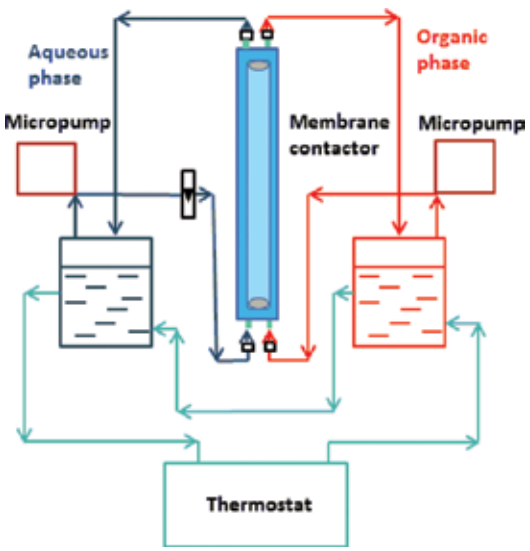

Figure 8. The scheme of the installation for extraction of uranium using membrane contactor.

hydrodynamic conditions in the membrane contactor eliminated the possibility of wetting the membrane and allowed stable working conditions of the apparatus. After a series of preliminary studies, it was found that a proper flow rate for the aqueous and organic phase (feed) is 98.11 and 5.95 L/h, accordingly. The flow of two phases in the system was arranged in co-current mode.

The next step of the work was a selection of extracting agents appropriate for the membrane process. Tributyl phosphate (TBP), triethylamine (TEA), di(2-ethylhexyl)phosphoric acid (DEHPA), tri-n-octylamine (TnOA) and trioctylphosphine oxide (TOPO) (see **Figure 4**) were considered as a potential extracting agents. The extraction efficiency (%E) was calculated by Eq. 6 (see above).

After preliminary experiments comprising determination of extraction efficiency, di(2-ethylhexyl)phosphoric acid (DEHPA) was found to be most favorable. The tests were performed using both model and real solutions. The results of experiments carried out using the model solution of uranyl nitrate in 5% H_2SO_4 are summarized in **Figure 9**. They show that the kinetics of membrane extraction is similar for different concentrations of uranium. However, the fastest extraction occurred for solutions with low concentrations of uranium. For concentration of 0.1 g/L, extraction efficiency reached a constant value after less than 1 h, while for concentration of 0.3 g/L equilibrium state was reached after about 2 h. It was also proved that an initial uranium concentration has great importance for extraction efficiency. The highest efficiency of the extraction process, reaching over 90%, was achieved in case of the solution with a concentration of 0.1 g/L, while the lowest with a concentration of 0.3 g/L.

The integrated process of extraction and stripping conducted in continuous mode was also investigated. This process includes two membrane modules, one for extraction and the other for back extraction. It was proved that in case of extraction/stripping process of real post-leaching solutions the high values of stripping and recovery of uranium were obtained. Using this process, it is possible to remove some metallic components from post-leaching liquors like Cu, Co and Ni. Such metals like Zn, Cr, Mo and Sb present in the ores were removed at the acid leaching stage.

Application of the membrane processes in the technology of the uranium recovery is very beneficial. The membrane contactors can be applied for recovery of uranium and associated metals from uranium ores as well as for the extraction of uranium from the post-leaching solutions.

Extraction with the use of membrane contactors has many advantages over conventional methods of the extraction of uranium, like no fluid/fluid dispersion, no emulsion formation, no flooding at high flow rates, low solvent holdup, known and constant interfacial area, easy

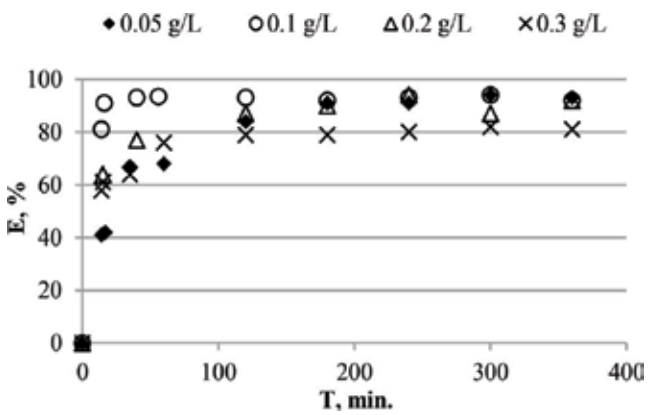

Figure 9. Efficiency of the extraction of uranium in the membrane contactor depending on the initial concentration of uranium in the feed solution.

upscaling, etc. However, some drawbacks also exist, among others concentration polarization and fouling [39]. There is also the risk of wetting the membranes during long-term operation of the module resulting in mixing of the two phases. For the proper operation of membrane contactors, it is important to maintain appropriate hydrodynamic conditions for flow of solutions over the membrane surface in order to eliminate such unfavorable phenomena.

5. Tentative economic analysis

In the case of low-grade uranium ores it is important to carry out a detailed geo-economic analysis, which will be aimed at reliable estimation of the cost of ore extraction. The costs of further technological processes of uranium recovery from the extracted ore in the initial phase are less important, because they can be very different, taking into account technological progress. While the cost of the mine construction and extraction of rocks on the surface, even in the long term, are not subject of significant changes.

In the case of the so-called Rajsk deposit, detailed geological and geochemical data were available. This allowed the development of a detailed mine model. Moreover, because the structure and form of uranium concentration of Lower Ordovician dictyonema Shales are similar to the Zechstein copper deposits exploited on a large scale on the Fore-Sudetic Monocline, there was a possibility to apply current costs of mining excavations, machinery and equipment as well as human labor.

In developing the model of mine adopted a number of assumptions resulting from the analysis of geological data and technology as well as the assumed concept of mining operation.

The deposit has an area of 16 km^2, occurs at a depth of 400 to 550 m, the average thickness of the uranium-rich rocks is 2.88 m, and the average uranium content is 69 ppm. Recovery of uranium from the ore was assumed at 65% [12]. Based on these parameters of deposits, it was assumed that the operating time of the potential mine will be 24 years, with an annual production capacity of the mine about 4 million Mg/year, which will allow uranium mining about 270–300 Mg per year, and taking into account the uranium recovery from the ore will allow the uranium production of approximately 200 Mg/year [40]. This quantity is necessary for the operation of 1 GWe nuclear power plant.

Taking into account all the above assumptions, it was calculated that the cost of extraction of the ore needed to production of 1 kg yellow cake (commercial product of uranium) will be about $ 800. This cost does not include the cost of technological processing of the ore, which will be quite high due to the low uranium content in the ore and its occurrence mainly in the form of organometallic compounds, which significantly reduce the uranium recovery. To assess the economic value of this occurrence of uranium ore, it should be compared to the price of a commercial product on the world market. Historically, the highest price of yellow cake at the turn of 2007/2008 was around $ 175/kg and was extremely speculative. The price of this product in 2015 was about $ 80/kg. The developed model of the exploitation of the deposit and based on it the evaluation of the cost of obtaining uranium ore from Lower Ordovician dictyonema shale (Podlasie Depression) justifies the statement of unprofitable extraction of uranium from this rock formation in a very long time perspective [3].

6. Environmental impact and radiation protection connected to uranium production in Poland

Radiation protection aims at protecting the health and life of humans and animals as well as protecting the environment from the harmful effects of ionizing radiation. Working with uranium is associated with the risk of exposure to ionizing radiation. In order to reduce the risk to a reasonable minimum, strategies and rules for radiological protection have been introduced worldwide. Radiological protection is largely based on the recommendations of three institutions: the International Commission for Radiation Protection (ICRP), the International Atomic Energy Agency (IAEA) and the Euratom Directives. Usually, the guidelines described in the publications of these institutions are implemented in the law of each country.

Of the various uranium isotopes, U-238 is the most common, accounting for 99.3% of uranium in the earth's crust. U-238 is the beginning of a uranium series of decay chain consisting of 15 radioactive elements with different half-life and terminating with Pb-206 permanent lead isotope. The radioactivity associated with uranium corresponds not only to uranium but also to a greater extent to its decay products and, in particular, to the noble gas radon (Rn-222). It should be emphasized that radiation exposure from uranium and its derivatives is considered natural and present in every corner of the earth. Radon exposure is the largest part of the effective dose received from the environment by a statistical person in Poland and it approximately equals 1.36 mSv/year [41]. Isotopes from the uranium decay series emit both α and β particles. During α-decay, γ-radiation is also emitted. From the radiation protection point of view matter both the type of emitted radiation and the physical form of the emitter. The α radiation is 20 times more effective than the β or γ radiation, but its penetration is small—it is completely retained by a sheet of paper or skin. Generally, the α radiation is not harmful to health as long as the emitter does not get inside the body. This happens mainly through drinking water or—in the form of dust, aerosol or noble gas—transferred to the lungs. The γ-radiation has a greater penetrating power than β-radiation and can therefore be an important component of the absorbed dose.

Uranium is being mined in many parts of the world because it is a basic element used as a fuel for nuclear power and for military purposes. Radiation protection refers to uranium at each stage of the fuel cycle: from ore extraction, milling, to yellowcake (triuranium octoxide) production, further enrichment, fuel elements production, fission reaction at power plants for processing, to storage and disposal of spent fuel.

From the late 1940s to the 1970s, in Poland, uranium ore was mined and processed in Lower Silesia. The ore was extracted by the classical method—the material was brought out from the underground to the surface and collected in heaps [3]. The uranium ore was then split to the rich ore, the poor ore and the gangue rocks [42]. The rich ore went directly to the Soviet Union. The poor ore was enriched on site and the resulting concentrate was exported to the Soviet Union. Mining and reprocessing of uranium was performed by the "Kowary Mines. State-owned Extraordinary Enterprise," based in Kowary, later renamed "R1 Industrial Plant." At that time, probably no radiological protection standards were met, and miners may not exactly know what they were extracting and how it could affect their health.

There are a number of uranium ore mining sites in 13 locations at Lower Silesia: heaps with varied concentration of uranium ore—the highest values up to 2000 ppm, open shafts, mine

tunnels, and sedimentation ponds [43]. Most shafts and tunnels are protected against unauthorized entry. So far, almost no attempts have been made to reclaim these areas. Exceptions are reclamation of the sediment tank in Kowary and the protection of some dumps being washed by water [44]. This area is covered by radiation monitoring of the National Atomic Energy Agency (PAA) as an area with increased levels of ionizing radiation from naturally occurring radioactive materials as a result of human activity [for example, see [41, 45]]. The monitoring consists mainly of investigating the α and β total activity and the level of radon in drinking water and mining effluents—60 measuring points, measuring gamma radiation dose in air (62 measurement points) and radon concentration in air. Measured levels in drinking water do not exceed the reference levels specified in the recommendations of the World Health Organization Guidelines for drinking-water quality, Vol. 1 Recommendations. Geneva, 1993: 100 mBq/dm^3 for total α activity and 1000 mBq/dm^3 for total β activity. These levels are often exceeded in mined water. As far as radon is concerned, the activity happens to exceed the limit of 100 Bq/dm^3, which is acceptable for drinking water points established by the EU Directive 2013/59/ EURATOM and for water from excavation can exceed 700 Bq/dm^3. Despite this, the PAA's annual reports state that "although water from mining excavations, surface water and groundwater are not intended for use as drinking water and do not present a direct health risk, they should continue to be systematically monitored for their increased radioactivity" and "generally speaking, even in this region of Poland, with the highest possible risk from radon and from natural radioactive elements in the soil, this threat to the local population is negligibly small" [41]. The PAA reports lack of information about the increased radioactivity of uranium heaps. Meanwhile, research carried out under the Strategic Research Project, "Technologies supporting the development of safe nuclear power" in 2010–2012 by a consortium led by the University of Warsaw showed elevated levels of radiation and elevated uranium in the soil in many places (among other uranium heaps in Lower Silesia) in Poland. The authors suggested that such places should be labeled, and preferably fenced [46].

The possible impact of uranium heaps on the environment is further taken into consideration. This can happen through water erosion of heaps and migration of heavy metals, including uranium and radium isotopes to groundwater and underground waters, and to soils in the area. Increased uranium content and radioactivity were observed in river beds flowing from these areas, even up to 20 km from the heaps (e.g. Jedlica river) [44]. Uranium, radium and associated heavy metals can spread and accumulate in organisms—through the food chain. The elevated level of radionuclides possibly increases the natural radiation dose to organisms. It seems that the harmfulness of uranium for organisms is not determined by its radioactivity, but rather by its chemical toxicity and that of the other accompanying heavy metals. So far, there has been no systematic study aimed to determine how uranium concentrations and elevated background radiation affect the individual organisms and ecosystems.

Lower Silesia is not the only area where elevated uranium level can have an impact on the environment. Uranium is also abundant in the material deposited on heaps after copper mining in Legnica-Głogów Copper District or on heaps formed after the production of phosphoric acid and phosphate fertilizers in Police, Wizów and Wiślinka near Gdańsk [47]. Radiological risk in these places should be considered negligible. The threat to the environment probably is related to other heavy metals and elements rather than to uranium.

From the point of view of radiation protection and environmental impact, the uranium industry in Poland does not cause any major threat. Uranium mining and processing activities were completed 40 years ago—at present, there is no nuclear power industry or military technology related to uranium. There are uranium mine residues in Lower Silesia, and there is an increase in the levels of ionizing radiation caused by human activity associated with uranium, but there is no evidence of a radiological hazard to humans or a significant environmental hazard connected to it.

7. Conclusion

The characteristics of Polish low-grade uranium resources were presented in the paper.

The set of methods and technology scheme that could be implemented to extract uranium from low-grade ores and other raw materials were shown. Uranium can be recovered with high efficiency by solid–liquid extraction (almost 100% efficiency), followed by liquid–liquid extraction or/and ion exchange methods. The synergistic mixture of DEHPA and TBP (0.2 M:0.2 M) together with $(NH_4)_2CO_3$ as a stripping agent were found as a good route for uranium recovery (99% of yield). The study of the precipitation of yellow cake in different forms, e.g. $(NH_4)_2U_2O_7$ and $UO_4{\cdot}H_2O$, was carried out with high efficiencies reaching 98%. The simultaneous recovery of other valuable metals, such as lanthanides, could improve the economics of proposed technology.

The studies performed revealed the feasibility of the proposed technology; however, its profitability in the current uranium supply could be questioned. The environmental impact and related risk from uranium mining and processing in Poland were discussed.

Acknowledgements

The work support by the financial resources for science in the years 2017–2018 granted for the implementation of the international project co-financed 3643/IAEA/16/2017/0 and IAEA Research Contract No: 18542.

Author details

Katarzyna Kiegiel[1]*, Agnieszka Miskiewicz[1], Dorota Gajda[1], Sylwester Sommer[1], Stanislaw Wolkowicz[2] and Grazyna Zakrzewska-Koltuniewicz[1]

*Address all correspondence to: k.kiegiel@ ichtj.waw. pl

1 Institute of Nuclear Chemistry and Technology, Warsaw, Poland

2 Polish Geological Institute, National Research Institute, Warsaw, Poland

References

[1] Klementowski R. In the shadow of Sudetic Uranium. Uranium mining in 1948-1973. IPN Wrocław; 2010 (in Polish) (ISBN: 978-83-61631-12-6l)

[2] Uranium 2016. Resources, Production and Demand, A Joint Report by the OECD Nuclear Energy Agency and the International Atomic Energy Agency, Paris: OECD; 2014 (ISBN: 978-92-64-17803-8)

[3] Miecznik B, Strzelecki R, Wołkowicz S. Uranium in Poland—History of prospecting and chances for finding new deposits. Przegląd Geologiczny. 2011;**59**:688-697 (in Polish, abstract in English)

[4] Dahlkamp FJ. Uranium Deposits of the World. Europe: Springer-Verlag GmbH; 2016 (ISBN 978-3-662-53462-5)

[5] Kiegiel K, Zakrzewska-Kołtuniewicz G, Gajda D, Miśkiewicz A, Abramowska A, Biełuszka P, Danko B, Chajduk E, Wołkowicz S. Dictyonema black shale and Triassic sandstones as a potential sources of uranium. Nukleonika. 2015;**60**:515-522. DOI:10.1515/nuka-2015-0096

[6] Gajda D, Kiegiel K, Zakrzewska-Kołtuniewicz G, Chajduk E, Bartosiewicz I, Wołkowicz S. Mineralogy and uranium leaching of ores from Triassic Peribaltic Sandstones. Journal of Radioanalytical and Nuclear Chemistry. 2015;**303**:251-529. DOI: 10.1007/s10967-014-3362-0

[7] Analysis of the possibility of uranium supply from domestic resources", No POIG 01.01.02-14-094/09 – project report (in Polish)

[8] Kiegiel K. Abramowska A, Biełuszka P, Zakrzewska-Kołtuniewicz G, Wołkowicz S. Solvent extraction of uranium leach solution obtained in processing of Polish low-grade ores. Journal of Radioanalytical and Nuclear Chemistry. 2017;**311**:589-598. DOI 10.1007/s10967-016-5029-5

[9] Zakrzewska-Koltuniewicz G, Herdzik-Koniecko I, Cojocaru C, Chajduk E. Experimental design and optimization of leaching process for recovery of valuable chemical elements (U, La, V, Mo and Yb and Th) from low-grade uranium ore. The Journal of Hazardous Materials. 2014;275136-145. DOI: 10.1016/j.jhazmat.2014.04.066

[10] Edwards CR, Oliver AJ. Uranium Processing: A Review of current methods and technology. Journal of Operations Management. 2000;**52**:12-20. DOI: 10.1007/s11837-000-0181-2

[11] Lunt D, Boshoff P, Boylett M, El-Ansary Z. Uranium Extraction: The key process drivers The Journal of the Southern African Institute of Mining and Metallurgy. 2007;**107**:419-426

[12] Frąckiewicz K, Kiegiel K, Herdzik-Koniecko I, Chajduk E, Zakrzewska-Trznadel G, Wołkowicz S, Chwastowska J, Bartosiewicz I. Extraction of uranium from low-grade Polish ores: Dictyonemic shales and sandstones. Nukleonika. 2012;**58**:451-459

[13] Chajduk E, Bartosiewicz I, Pyszynska M, Chwastowska J, Polkowska-Motrenko H. Determination of uranium and selected elements in Polish dictyonema shales and sandstones by ICP-MS. Journal of Radioanalytical and Nuclear Chemistry. 2013;**295**: 1913-1919. DOI: 10.1007/s10967-012-2330-9

[14] Lottering MJ, Lorenzen L, Phala NS, Smit JT, Schalkwyk GAC. Mineralogy and uranium leaching response of low grade South African ores. Minerals Engineering. 2008;**21**:16-22. DOI: 10.1016/j.mineng.2007.06.006

[15] Guettaf H, Becis A, Ferhat K, Hanou K, Bouchiha D, Yakoubi K, Ferrad F. Concentration-purification of uranium from an acid leaching solution. Physics Procedia. 2009;**2**:765-771. DOI: 10.1016/j.phpro.2009.11.023

[16] Kim JS, Chung KW, Lee HI, Yoon HS, Kumar JR. Leaching behaviour of uranium and vanadium using strong sulphuric acid from Korean black shale ore. Journal of Radioanalytical and Nuclear Chemistry. 2014;**299**:81-87. DOI: 10.1016/j.phpro.2009.11.023

[17] Mason CFV, Turney WRJR, Thomson BM, Lu N, Longmire PA, Chisholm-Brause CJ. Carbonate Leaching of Uranium from contamined Soils. Environmental Science & Technology. 1997;**31**:2707-2711. DOI: 10.1016/j.phpro.2009.11.023

[18] Bajwa I, Nawaz H, Bhatti TM. Uranium solubilization from rock phosphate in carbonate leaching media. International Journal of Agriculture and Biology. 2000;**2**:24-28. DOI: 1560-8530/2000/02-1-2-24-28

[19] El-Nadi YA, Daoud JA, Aly HF. Modified leaching and extraction of uranium from hydrous oxide cake of Egyptian monazite. International Journal of Mineral Processing. 2005;**76**:101-110. DOI:10.1016/j.minpro.2004.12.005

[20] Alsabbagh A, Zaidan L, Harahsheh I, Ba Sunbul N, Landsberger S. Investigation of Jordanian uranium resources in carbonate rocks. Journal of Radioanalytical and Nuclear Chemistry. 2016;**308**:1063-1070. DOI: 10.1007/s10967-015-4518-2

[21] Kumar JR, Kim J-S, Lee J-Y, Yoon H-SA. brief review on solvent extraction of uranium from acidic solution. Separation and Purification Reviews. 2011;**40**:77-125. DOI: 10.1080/15422119.2010.549760

[22] Zhu Z, Pranolo Y, Cheng CY. Uranium solvent extraction and separation from vanadium in alkaline solutions. Separation Science and Technology. 2013;**48**:1402-1408. DOI: 10.1080/01496395.2012.738277

[23] Awwad NS. Equilibrium and kinetic studies on the extraction and stripping of uranium(VI) from nitric acid medium into triphenylphosphine oxide using a single drop column technique. Chemical Engineering and Processing. 2004;**43**:1501-1509. DOI: 10.1016/j.cep.2004.02.005

[24] El-Reefy SA, Awwad NS, Aly HF. Liquid–liquid extraction of uranium from phosphoric acid by HDEHP–CYANEX-921 mixture. Journal of Chemical Technology & Biotechnology. 1997;**69**:271-275

[25] Khorfan S, Shino O, Wahoud A, Dahdouh A. Stripping of uranium from D2EHPA/TOPO solvent by ammonium carbonate solutions. Periodica Polytechnica Ser Chemical Engineering. 2000;**44**:123-132

[26] Daoud JA, Zeid MM, Aly HF. Tetravalent uranium extraction by HDEHP in kerosene from phosphate medium. Solvent Extraction and Ion Exchange. 1997;**15**:203-217. DOI: 10.1080/07366299708934474

[27] Ladeira ACQ, Gonçalves CR. Influence of anionic species on uranium separation from acid mine water using strong base resins. Journal of Hazardous Materials. 2007;**148**: 499-504. DOI: 10.1016/j.jhazmat.2007.03.003

[28] Danko B, Dybczyński RS, Samczyński Z, Gajda D, Herdzik-Koniecko I, Zakrzewska-Kołtuniewicz G, Chajduk E, Kulisa K. Ion exchange investigation for recovery of uranium from acidic pregnant leach solutions. Nukleonika. 2017;**62**:213-221. DOI: 10.1515/nuka-2017-0031

[29] Gutsche CD. Calixarenes. An introduction, 2nd ed., Cambridge: Royal Society of Chemistry; 2008. p. 86-87 and references therein. DOI: 10.1039/9781847558190

[30] Kiegiel K, Steczek L, Zakrzewska-Trznadel G. Application of calixarenes as macrocyclic ligands for uranium (VI): A Review. Journal of Chemistry. 2013, Article ID762819. 16 pages. DOI: 10.1155/2013/762819

[31] Musikas C, Schulz WW. Solvent extraction in nuclear science and technology. In: Rydberg J, Musikas C, Choppin GR, editors. Principles and Practices of Solvent Extraction. New York: Marcel Dekker; 1992. p. 413-447

[32] Kiegiel K, Abramowska A, Biełuszka P, Zakrzewska-Kołtuniewicz G, Wołkowicz S. Solvent extraction of uranium from leach solutions obtained in processing of Polish low grade ores. Journal of Radioanalytical and Nuclear Chemistry. 2017;**311**:589-598. DOI: 10.1007/s10967-016-5029-5

[33] Kumar JR, Kim JS, Lee JY, Yoon HAS. Brief review on solvent extraction of uranium form acidic solutions. Separation & Purification Reviews. 2014;**40**:77-125. DOI: 10.1080/15422119.2010.549760

[34] ElshafeeaHY AbowSlama, Ebraheem E, Sam AK. Precipitation and purification of uranium from rock phosphate. Journal of Radioanalytical and Nuclear Chemistry. 2014;**299**:815-818. DOI 10.1007/s10967-013-2703-8

[35] Paik S, Biswas S, Bhattacharya S, Roy SB. Effect of ammonium nitrate on precipitation of ammonium diuranate (ADU) and its characteristics. Journal of Nuclear Materials. 2013;**440**:34-38. DOI: 10.1016/j.jnucmat.2013.04.011

[36] Kiegiel K, Abramowska A, Gajda D, Zakrzewska-Kołtuniewicz G. The study of precipitation of yellow cake for production of nuclear fuel. Annual Report 2014, Institute of Nuclear Chemistry and Technology, 36-37

[37] Miśkiewicz A, Zakrzewska-Kołtuniewicz G, Dłuska E, Walo PF. Application of membrane contactor with helical flow for processing uranium ores. Hydrometallurgy. 2016:163108-163114. DOI: 10.1016/j.hydromet.2016.03.017

[38] Biełuszka P, Zakrzewska-Trznadel G, Chajduk E, Dudek J. Liquid-liquid extraction of uranium(VI) in the system with a membrane contactor. Journal of Radioanalytical and Nuclear Chemistry. 2014;**299**:611-619. DOI: 10.1007/s10967-013-2796-0

[39] Pabby AK, Sastre AM. State-of-the-art review on hollow fibre contactor technology and membrane-based extraction processes. Journal of Membrane Science. 2013:430263-430303. DOI: 10.1016/j.memsci.2012.11.060

[40] Galica D Dunst N, Wołkowicz S. The use of a digital model of the deposit and the production schedule to create a concept of a uranium deposit Rajsk. Wiadomości Górnicze. 2016;**67**:94-99 (in Polish, abstract in English)

[41] Niewodniczański J. Activities of the President of the National Atomic Energy Agency and assessment of nuclear safety and radiological protection in Poland in 2007 (in Polish). Warsaw. 2008. Available from: http://www.paa.gov.pl/sites/default/files/Raport_PAA_2007.pdf

[42] Koszela J. Engineering geological aspects of the pond remediation of the uranium mills tailings in Kowary (in Polish). Geologos. 2007;**11**:227-237

[43] Zakrzewska-Kołtuniewicz G, Kiegiel K, Miśkiewicz A, Sommer S, Roubinek O, Gajda O, Abramowska A, Kalbarczyk P, Bartosiewicz I. Unconventional resources of uranium in Poland (in Polish). Warsaw: Report filed in Institute of Nuclear Chemistry and Technology; 2015

[44] Grabas K. Environmental hazard in the area of the former uranium ore mine "Podgórze" in Kowary. Environment Protection Engineering. 2009;**35**:127-137

[45] Przybycin A. Annual Report. Activities of the President of the National Atomic Energy Agency and assessment of nuclear safety and radiological protection in Poland in 2016. Warsaw 2017. Available from: http://www.paa.gov.pl/paa/web/uploads/pub/pages/page_156/text_images/PAA_ Annual_Report_2016_printable.pdf

[46] Drewniak Ł. Waste repository of uranium mining in the Sudeten—The level of radiation and the possibility of its limitation. Bezpieczeństwo Jądrowej i Ochrona Radiologiczna, Biuletyn PAA. 2014;**4**:22-26

[47] Skwarzec B, Boryło A, Kosińska A, Radzajewska S. Polonium (210Po) and uranium (234U, 238U) in water, phosphogypsum and their bioaccumulation in plants around phosphogypsum waste heap at Wiślinka (northern Poland). Nukleonika. 2010;**55**:187-193

Chapter 5

Remotely Monitoring Uranium-Enrichment Plants with Detection of Gaseous Uranium Hexafluoride and HF Using Lidar

Gholamreza Shayeganrad

Additional information is available at the end of the chapter

http://dx.doi.org/10.5772/intechopen.73356

Abstract

A sudden release of UF_6 inside a building or to the atmosphere could conceivably cause undesirable health effects to workers and the public in general, mainly associated with the exposure to hydrolysis products HF and UO_2F_2. Although the hydrolysis reaction of UF_6 is fast, after escaping of UF_6 into the atmosphere, besides HF and UO_2F_2, UF_6 may also be found in the atmosphere. This chapter proposes a real-time technique to provide information to technical personnel and facility operators on the atmospheric release of UF_6 to ensure that the workers, the public, and the environment are adequately protected. The system comprises a combined differential absorption lidar (DIAL) and Raman lidar to detect gaseous UF_6 and HF, simultaneously. The DIAL provides information on UF_6 concentration using a frequency-quadrupled Nd:YAG laser at 266 nm as the off-wavelength and a Nd:-YAG-pumped Coumarin 450 dye laser using a Littrow grating mounting operating in the frequency doubled at 245 nm as the on-wavelength. Recording Raman scattering of molecular HF at wavelength of 297.3 nm (with Raman frequency shift of 3959 cm^{-1}) is a versatile technique to identify HF as a probe for real-time detection and localization of UF_6 leaks.

Keywords: uranium hexafluoride, hydrogen fluoride, uranium-enrichment plants, fuel cycle facilities, differential absorption lidar (DIAL), Raman lidar

1. Introduction

The raw material for today's nuclear fuel is uranium which first discovered in eighteenth century. Natural uranium consists primarily of two isotopes, 99.3% is U-238 and 0.7% is U-235. The fission process, by which heat energy is released in a nuclear reactor, takes place

mainly in U-235 which can sustain a chain reaction; a reaction in which each fission produces enough neutrons to trigger another, so that the fission process can maintain without any external source of neutrons. In contrast, uranium-238 cannot sustain a chain reaction, but it can be converted to plutonium-239 by high-energy neutrons, which can sustain a chain reaction and release large amounts of energy and is therefore often used to enhance the explosive power of thermonuclear, or hydrogen, bombs [1]. Plutonium-239, virtually nonexistent in nature, was used in the first atomic bomb tested July 16, 1945 and in the one that was dropped on Nagasaki on August 9, 1945. U-234 is a highly radioactive, but it is not useful in any applications.

In 1938, German physicists Otto Hahn and Fritz Strassmann showed that uranium could split into parts to yield lighter elements, neutrons, and energy. For instance, U-238, with half-life of about 4.5 billion years, decays by alpha emission into daughters like thorium-234, which itself decays by beta emission to protactinium-234, which decays by beta emission to uranium-234, and so on. After several more alpha and beta decays, the series ends with the stable isotope lead-206 [1]. Alpha particles have less penetrating than other forms of radiations and weak gamma rays. As long as uranium remains outside the body, it poses little health hazard (mainly from the gamma-rays). If inhaled or ingested, however, its radioactivity poses increased risks of lung cancer and bone cancer. Uranium is also chemically toxic at high concentrations and can cause damage to internal organs, notably the kidneys.

Most nuclear power plants require fuel with U-235 enriched to a level of 3–5%. The uranium fuel cycle begins with the mining and milling uranium ore to produce "yellow cake," a yellow powder of uranium oxide (U_3O_8), which is shipped to conversion facilities for converting to UF_6; the form in which uranium is accepted at current isotope enrichment plants. UF_6 gas is filled into large cylinders where it solidifies. The cylinders are loaded into strong metal containers and shipped to the uranium-enrichment plant. After enrichment, UF_6 is chemically converted to uranium dioxide (UO_2) or metal. Yellow cake has a pungent odor, is insoluble in water, and contains about 80% UO_2, which melts at approximately 2880°C.

A major concern in nuclear fuel cycle facilities, therefore, is the potential of accidental release of UF_6 inside a building or to the atmosphere. UF_6 is rapidly hydrolyzed by ambient moisture to form HF and uranyl fluoride (UO_2F_2). HF is not in itself radioactive; however, it is an extremely corrosive substance that causes severe skin burns, damage to the eyes, and lung injury when inhaled. The effect from acute exposure to HF is a function of the HF concentration and the exposure time. The accumulation of HF in the atmosphere may attack carbon steel and cause corrosion, rupture, or worker exposure via inhalation and skin problem. UO_2F_2 is a water-soluble compound, which in addition to being radioactive can also have toxic chemical effects. If ingested or inhaled, it will enter the bloodstream and will act primarily on the kidneys.

Conversion and enrichment facilities have had a number of accidents involving uranium hexafluoride. One such accident at the Sequoyah Fuels conversion plant in Gore, Oklahoma, on January 4, 1986, killed one worker, hospitalized 37 of the 42 onsite workers, and sent approximately 100 residents to the hospital as well [3]. The most important steps in

http://dx.doi.org/10.5772/intechopen.73356

the nuclear fuel cycle, namely, uranium refining, conversion, and enrichment, involve the production, handling, transportation, and waste management of UF_6 and related products. Due to the hazardous properties (radioactive, corrosive, and toxic) of UF_6, these operations must be carried out in a safe manner to protect plant workers, the public, and the environment.

It should be pointed out that UF_6 concentration in the environment should be restricted to less than 0.2 mg/m^3 or 13.8 ppb [2]. A common problem associated with the complex flow systems is the detection of gas leaks that cannot be directly observed. At present, there is no common and sensitive remote sensor for real-time monitoring the health and safeguarding uranium enrichment plants. To the author's knowledge, there are some passive and time-consuming methods utilizing the nondestructive measurement of U-235 and U-238 concentrations (or evaluation U-235/U-238 isotope ratio) known as "enrichment meter" based on detection main gamma radiation at 185.7 and 1001.0 keV, respectively [3, 4]. This method can be used on UF_6 released into the atmosphere with either germanium or NaI detector-based systems [5] but is limited in accuracy and requires calibration for each type of sample material and range. Although the 186- and 1001-keV peaks are easy to measure, it is difficult to determine the relative detection efficiency of these two gamma rays because of the large difference in their energies. On the other hand, laser-induced fluorescence can be used for remotely measuring UO_2F_2 concentration. This technique can provide specific chemical information like Raman scattering method; however, the fluorescence of solid-phase uranyl appears to be strongly affected by crystal properties and the extent of hydration [6]. Another method is elastic Mie scattering combined with absorption spectroscopy. The uranyl ion absorption near 10.5 μm overlaps a major lasing transition of the CO_2 laser, which can be used for detection of uranyl fluoride aerosol with minimal interference from major atmospheric gases. However, this wavelength is large relative to the average sizes of UO_2F_2 in the released Uf_6 plume, and thus, the intensity of the scattered light is very weak (Mie scattering).

In the previous works, we proposed an UV-DIAL for measuring UF_6 concentration in the atmosphere [7, 8]. In the UV region, signal to noise ratio (SNR) can be enhanced due to the varying of the Rayleigh and Raman backscattered signal as λ^{-4}, where λ is wavelength. Also, available shot-noise limited photomultiplier tubes (PMTs) with a high sensitivity and high-specific detectivity may increase the improvement of SNR in the UV region. UV-DIAL and Raman lidars are the most promising remote sensing techniques with high sensitivity and accuracy for remotely monitoring gaseous uranium hexafluoride [9]. In contrast, Raman lidar has a unique capability to provide additional information on the structure of the molecular species [10]. In Raman scattering, the frequency shifts are characteristic of the molecule and can be used as a molecular fingerprint. It is a weak process, typically only 1 in 10^6–10^8 photons undergo the Raman inelastic scattering event. This drawback may compensate by using a high power and high repetition rate UV laser (in the order of several tens of Hz), telescope with large area, sensitive PMT detector, and decreasing background noise. It should be emphasized that the elastic lidar near the surface detects combined signals of the Rayleigh and the Mie scattering that may limit the quantitative measurement of properties of molecules in the long-path remote sensing. However, in the DIAL technique, the systematic

error due to the aerosol scattering is negligible, and errors may arise when the wavelengths are significantly separated.

In this chapter, a system consists of UV-DIAL and Raman lidar for real-time actively remote monitoring uranium-enrichment plants has been proposed [9]. Because of the fast reaction of UF_6 with water vapor in the atmosphere (see **Figure 1**), simultaneous measurement of UF_6 and HF may decrease the measurement's uncertainty and improve the sensitivity. A green targeting laser diode can be used to visualize and help the operator to determine where is aiming with invisible UV laser beam during the screening. The system comprises a frequency-quadrupled, compact, pulsed Nd:YAG laser at 10 Hz repetition rate for the off-wavelength at 266 nm and a frequency-doubled Nd:YAG-pumped Coumarin 450 using a Blazed grating mounted in Littrow configuration operating in the frequency doubled for the on-wavelength at 245 nm. The grating is invariably used to allow tuning of the laser across the wide gain bandwidth of the laser. Raman scattering measurements of HF at 297.3 nm with Raman frequency shift 3959 cm^{-1} are helpful to identify HF as a probe for real-time detection and localization of toxic UF_6 leaks.

It should be mentioned that the absorption spectroscopy is also utilized for remotely detection of HF at 1.28 μm [12]. However, it has a drawback of inability to distinguish HF and also limitation due to the strong absorption of water vapor in the region which hampers the measurements, especially at relatively low HF concentrations. Hence, because of the very weakness of Raman scattering of water [10], Raman lidar may be a versatile technique to study HF in the wet environment. Moreover, Raman signal and thereby SNR can be significantly enhanced using UV light especially in the solar blind ultraviolet (200 –310 nm). We believe combined UV-DIAL and Raman lidars is a promising and reliable real-time tool for measuring

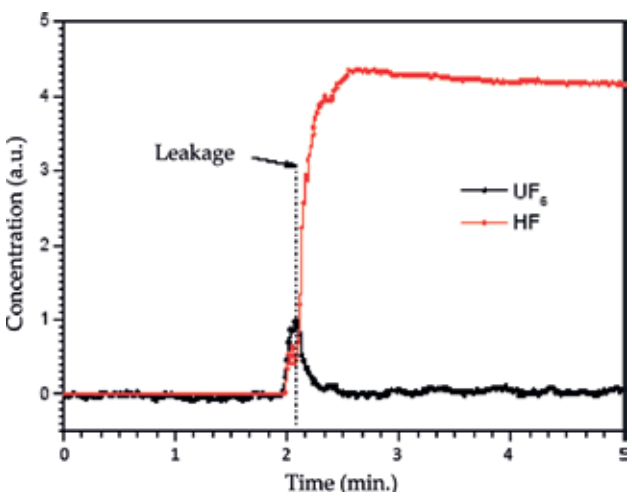

Figure 1. Varying UF_6 and HF concentration in the moisture atmosphere versus time [11].

and tracing UF_6 and HF components in the atmosphere to greatly decrease probable disaster results by releasing gaseous UF_6 in the atmosphere.

2. Physical and chemical properties of UF_6

Uranium hexafluoride can be a solid, liquid, or gas, depending on its temperature and pressure. The phase diagram of UF_6 is schematically shown in **Figure 2**, which presents different physical forms of UF_6 as a function of temperature and pressure [13]. At atmospheric pressure (14.7 psia), UF_6 is a solid below a temperature of 134°F (56.6°C) and a gas at temperatures above 134°F. Liquid UF_6 is formed only at temperatures greater than 147.2°F (64.02°C) and at pressures greater than 1.5 times atmospheric pressure (~22 psia). At atmospheric pressure, solid UF_6 will transform directly to UF_6 gas (sublimation) when the temperature is raised to 134°F, without going through a liquid phase. Detail description on its physical properties can be found in Ref. [14]. All three phases, solid, liquid, and gas, coexist at 64.02°C (147.2°F, the triple point) and P = 1.497 atm. Only the gaseous phase exists above 446°F (230.2°C, the critical temperature), at which critical pressure is 45.5 atm.

Uranium hexafluoride is the substance most suitable for use in the fuel cycle facilities processes because of its exotic physical properties. Since fluorine exists naturally in only one isotopic form (F-19), the physical processes widely used for enrichment of U-235, such as diffusion, centrifugation, and molecular laser isotope separation (MLIS), increase only the concentrations of uranium isotopes. The process of fluorination of uranium dioxide to produce UF_6 can be subdivided into the following chemical reactions:

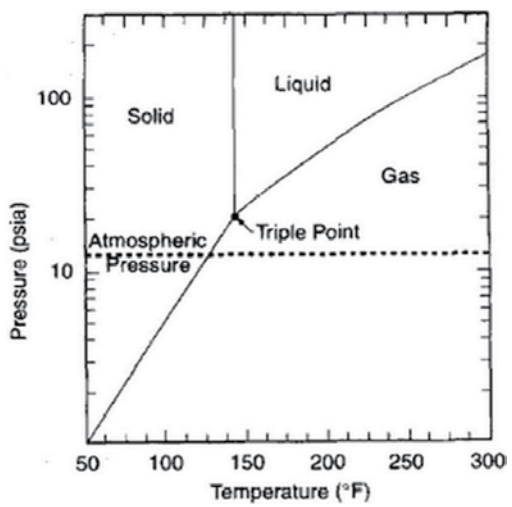

Figure 2. UF_6 phase diagram, showing relationship between pressure, temperature, and physical form [13].

$$U_3O_8 + 2H_2 \rightarrow 3UO_2 + 2H_2O \tag{1}$$

$$UO_2 + 4HF \rightarrow UF_4 + 2H_2O \tag{2}$$

$$UF_4 + F_2 \rightarrow UF_6 \tag{3}$$

The density of UF_6 changes with temperature and for the solid phase can be described by the following equation [15]:

$$\rho_s = 5194 - 5.168T \ \text{kg/m}^3 \tag{4}$$

for 0°C ≤ T ≤ 64°C. In the liquid state, its density varies in a nonlinear fashion and can be summarized by the following equation [15]:

$$\rho_l = 1670 + 152.03(T_c - T)^{0.5} \ \text{kg/m}^3 \tag{5}$$

where T_c = 230.2°C, which is accurate close to triple point (T = 64.02°C, p = 1.497 atm), and

$$\rho_l = 2084.3 - 3.1T + 371(T_c - T)^{0.3045} \ \text{kg/m}^3 \tag{6}$$

which is more accurate close to the critical point (T = 230°C, p = 45.5 atm). Note that T in Eqs. (4)–(6) is measured in °C.

In the vapor phase, the density of UF_6 can be described according to an equation which is similar in form to the ideal gas law [15]:

$$\rho_v = \frac{4291p}{T\left(1 - 1.3769 \times 10^6 p/T^3\right)} \ \text{kg/m}^3 \tag{7}$$

where p is in atm, and T is in K. In the range of 50–140°C, Eq. (8) gives density values [16], which is similar to those obtained using Eq. (7), but it is applicable over a wider temperature range and does not have a singularity limit, i.e.

$$\rho_v = \frac{4291p}{T}\left(1 + 1.2328 \times 10^6 p/T^3\right) \ \text{kg/m}^3 \tag{8}$$

Comparing Eqs. (4) and (5), we can see that during the change from solid to liquid at 64.02°C, a volume expansion of 25.36% takes place (density changes from 4863.25 kg/m^3 (solid) to 3629.95 kg/m^3 (liquid)).

When gaseous UF_6 escapes into the moist atmosphere, it rapidly reacts and hydrolyzes with the ambient water vapor to form hydrogen fluoride (HF) gas and uranyl fluoride (UO_2F_2) particles with diameters of a few microns, both of which are very toxic. This exothermic reaction can be written in the following forms:

$$UF_6 + 2H_2O \ \rightarrow UO_2F_2 + 4HF + \text{heat} \tag{9}$$

or

$$UF_6 + H_2O \rightarrow UOF_4 + 2HF \quad (10.a)$$

$$UOF_4 + H_2O \rightarrow UO_2F_2 + 2HF + \text{heat} \quad (10.b)$$

The UF_6 hydrolysis reaction releases approximately 58 kJ/g mole of H_2O, which heats the plume and causes plume rise that afterward slowly sink to the ground. This hydrolysis reaction plays an important role in determining the fate of UF_6 that is released into the atmosphere. If a release occurs inside a building, this fog may impair escape from the release area or may difficult planned emergency actions. A dense fog was observed, for example, at the Hanau conversion plant, in 1987, during a UF_6 release from an autoclave [17]. It has been reported that UO_2F_2 concentrations as low as 1 g/m^3 are visible, and visibility is less than 90 cm [18]. Fog can also occur in unconfined areas if the humidity is high.

The hydrolysis reaction is very fast and is limited by the availability of water. To hydrolyze 1000 kg of UF_6, 100 kg of water is required; at 25°C and 70% relative humidity, this amount of water is contained in 6000 m^3 of air. Following a large-scale release of UF_6 outside, the dispersion is governed by meteorological conditions. The plume could still contain unhydrolyzed UF_6 even after traveling a distance of several 100 meters. In other words, although the hydrolysis reaction of UF_6 is fast, after escaping of UF_6 into the atmosphere, besides HF and UO_2F_2, UF_6 may also be found in the atmosphere. Only escaping a few 100 g of UF_6 into the atmosphere will raise the formation toxic and opaque cloud of uranyl fluoride [19]. UO_2F_2 is a particulate that is very soluble in the lungs, and the uranium acts as a heavy metal poison that can affect the kidneys. HF is an acid vapor that can cause acid burns on the skin or lungs. In the event of an accidental release, its toxicity level can be reached in minutes.

It should be emphasized that enriched UF_6 cannot be directly used in reactors, as it does not withstand high temperatures or pressures. It is therefore converted into UO_2. Fuel pellets are formed by pressing UO_2, which is sintered (baked) at temperatures of over 1400°C to achieve high density and stability. The pellets are cylindrical and are typically 8–15 mm in diameter and 10–15 mm long. They are packed in long metal tubes to form fuel rods, which are grouped in "fuel assemblies" for introduction into a reactor. The spent fuel contains uranium (96%), plutonium (1%), and high-level waste products (3%). The uranium with less than 1% fissile U-235 and the plutonium can be reused. Some countries chemically reprocess usable uranium and plutonium to separate them from unusable waste. Recovered uranium from reprocessing can be returned to the conversion plant, converted to UF_6, and subsequently re-enriched. Recovered plutonium, mixed with uranium, can be used to fabricate mixed oxide fuel (MOX).

3. Materials and methods

A schematic diagram of the combination of DIAL and Raman lidar is shown in **Figure 3**. The description of our DIAL system is provided in details in the earlier papers [8]. The Nd:YAG laser is a Q-switched with pulse repetition rate of 10 Hz and pulsewidth of 10 ns with an output power of several 100 mJ per pulse at the fundamental wavelength, 1064 nm. In the laser unit, the 1064-nm laser beam is sent through the frequency doubling and quadrupling harmonic

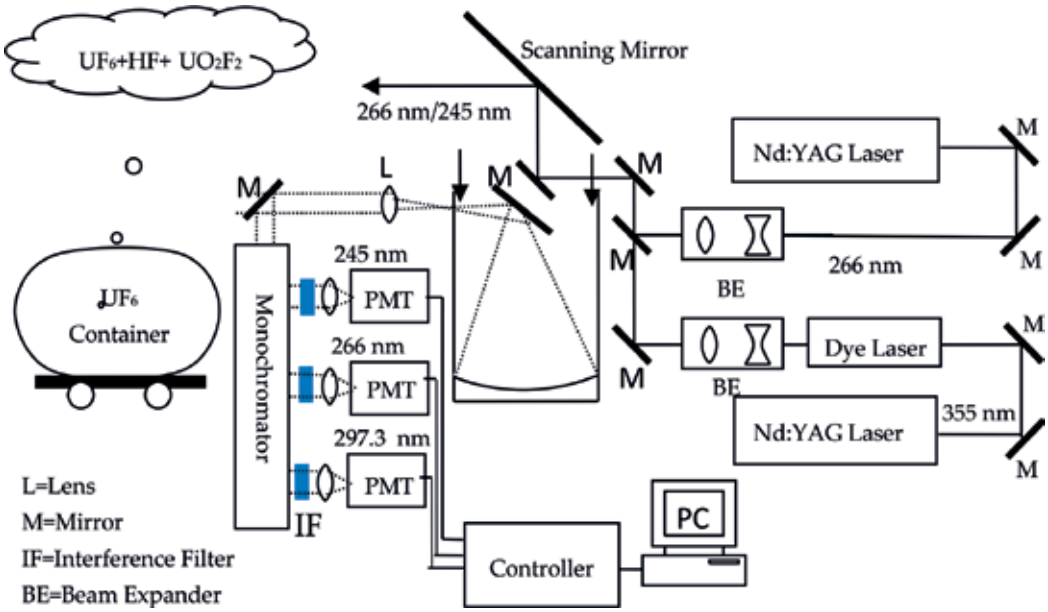

Figure 3. Schematic diagram of the combined differential absorption/Raman lidars for simultaneously remote detection of UF_6 and HF.

crystal modules to deliver a laser beam at 266 nm (4th harmonic) for the off-wavelength. A practical reason for choosing fourth harmonic of Nd:YAG laser as off-wavelength is its reliability, compactness, long lifetime, and low running costs. However, its main drawback is the strong absorption by ozone at 266 nm [20].

A frequency-tripled Nd:YAG-pumped Coumarin 450 dye laser using a Littrow grating mounting operates in the frequency doubled mode for the on-wavelength, 245 nm. The grating is invariably used to allow tuning the laser across the wide gain bandwidth of the laser, the biggest advantage of dye lasers. Use of a diffraction grating alone as a wavelength selector (with suitable beam expanding optics allowing utilization of a large area of the grating surface) renders a spectral width of 0.01 nm. To reduce linewidth, an intracavity etalon is often included in the optical path. Use of an etalon along with a diffraction grating can render spectral widths as low as 0.0005 nm [21]. Coumarin 450 dye lasers with the spectral emission 427–488 nm is considered because of tunability, compactness, output stability, design simplicity, and good beam quality. Coumarin 450 has an absorption peak at 366 nm and an emission peak at 440 nm.

The laser output radiations are expanded by a beam expander (BE). The expanded beams are folded 90° by UV-enhanced aluminum-coated mirrors which have a good reflectivity in the region of 250–300 nm (R > 86%) and subsequently steered them toward the UF_6 and hydrolyzed products plume released into the atmosphere. After interaction with particles and molecules of the atmosphere and plume, the elastic and inelastic backscattered radiations at 266, 245, and 297.3 nm are collected by a Newtonian-type telescope. It has an aspheric primary mirror with the focal length F. A secondary flat mirror reflects the converging light through a

http://dx.doi.org/10.5772/intechopen.73356

diaphragm with a diameter D. An MgF_2 plano-convex lens (L) after the diaphragm is used to provide a collimated beam. The collimated beam after passing through a monochromator is focused on the entrance pupil of the detector through a Lyot tunable birefringent or Fabry-Pérot interference filters (IF). The diaphragm is in the focal plane of the telescope and sets the field of view (FOV) of the receiver, FOV ≈ D/F. To obtain a required FOV, we select the diameter of the diaphragm for a given focal length of the telescope. The FOV of the receiver is usually set small (about 100 micro-radians full angle FOV) to reject the background noise and achieve acceptable SNR.

As mentioned above, along with the power of the laser, the size of the primary optics is an important factor in determining the effectiveness of the system. Since the returned signal from the far distance is relatively weak, to improve the SNR and increase the detection range, a reasonable FOV is essential to suppress the sky background light, especially during the daytime measurements under sunlit conditions. The smaller aperture optics is used to work in close ranges, for example, a few 100 m, where the returned signal is a larger fraction of the transmitted power. To address the minimum distance at which returning signals are completely in the instrument's FOV, the FOV of the instruments needs to be wide enough. The wide field angle of the receiver reduces the overlap range to several 100 meters. However, the increase in FOV increases the collection of unwanted solar background, resulting in unacceptably poor SNR during daytime measurements. One way to reduce the background solar radiation in the wide FOV lidars is working in the solar blind region. Moreover, by adding an AR coating, the overall transmission of the lenses can be increased. The UV folding mirrors also can reduce the nonresonant background noise.

Monochromator is used to separate the signals, and narrowband filters (IF) are used to extract the Raman and elastic signals at 266, 245, and 297.3 nm. Narrow bandpass filters designed for these center wavelengths allow isolation of the Raman line and increase the SNR by rejecting the out-of-band radiations. Some of the channels may use neutral density filters for reducing the signal intensity to a level that does not saturate the PMT. The high-resolution reflection grating of the monochromator diffracts the background noise as well and makes it possible to separate and block the majority of background noises with combination of a small diaphragm. Most detectors have a window or a lens between the active area of the detector and the energy source. The solid angle cone from which energy can reach the detector is determined by the distance of the detector surface from the front surface of the window or by curvature of the lens. Antireflection coatings are applied to the detector materials or, where applicable, windows and lenses to reduce the reflection losses. The acquisition system is based on a three-channel transient digitizer working in the photon counting mode for increased sensitivity at low signal levels.

4. Results and discussion

The total photon counts received by the elastic-DIAL at the distance R from both the aerosol and molecular backscattering species, $N_{sig}(R)$, is given by the general lidar equation:

$$N_{sig}(\lambda_L, R) = \frac{E_L(\lambda_L)}{h\nu}\eta_{tot}\beta(\lambda_L, R)\Delta R\ \frac{A}{R^2}\exp[-2\tau(\lambda_L, R)] \tag{11}$$

where E_L is the transmitting energy, h and ν are Planck's constant and the laser frequency, $\eta_{tot} = \eta_t\eta_r\eta_{FOV}\eta_{IF}\eta_{PMT}$ is the total efficiency of the lidar, η_t is the transmitting efficiency owing to the beam expander and mirrors, η_r is the receiving efficiency owing to the mirrors, lenses, and telescope, η_{FOV} and η_{IF} are the efficiency of the FOV and interference filters, η_{PMT} is the quantum efficiency of the PMT, ΔR is the range resolution of the photon counter, β(R) is the total backscatter coefficient of molecules and aerosols, A is the area of the telescope, and the optical depth or optical thickness $\tau(\lambda, R) = \int_0^R \alpha(\lambda, r)dr$ is the integral of the extinction coefficient $\alpha(\lambda, r)$ along the path which is a function of the laser wavelength and distance.

Usually backscatter coefficient β for elastically backscattered light consists of contribution of both air molecules and aerosols, i.e., $\beta(R) = \beta_{ms}(R) + \beta_{as}(R)$. For molecular species, backscatter and extinction coefficient differs by a constant factor $\beta_{ms} = (3/8\pi)\alpha_{ms}$ and can easily be substituted. While for the aerosol species, this procedure is not possible and must define "lidar-ratio" [22, 23]:

$$S(R) = \frac{\alpha_{as}}{\beta_{as}} \tag{12}$$

The result of the inversion is the backscatter ratio which is defined as:

$$B(R) = \frac{\beta_{as} + \beta_{ms}}{\beta_{ms}} = \frac{8\pi\alpha_{as}}{3\alpha_{ms}}\frac{1}{S} + 1 \tag{13}$$

For a lidar system with a narrow FOV and a separation between transmitter and receiver optical axes, the incomplete overlap between the laser beam and the receiver FOV significantly affects lidar observation in the short range. When separation of the laser and telescope axes is negligible or small enough in which the area of the laser illumination lies totally within the receiver-optical FOV or vice versa, the overlap distance and efficiency may be adjusted by controlling the FOV of the telescope or the divergence of the laser beam (DIV). As the transmitting laser has nearly a TEM_{00} mode Gaussian shape, for a given beam divergence, the FOV receiving efficiency, η_{FOV}, increases with FOV and saturates for FOV ≥ 1.5DIV as described in Eq. (14), which can be derived from the integral of the radial intensity distribution of TEM_{00} mode:

$$\eta_{FOV} = 1 - \exp\left(-2\frac{FOV^2}{DIV^2}\right) \tag{14}$$

It indicates that the FOV of the telescope optics must be larger than the laser beam divergence so that the lidar can see the entire illuminated volume.

The volume density N_{spcies} (in ppb) of the measurement target species in the range between R and R + ΔR can be derived from Eq. (15), which is known as the DIAL equation:

$$N_{species} = \frac{10^9}{2N_{atm}\Delta\sigma}\frac{\partial}{\partial R}\ln\left[\frac{N_{sig}(\lambda_{off}, R)}{N_{sigs}(\lambda_{on}, R)}\right] - \frac{10^9}{2N_{atm}\Delta\sigma}\frac{\partial}{\partial R}\ln\left[\frac{\beta(\lambda_{off}, R)}{\beta(\lambda_{on}, R)}\right] - \frac{\Delta\alpha_{atm}}{N_{atm}\Delta\sigma} \times 10^9 \quad (15)$$

Here $\Delta\sigma = \sigma_{abs}(\lambda_{on}) - \sigma_{abs}(\lambda_{off})$ is the differential absorption cross-section of the species of interest, and $N_{atm} = 2.55 \times 10^{19}$ cm^{-3} is the total number density of molecules in the atmosphere at sea level. At 266 nm, the absorption cross section of UF_6 appears to be constant, $\sigma = (1.15 \pm 0.01) \times 10^{-18}$ cm^2 from 0 to 100°C. The absorption cross section at 245 nm over the same temperature range may be represented with the empirical polynomial σ = [1.37 ± 0.05 + (9.7 ± 1.5) × 10^{-3}.*T* - (4.2 ± 1.1)10^{-5}.T^2] × 10^{-18} cm^2, where T is in degrees Celsius [24]. One can obtain the differential absorption cross section of $\Delta\sigma = 4.2 \times 10^{-19}$ cm^2 at room temperature T = 23°C for λ_{on} = 245 nm and λ_{off} = 266 nm. Since aerosol concentration is typically high enough near the ground surface, it is reasonable to approximate $\beta = \beta_{as}$. For the horizontal homogenous atmospheric path, β_{as} is a slowly decreasing function of wavelength; therefore, the second term on the right hand side of the Eq. (15) can be negligible. However, for wavelengths below 300 nm, the wavelength dependent aerosol backscatter coefficient, β_{as}, can significantly deviate from λ^{-1} law, depending on the aerosol type. Therefore, a long distance between λ_{on} and λ_{off} can introduce noticeable systematic error in regions of the atmosphere, where the aerosol size gradient is large.

In Eq. (15), $\Delta\alpha_{atm} = \alpha_{atm}(\lambda_{off}) - \alpha_{atm}(\lambda_{on})$ is the differential extinction coefficient of the atmosphere, described as:

$$\begin{aligned}\Delta\alpha_{atm} = \Delta\alpha_{ma} + \Delta\alpha_{ms} + \Delta\alpha_{as} = &[\alpha_{ma}(\lambda_{off}, R) - \alpha_{ma}(\lambda_{on}, R)] \\ &+ [\alpha_{ms}(\lambda_{off}, R) - \alpha_{ms}(\lambda_{on}, R)] \\ &+ [\alpha_{as}(\lambda_{off}, R) - \alpha_{as}(\lambda_{on}, R)]\end{aligned} \quad (16)$$

where $\Delta\alpha_{ma}$, $\Delta\alpha_{ms}$, and $\Delta\alpha_{as}$ are the differential molecular absorption, molecular scattering, and aerosol scattering coefficients, respectively. The measurement accuracy of DIAL depends very strongly on accuracy of species absorption cross-section and evolution of atmospheric extinction. The main errors of the measurement gas concentration lie with the high aerosol and air molecule concentrations in the troposphere, and errors are caused by the large wavelength separation between the "on" and "off" signals and different absorption by gases other than the species of interest and scattering caused by aerosols and molecules. Simplifying conditions can be hold when the "on" and "off" wavelengths are much more close together, and differential extinction coefficient of the atmosphere is negligible. In addition, differential backscatter error is negligible under the condition of spatially homogeneous backscatter. If the simplifications cannot be made, each of the error terms must be considered [20]. The total error caused from the atmosphere for detection UF_6 can be obtained as:

$$Error_{atm}(ppb) = 1.3 \times 10^8(\Delta\alpha_{ms} + \Delta\alpha_{ma} + \Delta\alpha_{as}) \quad (17)$$

Among the expected noise from constituents in the atmosphere, O_3 is considered as the dominant constituent in the UV region. **Figure 4** shows ozone absorption extinction as a function of

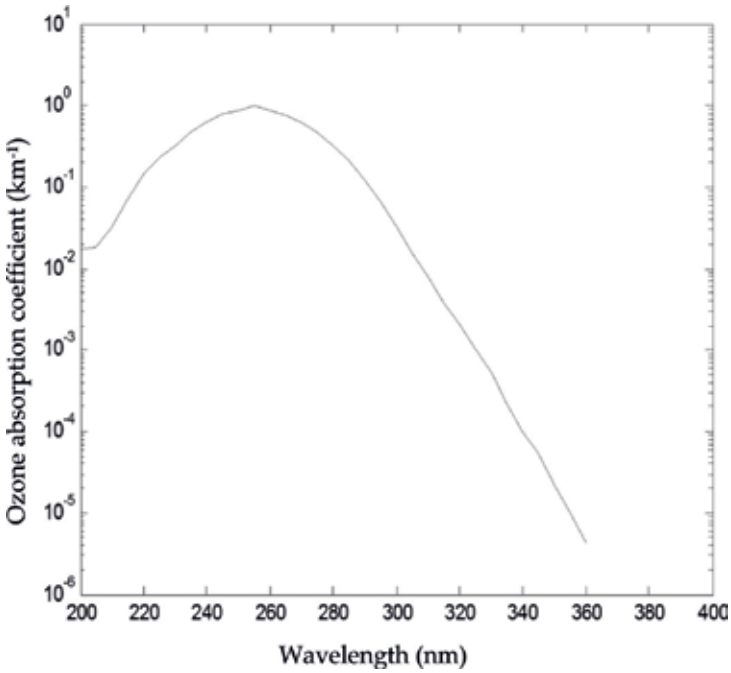

Figure 4. The ozone absorption extinction as a function of wavelength [20].

wavelength in the UV region. The ozone concentration near the surface is considered to be about 0.8×10^{12} cm^{-3}, corresponding to 30 μg/cm^{-3} or 30 parts in 10^9 volumes (ppbv). From ~200 to ~310 nm, the ozone absorption coefficient is large with a maximum absorption extinction ~1 km^{-1} at 255 nm, and it reduces rapidly to ~10^{-6} km^{-1} by increasing wavelength near 360 nm [20, 25].

Before designing a DIAL system, the differential absorption of the target species must be known to derive the necessary parameters such as laser energy, linewidth, and detector area. Also, the sensitivity and lower detection limit of the DIAL measurement are directly dependent on the accuracy of the differential absorption cross-section. From Eq. (15), it follows that if differential extinction and backscatter coefficients of the atmosphere as a function of wavelength are known, a measurement of backscatter power is adequate to precisely determine concentration.

In photodetectors, such as PMT or APD, that have an internal gain, both signal and noise are amplified. Usually, in photon counting regime, the random errors caused by shot noise is the dominant factor to fluctuate the detected signal and background. The SNR at each wavelength can be computed for each laser shot from:

$$SNR_i = \frac{N_{sig}}{\sqrt{N_{sig} + N_{bg} + N_n}} \tag{18}$$

where N_{bg}, N_n, and N_{sig} are the detected background, dark counts accumulated over the laser pulsewidth, and the detected signal photons, respectively. From Eq. (18), the SNR is maximum when $N_n = N_{bg} = 0$; i.e., $SNR_{max} = \sqrt{N_{sig}}$. The SNR decreases rapidly once the received light intensity drops below the noise intensity.

The total detector noise counts within the laser pulsewidth, N, which is caused by the detected sunlight and the detector dark noise, is given by:

$$N = N_{bg} + \dot{N}_d \tau_{PMT} \tag{19}$$

where dN_d/dt is the detector dark noise count rate (Hz), τ_{PMT} is the PMT response time constant or receiver pulse integration time, usually slightly larger than the laser pulsewidth, and N_{bg} is the photon counts of the background light received by the lidar is expressed by:

$$N_{bg} = \frac{1}{h\nu}\eta_r\eta_{IF}\eta_{PMT}B_{bg}\Omega A\Delta\lambda_{BIF}\tau_{PMT} \tag{20}$$

where B_{bg} is the sky background radiation that is negligible in the solar blind region, $\Delta\lambda_{BIF}$ is the bandwidth of the narrow-band interference filter, and $\Omega = \pi FOV^2/4$ is the viewing solid angle. For a low dark count detector in the solar blind region, total detector noise count can be approximated as $N \approx 0$. After accumulating photon counts for an integration time T_{int}, the averaged SNR at each wavelength is given by:

$$SNR(\lambda_i) = \sqrt{f(\lambda_i)_{las}T_{int}}SNR_i \tag{21.a}$$

where $f(\lambda)_{las}$ is the laser repetition rate at wavelength λ, and $f(\lambda)_{las}T_{int}$ is the total number of pulse measurements averaged. For a low dark count detector in the solar blind region, we can simplify Eq. (21.a) as below:

$$SNR(\lambda_i) = \sqrt{f(\lambda_i)_{las}T_{int}}\sqrt{N_{sig}} \tag{21.b}$$

The feasibility of the system is simulated by taking into account the contribution of molecules and aerosols in the backscatter lidar photon rate. The aerosol backscatter has been included in the simulation considering the lidar ratio of 50 Sr corresponding to extinction and back-scattered coefficients of 5×10^{-4} m^{-1} and 1×10^{-5} $m^{-1}Sr^{-1}$, respectively. The simulation results are organized using the parameter introduced in **Table 1**. In **Figure 5**, the minimum detectable concentration of UF_6 as a function of range for a typical detector having a low SNR of 1.5 is depicted. It can be seen that the minimum detectable concentration of UF_6 is limited to 1.21 ppm for range of 1000 m. Note that each system parameter should be carefully considered in a trade-off analyses, including the distances (or ranges) from which the measurements are to be taken, to determine the best overall solution for a given lidar application. In other words, if the determined set of lidar parameters yields a SNR that is below specification, it may be adjusted simply by reducing the DIV, and thus, the SNR will increase, or by increasing the integration time (number of shots) as shown in **Figure 6**. It may also possibly increase the

Transmitting subsystems	
Energy per pulse	300 mJ
Repetition rate	10 Hz
Pulsewidth (FWHM)	10 ns
Pulse laser linewidth (FWHM)	0.1 nm
Optical transmission efficiency	0.7
Far-Field Full angle divergence (beam expanded)	100 μRad
Receiving subsystems	
Telescope aperture (diameter)	35 cm
FOV	200 μRad
Interference filter bandwidth	0.1 nm
Receiving efficiency	0.5
PMT quantum efficiency	0.1
Range resolution of photon counter	30 m

Table 1. Major parameters of the lidar system considered in simulation.

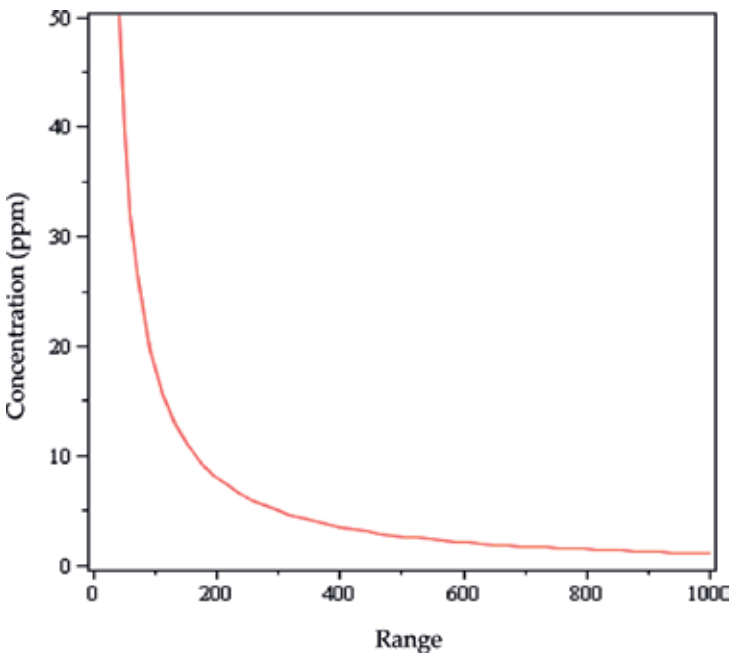

Figure 5. The minimum detectable UF_6 concentration by DIAL (λ_{on} = 245 nm and λ_{off} = 266 nm) versus range for one pulse for a very low dark count detector. The SNR is considered to be 1.5. Other parameters of the lidar system are shown in **Table 1**.

http://dx.doi.org/10.5772/intechopen.73356

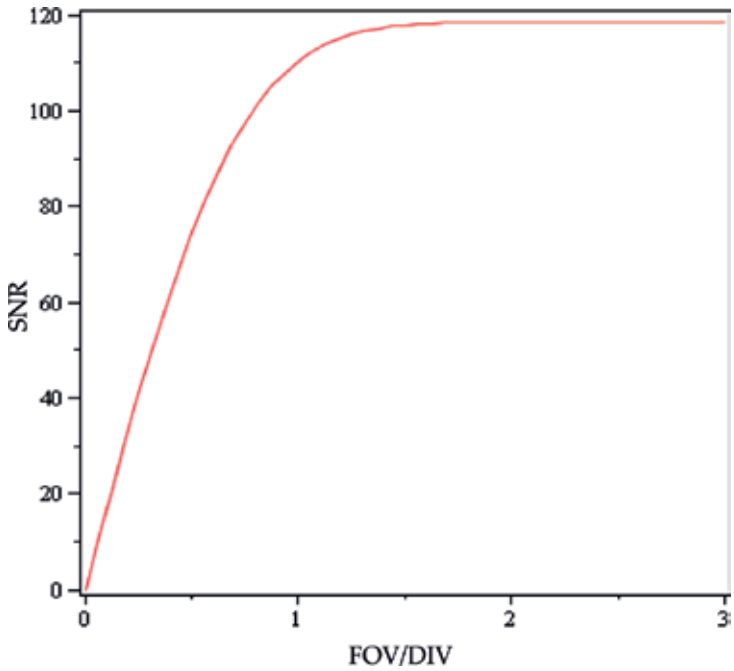

Figure 6. Calculated SNR as a function of FOV/DIV for a UF_6 cloud with 1.1 ppm concentration at 1 km. The integration time is 300 second (3000 shots). Other parameters of the lidar system are shown in **Table 1**.

receiver diameter; however, it increases both the received signal and noise in the same proportion. An increase in the laser beam diameter will increase the received signal, as well as SNR.

Despite the advantage of large Mie- and Rayleigh-scattering and therefore high SNR of the conventional elastic lidar systems, they cannot provide species selectivity. In contrast, inelastic Raman scattering where the frequency of the scattered radiation is shifted by an amount that is a unique of the molecule can be used like fingerprint to distinguish molecular species. In other words, the Raman spectrum contains characteristic signatures of each target molecules with high spectral resolution which makes the Raman spectroscopy a very powerful technique for characterization and identification of unknown species. The intensity of the Raman signal is directly proportional to the density of the scattering molecules independent of other molecular or particulate species:

$$N_{sig}(\lambda_{Ra}, R) = \frac{E_L(\lambda_L)}{h\nu}\eta_{tot}\beta_{Ra}(\lambda_L, R)\Delta R\ \frac{A}{R^2}\exp[-\tau(\lambda_L, R)-\tau(\lambda_{Ra}, R)] \tag{22}$$

where

$$\beta_{Ra}(\lambda_L, R) = N_{Ra}(R)\frac{d\sigma_{Ra}(\pi, \lambda_L)}{d\Omega} \tag{23}$$

is the Raman backscatter coefficient, λ_L and λ_{Ra} are the wavelength of laser and Raman, respectively. The wavelength shift and also narrow spectral width of the Raman scattered

signal respectively at 266 and 297.3 nm allows distinguishing HF from the other species which elastically scatter 266 nm radiation [10]. Simultaneous measurement of the elastic-backscatter signals at 266 nm and 245 nm and the HF inelastic-backscatter signal at 297.3 nm permit the determination of the concentration of UF_6 and HF, independently, and therefore detection and localization of UF_6 leaks. Notice that both Rayleigh and Raman scattering are two-photon processes involving scattered incident light from a virtual state. The main problem of the Raman scattering is its weak interaction compared to Rayleigh scattering, with a cross-section that is typically 3–4 orders of magnitude smaller. Therefore, the strong Rayleigh scattered radiation must be eliminated when analyzing the weak Raman scattered radiation. The Raman lidar typically consists of an untunable laser excitation source, collection optics like a telescope to collect the rotational-vibrational backscattered radiation from the molecular HF, a spectral analyzer such as monochromator, and a high-sensitive detector such as PMT. The collection optics must be carefully designed to collect as much as the Raman scattered radiation from HF and transfer it into the monochromator. Using a high-sensitive PMT and a high-throughput monochromator with Rayleigh rejection filters may dramatically improve the performance of the Raman lidar. The low intensity of the Raman backscattered signal can be improved by using a high-power laser, high-efficient receiver, low-noise detector, and operation in the solar blind region. It is well known that tropospheric and stratospheric ozone absorb practically all of the incoming solar radiation in this region of the spectrum, providing a black background for detection of the weak Raman signals in the region of 200–310 nm. Natural ozone mainly occurs in the stratosphere between heights of 15 and 50 km. The solar blind region provides conditions that make it possible to operate lidar with a wide FOV telescope and sensitive quantum noise–limited photon counting detectors. The magnitude of the Raman shift is specific of the excited molecule, and the detected light is proportional to the concentration of molecule and Raman cross-section as well. At wavelengths greater than 310 nm, the background noise radiation is significant. Below 200 nm, absorption by oxygen is so strong that propagation is severely limited, and it is not feasible to operate within the atmosphere.

So far, a single grating monochromator and a double grating monochromator in combination with an interference filter have been employed to separate wavelengths effectively in practice [26]. Moreover, for further suppressing the elastic Mie- and Rayleigh-scattering signals, two sets of interference filters can be employed. To improve the optical efficiency of spectroscopic filters, the filters are designed with a peak transmittance at non-normal incidence angle. The function relationship between the central wavelength at normal incidence, λ_n, and wavelength at non-normal incidence angle of θ is given by:

$$\lambda(\theta) = \lambda_n \sqrt{1 - (\sin\theta/n)^2} \tag{24}$$

where n is the effective refractive index of the filter. λ/λ_n decreases slowly with angle from 1 to 0.75, as angle is increased from normal to 90° for the case of n = 1.5. In many applications, angle shifts can be safely ignored. Using a high-index material such as zinc sulfide (n = 2.355 at 632.8 nm), the feature of the spectrum shift to the shorter wavelength versus angle decreases. Sometime, two narrow-band interference filters combined with a high resolution grating are

used to construct a powerful spectroscopic system for achieving the required high rejection rate of 10^7.

The grating diffracts the spectra of the backscattered signal spatially according to the Fraunhofer diffraction. If the incident light beam is not perpendicular to the grooves, the grating equation is given by the modified equation as [27]:

$$Gm\lambda = \cos\gamma\left(\sin\alpha + \sin\beta\right) \tag{25}$$

Here, m is diffraction order, α is the angle of incidence, λ is the diffracted light at angle of β, G = 1/d is the groove frequency or groove density, and γ is the angle between the incident light path and the plane perpendicular to the grooves at the grating center. If the incident light lies in this plane, γ = 0, and Eq. (25) reduces to the famous grating equation. In geometries for which $\gamma \neq 0$, the diffracted spectra lie on a cone rather than in a plane, so such cases are termed conical diffraction. In the most fundamental senses, both spectral bandpass and resolution are used as a measure of an instrument's ability to separate adjacent spectral lines called resolving power. The spectral bandpass is the wavelength interval passed through the exit slit or falls onto the detector. Resolution is related to the bandpass but determines whether the separation of two adjacent peaks can be distinguished. The spectral resolution $\Delta\lambda$ is measured by convolution of the image of the entrance aperture with the exit aperture. It determines resolving power RP = $\lambda/\Delta\lambda$. However, the practical resolving power is limited by the spectral width of the spectral lines emitted by the source.

Spectral bandpass resolved by a monochromator is the difference in wavelength between the points of the half-maximum intensity on either side of the intensity maximum. For an optical system, bandpass is given by:

$$BP = W.R_d \tag{26}$$

where R_d is reciprocal of linear dispersion, and W is the width of the entrance or exit slit (larger one). An instrument with smaller bandpass can resolve wavelengths that are closer together than an instrument with a larger bandpass. Bandpass can be reduced by decreasing the width of the exit slit but usually at the cost of decreasing light intensity. The reciprocal linear dispersion represents the number of wavelength intervals (e.g., nm) contained in each interval of distance (e.g., mm) along the focal plane:

$$R_d = \frac{\partial\lambda}{\partial x} = \frac{d\cos\left(\beta\right)}{f.m} \tag{27}$$

where d is the ruled width of grating and f is the focal length of the grating (in the case of curved grating). At small angles of diffraction, Eq. (27) is simplified as:

$$R_d = \frac{d}{f.m} \tag{28}$$

By substituting Eq. (28) into Eq. (26), one can obtain:

$$BP = \frac{W.d}{f.m} \tag{29}$$

For instance, considering G = 1200 gr/mm, W = 0.05 mm, f = 500 mm, and m = 1, the obtained bandpass is 0.083 nm. For selecting grating, one should consider that the grating equation reveals only the spectral orders for which $|m\lambda/d| < 2$ exist. This restriction prevents light of wavelength λ from being diffracted in more than a finite number of order m. Once angle of incidence has been determined, the choice must be made whether a small width grating should be used in a low order, or a large width grating such as an echelle grating should be used in a high order; though, the small width grating will provide a larger free spectral range, $\Delta\lambda_{FSR} = \lambda/m$.

The minimum attainable spectral resolution is given by:

$$\Delta\lambda = \lambda^2/2D \tag{30}$$

regardless of the order m or number of grooves N under illumination. Here D = Nd is the rules width of the grating. This minimum condition corresponds to the grazing Littrow configuration. Noticeably when the grating is incorporated in a spectrometer or monochromator, however, aberrations and imperfections in other elements (e.g., lenses and mirrors) rather than grating and factors related to the size of the slits and detector elements may result in even wider spectral resolution. This means that the minimum wavelength difference $\Delta\lambda$ that can be resolved will be larger that for the grating only defined by Eq. (30), and, in general, the resolving power for the optical system degrades.

5. Conclusion

A sudden release of UF_6 into the atmosphere can conceivably cause undesirable health effects to the workers and the public in general associated with high level of toxicity of the hydrolysis products HF and UO_2F_2. Although the hydrolyze reaction of UF_6 is fast, however, after escaping of UF_6 into the atmosphere, besides HF and UO_2F_2, UF_6 may also be found in the atmosphere. Therefore, the combination of DIAL and Raman lidar for simultaneously detection of UF_6 and HF can be a reliable technique for remotely detection and monitoring UF_6 leaks and further improving the safety and economically operation of a uranium-enrichment plant. The DIAL provides information on UF_6 concentration using the off- and on-wavelength at 266 and 245 nm, respectively, while Raman scattering of HF at 297.3 nm can identify and quantify HF as a probe for real-time detection and localization of toxic UF_6 leaks. This system might be mounted on a helicopter for quickly and remotely surveying the leaks from the large facilities. Since the system is working in the solar blind ultraviolet (200–310 nm), the Raman signal may simply be enhanced by increasing FOV or increasing the integration time (or number of shots).

Author details

Gholamreza Shayeganrad

Address all correspondence to: gholamreza.shayeganrad@unibas.ch; shayeganrad@yahoo.com

Department of Biomedical Engineering, University of Basel, Gewerbestr, Allschwil, Switzerland

References

[1] Knoll GE. Radiation Detection and Measurement. 3rd ed. New York: John Wiley & Sons, Inc; 2000

[2] Safety requrements, Safety of nuclear fuel cycle facilities. IAEA, No. NS-R-5 (Rev.1) 2007

[3] Railly D, Ensslin N, Smith H, eds, Passive Nondestructive Assay on Nuclear Materials. 1991

[4] Reilly TD, Walton RB, Parker JL. A-1 Progress Report LA-4605-MS. 1970. p. 19

[5] Shayeganrad G, Parvin P. DIAL–phoswich hybrid system for remote sensing of radioactive plumes in order to evaluate external dose rate. Progress in Nuclear Energy. 2008;**51**: 420-433

[6] Rabinwitch E, Linn Belford R, Dunworth JV. Spectroscopy and Photochemistry of Uranyl Compounds. Oxford: Program Press; 1964

[7] Shayeganrad G, Mashhadi L. Remote leak detection of UF6 by UV-DIAL. 2009: Iranan Patent, No. 59319

[8] Shayeganrad G, Mashhadi L. High speed remote monitoring of hazardous uranium hexafluoride by lidar. In: Proceedings of the 25th international laser radar conference. 2010: St.-Petersburg. pp. 814-817

[9] Shayeganrad G. On the remote monitoring of gaseous uranium hexafluoride in the lower atmosphere using lidar. Optics and Lasers in Engineering. 2013;**51**:1192-1198

[10] Chalmers JM, Griffiths PK. eds, Handbook of Vibrational Spectroscopy. Chichester: John Wiley & Sons Ltd; 2002

[11] Grigoriev GY et al. Remote detection of HF molecules in open atmosphere with the use of tunable diode lasers. Applied Physics B. 2010;**101**:683-688

[12] Gibson G et al. Remote detection of HF molecules in open atmosphere with the use of tunable diode lasers. Applied Physics B: Lasers and Optics. 2010;**101**:683-688

[13] Hanna SR, Chang JC. Modeling accidental releases to the atmosphere of a dense reactive chemical. Atmospheric Environment. 1997;**31**:901-908

[14] Sazhin SS, Jeapes AP. Fluorination of uranium dioxide particles: A review of physical and chemical properties of the compounds involved. Journal of Nuclear Materials. 1999;**275**: 231-245

[15] Lewis RW, Zheng Y, Gethin DT. An adaptive finite element model for the behaviour of uranium hexafluoride filled container in a fire. Nuclear Engineering and Design. 1993; **140**:229-250

[16] Masi JF. The heats of vaporization of uranium hexafluoride. The Journal of Chemical Physics. 1949;**17**:755

[17] Bayer H. UF_6 Release in a German Fuel Fabrication Plant-Sequence and Consequences. In: Conference Proceedings, Uranium Hexafluoride- Safe Handling, Processing and Transporting, Oak Ridge, Tennessee, USA. 1988

[18] Bouzigues H, et al. The safety problems associated with the handling and storage of UF_6. In: Proceedings of the Specialists Meeting. 1978: Boekelo, The Netherlands. p. 344

[19] Zherin II, Penin ST, Chistyakova LK, Kokhanov VI. Experimental study of the aerosol formation by hydrolysis of UF6 in gaseous phase under atmospheric conditions. Journal of Aerosol Science. 1996;**27**:S405-S406

[20] Shayeganrad G, Mashhadi L. Study of aerosols and molecular extinction effects in ultraviolet DIAL remote sensing in the lower atmosphere. International Journal of Remote Sensing. 2012;**33**:887-904

[21] Csele M. Fundamentals of Light Sources and Lasers. Hoboken, New Jersey: John Wiley & Sons, Inc; 2004

[22] Klett JD. Stable analytical inversion solution for processing lidar returns. Applied Optics. 1981;**20**:211-220

[23] Klett JD. Lidar inversion with variable backscatter/extinction ratios. Applied Optics. 1985; **24**:1638-1643

[24] Rice WW, Oldenborg RC, Wampler FB, Tlee JJ. Gas temperature and density of UF6 determined by two-wavelength UV absorption. Applied Optics. 1981;**20**:2625-2629

[25] Bass AM, Paur aRJ. The ultraviolet cross-section of ozone, results and temperature dependence. In: Atmospheric Ozone, Proceedings of the Quadrennial Ozone Symposium. 1985

[26] Lakowicz JR. Principles of Fluorescence Spectroscopy. 3rd ed. New York: Springer; 2006

[27] Loewen E. Diffraction Grating Handbook. 6th ed: Newport Corporation; 2005

Chapter 6

Thermodynamics and Separation Factor of Uranium from Fission Products in "Liquid Metal-Molten Salt" System

Valeri Smolenski, Alena Novoselova,
Alexander Bychkov, Vladimir Volkovich,
Yana Luk'yanova and Alexander Osipenko

Additional information is available at the end of the chapter

http://dx.doi.org/10.5772/intechopen.72451

Abstract

The present chapter contains the results of studying electrochemical and thermodynamic properties of La, Nd, and U in "liquid metal-molten salt" systems, where liquid metals were binary Ga-Al and Ga-In alloys of various compositions. The apparent standard potentials of ternary U-Ga-In, U-Ga-Al, La-Ga-In, La-Ga-Al, Nd-Ga-In, and Nd-Ga-Al alloys at various temperatures were determined, and the temperature dependencies were obtained. Primary thermodynamic properties (activity coefficients, partial excess Gibbs free energy change, partial enthalpy change of mixing, and excess entropy change) were calculated. The influence of the bimetallic alloy composition and the nature of lanthanide on thermodynamic properties of compounds are discussed. The values of U/Nd separation factors on gallium-aluminum and U/La on gallium-indium alloys were calculated. The value of the separation factors strongly depends on the alloy composition. Uranium in this case is accumulating in the metallic phase and lanthanides in the salt melt. Analysis of the data obtained showed the perspective use of the active cathodes (Ga-Al and Ga-In instead of single Cd) in future innovative methods for reprocessing spent nuclear fuels (SNF) and high-active nuclear wastes in the future of closed nuclear fuel cycle.

Keywords: uranium, lanthanum, neodymium, gallium-aluminum alloys, gallium-indium alloys, molten salts, liquid metals, thermodynamic properties, separation factor

1. Introduction

Pyrochemical technologies of reprocessing spent nuclear fuels (SNF) attract growing interest due to the necessity to ensure safety and efficiency of the nuclear fuel cycle. These technologies

have a number of significant advantages compared to the existing hydrometallurgical technology, which include a drastic decrease of radioactive wastes, engineering support of nonproliferation principle of using the fissile materials, and lowering cost of SNF reprocessing. Development of nonaqueous SNF reprocessing technologies allows closing nuclear fuel cycle on the basis of the expanded construction of fast reactors with inherent safety. Currently, several variants of pyrochemical technologies are under study: electrochemical technology in molten salts, fluoride volatility process, extraction of technology in molten metals, and some others. The results obtained provide evidence for both the complexity of technological processes and equipment and their potential possibilities [1, 2].

Electrochemical reprocessing of SNF in chloride melts is one of the most developed and promising processes. It is going to be used in the experimental industrial complex of a fast neutron reactor with the solid fuel reprocessing. The major steps of the pyrochemical technology include electrorefining or reductive extraction in molten chloride/liquid metal systems for recovering actinides, including the minor actinides, from the spent metallic or nitride nuclear fuels and high-level radioactive wastes [3, 4]. Actinides recycling by separation and transmutation are considered worldwide as one of the most promising strategies for a more efficient use of the nuclear fuel as well as for nuclear waste minimization. The goal of one of the main strategies (partitioning and transmutation) is achieving the highest possible reduction of the nuclear waste radiotoxicity in the back end of the fuel cycle. High radiation resistance of molten chlorides and the absence of neutron moderators allow reprocessing spent nuclear fuels with high fissile materials content after a short cooling time. Selectivity of high-temperature separation process taking place at the molten salt-liquid metal interface depends on different characteristics of both phases. Knowing thermodynamics of the main fission products in working media is essential for determining applicability of a particular system for practical application [5].

In terms of the efficiency of separating lanthanide (Ln) and actinide (An) elements, the following sequence of the low-melting metals was proposed: Al > Ga > Sn > Bi > In > Zn > Cd [5]. Cadmium is currently considered as the low-melting metal electrode for separating actinides and fission products in the pyrochemical spent nuclear fuel reprocessing. This element has the advantages of compatibility with low-carbon steels and high vapor pressure at elevated temperatures, but it is not efficient in separating lanthanides and actinides. High melting point of aluminum (933.52 K) and low compatibility with the metallic construction materials limit its application in pyrochemical technologies utilizing chloride media. Gallium is next in the row and is considered as a prospective liquid metal electrode material. Ga, however, is a trace element and therefore is rather expensive for the industrial application. Alloys of gallium with other elements, for example, aluminum or indium, can be employed instead of pure Ga. Ga-In and Ga-Al alloys are very prospective for reprocessing SNF [6–11].

The goal of this work was to investigate the effect of Al and In concentration on the thermodynamic properties of La, Nd, and U in ternary Ga-In and Ga-Al-based alloys and the separation factor of Ln/Ac couple in a “molten salt-liquid metal” system.

http://dx.doi.org/10.5772/intechopen.72451

2. Experiment

The experiments were carried out at 723–823 K with the step 20–25 K under dry argon atmosphere in a three-electrode silica cell. All operations were performed in a SPEKS GB 02 M glovebox (< 1 ppm oxygen and <1 ppm moisture content). The electrochemical measurements were performed employing an Autolab 302 N potentiostat-galvanostat controlled by NOVA 1.11 software. Salts and metal mixtures of the required compositions were prepared from the individual components, LiCl (Sigma-Aldrich, 99.99%), KCl (Reachim, 99.9%), $LaCl_3$ (Sigma-Aldrich, 99.99%), $PrCl_3$ (Sigma-Aldrich, 99.99%), $NdCl_3$ (Sigma-Aldrich, 99.99%), Ga (GA-000, 99.99%), and In (IN-000, 99.98%). Ga-Al and Ga-In alloys of the specified composition were prepared from batches of the individual metals in the inert atmosphere in glovebox. The Ga-Al and Ga-In alloys prepared were metallic, silvery liquids free from any visible oxide films. Uranium (III) ions were introduced to electrolyte by electrolysis (anodic dissolution of U metal). The amount of lanthanum or uranium in the alloys was less than 0.40 wt.%. Liquid gallium-aluminum (gallium-indium) mixture was used as cathode and placed in a beryllium oxide crucible. The dilute solutions of prepared alloys were used directly in the experiments during the electromotive force (EMF) measurements vs. the Cl^-/Cl_2 reference electrode. The standard construction of it was described earlier in detail [12]. The following galvanic cell was used for measuring the electrode potentials of the alloys $E^{**}_{Me(Ga-In)}$:

$$(-)\ \mathrm{Me(alloy)}\ |\ 3\mathrm{LiCl}-2\mathrm{KCl},\mathrm{Me(III)}\ \|\ 3\mathrm{LiCl}-2\mathrm{KCl}\ |\ \mathrm{C_{(s)}},\mathrm{Cl_{2(g)}}\ (+) \tag{1}$$

The experimental procedure was the following. After preparation of the ternary alloy of a required composition, the potential-time dependence was recorded using potentiometric method at zero current at different temperatures in the experiment. The potential value of the horizontal part of the curve corresponded to the equilibrium potential of the alloy.

The lanthanide (uranium) concentrations in the chloride salts were determined by taking samples from the melts that were then dissolved in nitric acid solutions. Ln (U)-containing alloys were washed with water and then dried by ethanol. All solutions were analyzed by ICP-MS.

3. Results and discussion

3.1. Nd(U)-(Ga-Al)/3LiCl-2KCl system

Potentiometry method at zero current was used for determination of the apparent standard potentials of the alloys. The potential-time dependences were recorded at various temperatures and of the horizontal part of the curve corresponded to the equilibrium potential of the alloy [13–15]. In molten salts the activity coefficients of the solute species Me^{n+} are constant at concentrations below (3–5) $\times\ 10^{-2}$ mole fraction [12]. For the dilute solutions of Me in the alloys, the activity coefficients are also constant [5]. To characterize the electrochemical behavior of the alloy, an apparent standard potential of the alloy, $E^{**}_{Me(Ga-Al)}$, was used [5]:

$$E_{Me(Ga-Al)} = E^{**}_{Me(Ga-Al)} + \frac{RT}{nF} \ln \frac{C_{Me(III)}}{x_{Me(Ga-Al)}}, \quad (2)$$

where Me = Nd or U, $E_{Me(Ga-Al)}$ is the equilibrium potential of the alloy (V), $E^{**}_{Me(Ga-Al)}$ is the apparent standard potential of the alloy (V), n is the number of electrons exchanged, $C_{Me(III)}$ is the concentration of the metal ions in the solvent (mole fraction), and $x_{Me(Ga-Al)}$ is the concentration of the metal in the alloy (atomic fraction).

The apparent standard potentials of the alloys Me(Ga-Al) as a function of temperature were fitted to the following equations using OriginPro version 7.5 Software, Eqs. (3)–(8):

$$E^{**}_{Nd(Ga-Al)} = -(2.987 \pm 0.007) + (5.2 \pm 0.5) \cdot 10^{-4} \cdot T \pm 0.005 \text{ V} \quad 1.5 \text{ wt.\%Al} \quad (3)$$

$$E^{**}_{Nd(Ga-Al)} = -(3.068 \pm 0.004) + (6.0 \pm 0.2) \cdot 10^{-4} \cdot T \pm 0.003 \text{ V} \quad 5.0 \text{ wt.\%Al} \quad (4)$$

$$E^{**}_{Nd(Ga-Al)} = -(3.143 \pm 0.006) + (6.8 \pm 0.2) \cdot 10^{-4} \cdot T \pm 0.004 \text{ V} \quad 20.0 \text{ wt.\%Al} \quad (5)$$

$$E^{**}_{U(Ga-Al)} = -(2.715 \pm 0.006) + (5.1 \pm 0.1) \cdot 10^{-4} \cdot T \pm 0.003 \text{ V} \quad 1.5 \text{ wt.\%Al} \quad (6)$$

$$E^{**}_{U(Ga-Al)} = -(2.758 \pm 0.004) + (5.3 \pm 0.1) \cdot 10^{-4} \cdot T \pm 0.002 \text{ V} \quad 5.0 \text{ wt.\%Al} \quad (7)$$

$$E^{**}_{U(Ga-Al)} = -(2.791 \pm 0.005) + (5.5 \pm 0.1) \cdot 10^{-4} \cdot T \pm 0.003 \text{ V} \quad 20.0 \text{ wt.\%Al} \quad (8)$$

Newton interpolation polynomial expressions were obtained to construct three-dimensional $E^{**}_{Me(Ga-Al)} - C_{(Ga-Al)} - T$ graphs on the basis of the functional dependencies of the apparent standard electrode potentials of the alloys, Ga-Al mixture compositions, and temperature. Universal mathematical Maple 11 software was used for this purpose. Three-dimensional $E^{**}_{Me(Ga-Al)} - C_{(Ga-Al)} - T$ plots for Nd-(Ga-Al) and U-(Ga-Al) alloys and 3LiCl-2KCl eutectic-based melts are presented in **Figures 1** and **2**, respectively. The following expressions describe the three-dimensional graphs:

$$E^{**}_{Nd(Ga-Al)} = \left(4.8 \cdot 10^{-4} + 2.9 \cdot 10^{-5} \cdot C - 9.5 \cdot 10^{-7} \cdot C^2\right) \cdot T - 2.9 - 0.03 \cdot C + 9.8 \cdot 10^{-4} \cdot C^2 \text{ V} \quad (9)$$

$$E^{**}_{U(Ga-Al)} = \left(5 \cdot 10^{-4} + 7.2 \cdot 10^{-6} \cdot C - 2.4 \cdot 10^{-7} \cdot C^2\right) \cdot T - 2.7 - 0.02 \cdot C + 5.4 \cdot 10^{-4} \cdot C^2 \text{ V} \quad (10)$$

where C is the concentration of Al in Ga-Al alloy (wt. %).

The activity coefficients of Nd and U in liquid Ga-Al metallic alloys were determined from the following expression [5]:

$$\log \gamma_{Me(Ga-Al)} = \frac{3F}{2.303} \left(E^{*}_{Me(III)/Me} - E^{**}_{Me(Ga-Al)}\right) \quad (11)$$

http://dx.doi.org/10.5772/intechopen.72451

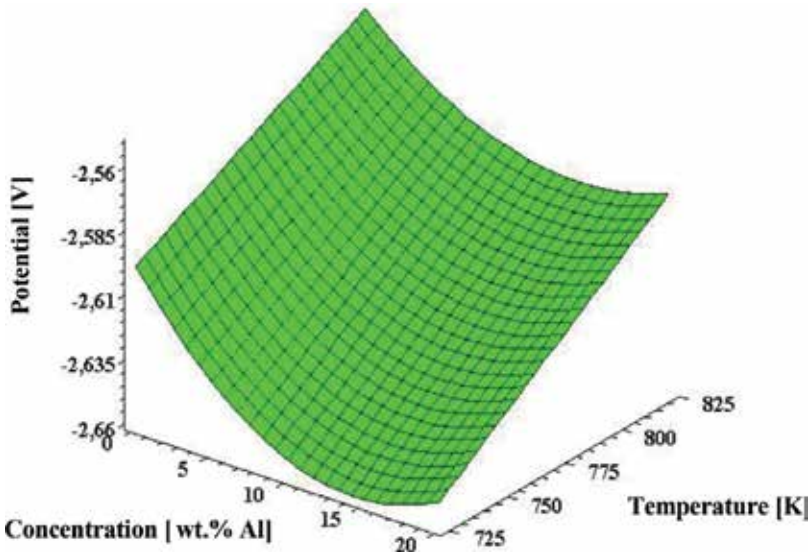

Figure 1. Apparent standard electrode potentials of Nd-Ga-Al alloys in fused Nd(Ga-Al)/3LiCl-2KCl system as a function of temperature and composition of Ga-Al alloy (3D diagram). Reference electrode: Cl^-/Cl_2.

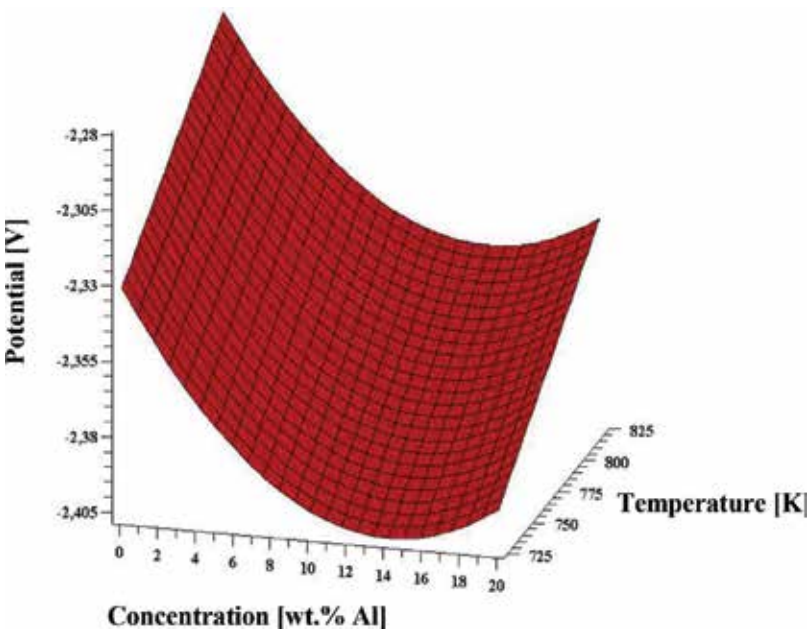

Figure 2. Apparent standard electrode potentials of U-Ga-Al alloy in the fused U(Ga-Al)/3LiCl-2KCl system as a function of temperature and composition of Ga-Al alloy (3D diagram). Reference electrode: Cl^-/Cl_2.

The data on Nd^{3+}/Nd and U^{3+}/U apparent standard electrode potentials in 3LiCl-2KCl eutectic were taken from the literature [7]. Temperature dependencies of Nd and U activity coefficients in liquid Ga-Al alloys were fitted to the Eqs. (12)–(17):

$$\log\gamma_{Nd(Ga-Al)} = 5.12 - \frac{11260}{T} \pm 0.06 \quad 1.5\ \text{wt.\%Al} \tag{12}$$

$$\log\gamma_{Nd(Ga-Al)} = 5.07 - \frac{11006}{T} \pm 0.04 \quad 5.0\ \text{wt.\%Al} \tag{13}$$

$$\log\gamma_{Nd(Ga-Al)} = 4.94 - \frac{10713}{T} \pm 0.05 \quad 20.0\ \text{wt.\%Al} \tag{14}$$

$$\log\gamma_{U(Ga-Al)} = 1.21 - \frac{4393}{T} \pm 0.05 \quad 1.5\ \text{wt.\% Al} \tag{15}$$

$$\log\gamma_{U(Ga-Al)} = 1.17 - \frac{3935}{T} \pm 0.05 \quad 5.0\ \text{wt.\%Al} \tag{16}$$

$$\log\gamma_{U(Ga-Al)} = 1.11 - \frac{3619}{T} \pm 0.06 \quad 20.0\ \text{wt.\%Al} \tag{17}$$

Three-dimensional $\log\gamma_{Nd(Ga-Al)} - C_{(Ga-Al)} - T$ and $\log\gamma_{U(Ga-Al)} - C_{(Ga-Al)} - T$ plots for fused Nd-(Ga-Al)/3LiCl-2KCl and U-(Ga-Al)/3LiCl-2KCl systems were presented in **Figures 3** and **4**, respectively. The following expressions describe these three-dimensional graphs:

$$\log\ \gamma_{Nd(Ga-Al)} = \left(-11390 + 91.2 \cdot C - 2.8 \cdot C^2\right)/T + 5.14 - 0.016 \cdot C + 3 \cdot 10^{-4} \cdot C^2 \tag{18}$$

$$\log\ \gamma_{U(Ga-Al)} = \left(-4638 + 169.4 \cdot C - 5.9 \cdot C^2\right)/T + 1.23 - 0.014 \cdot C + 4 \cdot 10^{-4} \cdot C^2 \tag{19}$$

where C is the concentration of Al in Ga-Al alloy (wt. %).

Low values of the activity coefficients show strong interaction between Ln (An) and the liquid alloy. Increasing temperature shifts the system toward more ideal behavior, in agreement with the literature.

Partial excess Gibbs free energy change of Nd and U in liquid Ga-Al-based alloys was calculated using Eq. (21) and previously obtained in expressions (12)–(17):

$$\Delta G^{ex.}_{Me(Ga-Al)} = \Delta H_{Me(Ga-Al)} - T\Delta S^{ex.}_{Me(Ga-Al)} \tag{20}$$

$$\Delta G^{ex.}_{Me(Ga-Al)} = 2.303RT\log\gamma_{Me(Ga-Al)} \tag{21}$$

$$\Delta G^{ex}_{Nd(Ga-Al)} = -229.1 + 115.0 \cdot 10^{-3}T \pm 3.7\ \text{kJ/mol} \quad 1.5\ \text{wt.\%Al} \tag{22}$$

$$\Delta G^{ex}_{Nd(Ga-Al)} = -211.7 + 100.1 \cdot 10^{-3}T \pm 3.6\ \text{kJ/mol} \quad 5.0\ \text{wt.\%Al} \tag{23}$$

$$\Delta G^{ex}_{Nd(Ga-Al)} = -175.8 + 57.9 \cdot 10^{-3}T \pm 3.4\ \text{kJ/mol} \quad 20.0\ \text{wt.\%Al} \tag{24}$$

$$\Delta G^{ex}_{U(Ga-Al)} = -83.9 + 23.2 \cdot 10^{-3}T \pm 3.6\ \text{kJ/mol} \quad 1.5\ \text{wt.\%Al} \tag{25}$$

http://dx.doi.org/10.5772/intechopen.72451

$$\Delta G^{ex}_{U(Ga-Al)} = -78.9 + 27.1 \cdot 10^{-3}T \pm 3.2 \text{ kJ/mol} \quad 5.0 \text{ wt.\%Al} \tag{26}$$

$$\Delta G^{ex}_{U(Ga-Al)} = -70.7 + 23.2 \cdot 10^{-3}T \pm 3.5 \text{ kJ/mol} \quad 20.0 \text{ wt.\%Al} \tag{27}$$

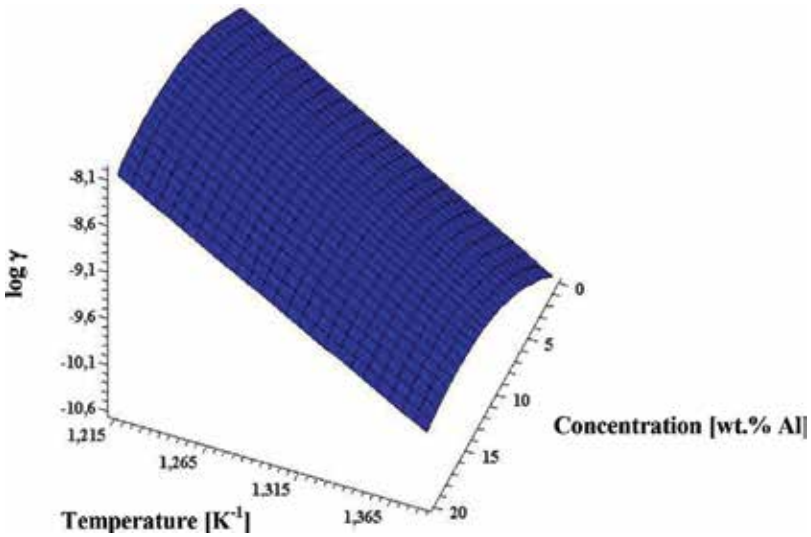

Figure 3. The activity coefficients of Nd in Ga-Al alloys as a function of temperature and composition of Ga-Al alloy (3D diagram).

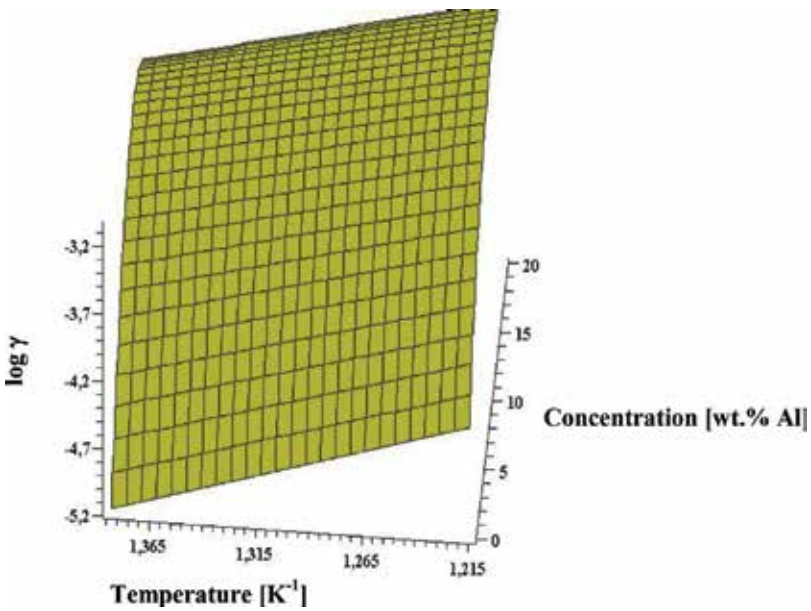

Figure 4. The activity coefficients of U in Ga-Al alloys as a function of temperature and composition of Ga-Al alloy (3D diagram).

where $\Delta G^{ex.}$ is the partial excess Gibbs free energy change (kJ/mol), ΔH is the partial enthalpy change of mixing (kJ/mol), $\Delta S^{ex.}$ is the partial excess entropy change (J/mol·K), and γ is the activity coefficient.

The general alloy formation reaction can be written in the following way:

$$[MeCl_6]^{3-} + 3\bar{e} + n(Ga - Al) = Me(Ga - In)_n + 6Cl^- \tag{28}$$

The efficiency of the electrochemical separation of metals in molten salts during their deposition is characterized by the value of the separation factor:

$$\Theta = \frac{C_2 x_1}{C_1 x_2} \tag{29}$$

where C_1 and C_2 are the concentrations of separated metals M_1 and M_2 in electrolyte in mole fraction and x_1 and x_2 are the quantity of separated metals M_1 and M_2 in alloy in atomic fraction.

The expression for calculation of the separation factor (SF) of uranium and neodymium in gallium-aluminum alloys can be written as follows [5]:

$$\log \Theta = \frac{3F}{2.303RT}\left(E^{**}_{U(Ga-Al)} - E^{**}_{Nd(Ga-Al)}\right) \tag{30}$$

where $E^{**}_{U(Ga-Al)}$ is the apparent standard potential of U-Ga-Al alloy (V) and $E^{**}_{Nd(Ga-Al)}$ is the apparent standard potential of Nd-Ga-Al alloy (V).

The following expressions for separation factor of uranium and neodymium were obtained in Eqs. (31)–(33):

$$\log \Theta_{U/Nd} = 1.18 + \frac{3088}{T} \pm 0.03 \quad 1.5\ \text{wt.\%Al} \tag{31}$$

$$\log \Theta_{U/Nd} = 1.05 + \frac{3003}{T} \pm 0.02 \quad 5.0\ \text{wt.\%Al} \tag{32}$$

$$\log \Theta_{U/Nd} = 1.01 + \frac{3004}{T} \pm 0.02 \quad 20.0\ \text{wt.\%Al} \tag{33}$$

A three-dimensional $\log \Theta_{Me(Ga-Al)} - C_{(Ga-Al)} - T$ graph showing the relationship between Nd/U separation factor, Al concentration in the Ga-Al solvent alloy, and temperature, for molten Me-(Ga-Al)/3LiCl-2KCl system, is presented in **Figure 5** and is described by the following equation:

$$\log\ \Theta_{U/Nd} = \left(3134.3 - 32.84 \cdot C + 1.32 \cdot C^2\right)/T + 1.25 - 0.05 \cdot C + 0.0019 \cdot C^2 \tag{34}$$

The separation of neodymium from uranium in molten chloride salts shows that uranium will be concentrated in the alloy phase, while neodymium will stay in the salt phase. The calculations of

http://dx.doi.org/10.5772/intechopen.72451

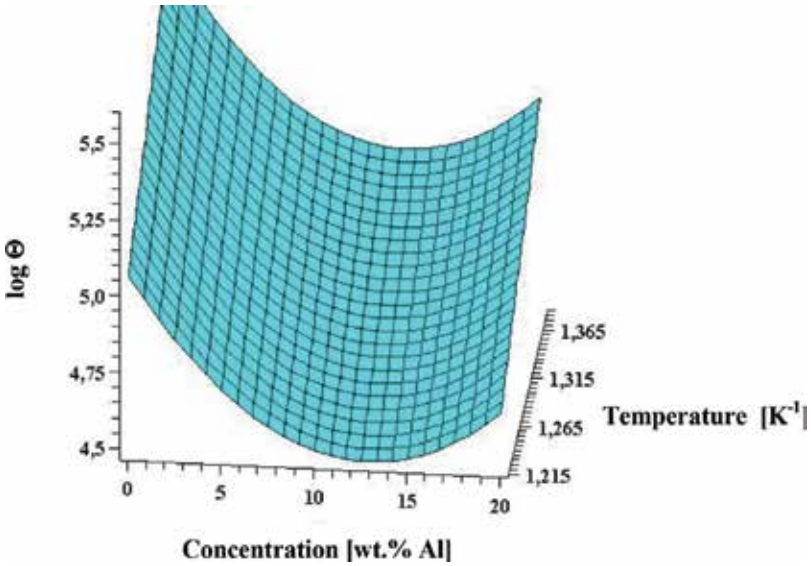

Figure 5. The separation factor of U/Nd couple as a function of temperature and composition of Ga-Al alloy (3D diagram).

SF for fused Nd/U(Ga-Al)/3LiCl-2KCl system show the high values of partitioning. For this technique the effect of lower temperatures should be preferred. Separation factor of Nd/U decreases by increasing the temperature due to the entropy factor.

3.2. La(U)-(Ga-In)/3LiCl-2KCl system

Potentiometry method at zero current was used for determination of the apparent standard potentials of the alloys. The dependencies of the apparent standard potential of Me(Ga-Al) alloys versus the temperature were fitted by the following equations using OriginPro version 7.5 Software:

$$E^{**}_{La(Ga)} = -2.851 + 5.18 \cdot 10^{-4} \cdot T \ V \quad [5] \tag{35}$$

$$E^{**}_{La(Ga-20wt.\%In)} = -(2.906 \pm 0.003) + (5.7 \pm 0.6) \cdot 10^{-4} \cdot T \pm 0.002 \ V \tag{36}$$

$$E^{**}_{La(Ga-40wt.\%In)} = -(3.357 \pm 0.005) + (10.9 \pm 0.1) \cdot 10^{-4} \cdot T \pm 0.002 \ V \tag{37}$$

$$E^{**}_{La(Ga-70wt.\%In)} = -(3.401 \pm 0.004) + (10.8 \pm 0.1) \cdot 10^{-4} \cdot T \pm 0.004 \ V \tag{38}$$

$$E^{**}_{La(In)} = -3.081 + 6.25 \cdot 10^{-4} \cdot T \ V \quad [5] \tag{39}$$

$$E^{**}_{U(Ga)} = -2.723 + 6.72 \cdot 10^{-4} \cdot T \ V \quad [5] \tag{40}$$

$$E^{**}_{U(Ga-20wt.\%In)} = -(2.508 \pm 0.006) + (3.8 \pm 0.1) \cdot 10^{-4} \cdot T \pm 0.003 \ V \tag{41}$$

$$E^{**}_{U(Ga-40wt.\%In)} = -(2.934 \pm 0.006) + (8.3 \pm 0.1) \cdot 10^{-4} \cdot T \pm 0.005 \ V \tag{42}$$

$$E^{**}_{U(Ga-70wt.\%In)} = -(2.950 \pm 0.008) + (7.3 \pm 0.1) \cdot 10^{-4} \cdot T \pm 0.006 \text{ V} \quad (43)$$

$$E^{**}_{U(In)} = -2.921 + 6.12 \cdot 10^{-4} \cdot T \text{ V} \quad [5] \quad (44)$$

Newton interpolation polynomial expressions were obtained to develop three-dimensional $\gamma_{Me(Ga-In)} - C_{(Ga-In)} - 1/T$ graphs on the basis of the functional dependencies of the apparent standard electrode potentials of the alloys, Ga-In mixture composition, and temperature (**Figures 6** and **7**).

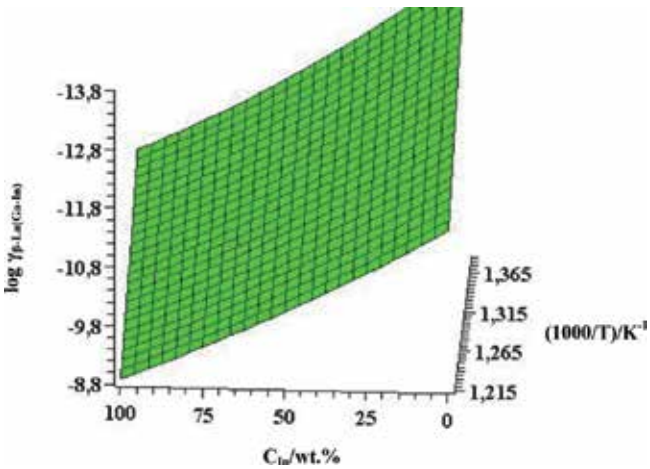

Figure 6. The activity coefficients of La in Ga-In alloys as a function of temperature and composition of Ga-In alloy (3D diagram).

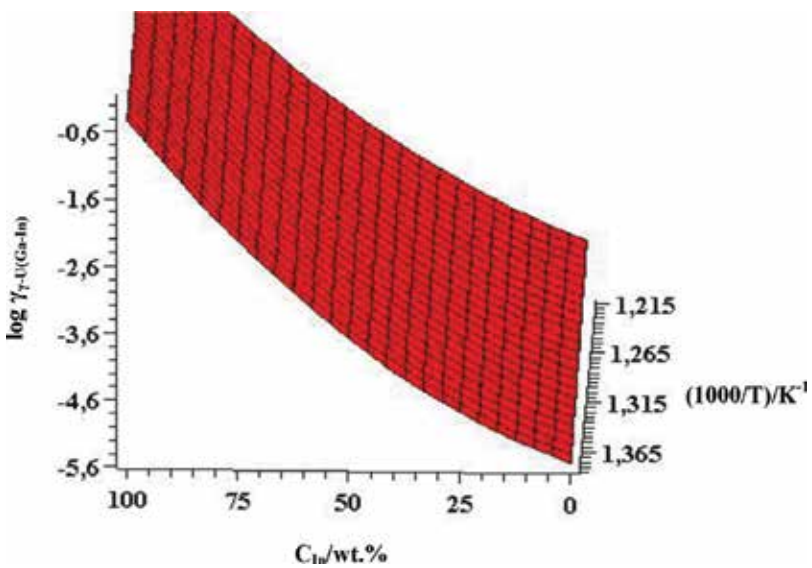

Figure 7. The activity coefficients of U in Ga-In alloys as a function of temperature and composition of Ga-In alloy (3D diagram).

The following expressions describe these three-dimensional graphs:

$$\log\gamma_{\beta-\mathrm{La(Ga-In)}} = \left(-13333 + 59\cdot \mathrm{C} - 0.24\cdot \mathrm{C}^2\right)/\mathrm{T} + 4.72 - 0.04\cdot \mathrm{C} + 0,0025\cdot \mathrm{C}^2 \quad (45)$$

$$\log\gamma_{\gamma-\mathrm{U(Ga-In)}} = \left(-4977 - 10\cdot \mathrm{C} + 0.4\cdot \mathrm{C}^2\right)/\mathrm{T} + 1.38 + 0.037\cdot \mathrm{C} - 0.0003\cdot \mathrm{C}^2 \quad (46)$$

where C is the concentration of In in Ga-In alloy (wt.%). The small values of activity coefficients show strong interaction of lanthanide and actinide with the liquid alloy. Increasing temperature shifts the system toward more ideal behavior.

Partial excess Gibbs free energy change of La and U in liquid Ga-In alloys was calculated:

$$\Delta G^{\mathrm{ex}}_{\mathrm{La(Ga)}} = -254.8 + 90.2\cdot 10^{-3}\mathrm{T}\ \ \mathrm{kJ/mol} \quad (47)$$

$$\Delta G^{\mathrm{ex}}_{\mathrm{La(Ga-20wt.\%In)}} = -233.6 + 68.6\cdot 10^{-3}\mathrm{T} \pm 3.2\ \ \mathrm{kJ/mol} \quad (48)$$

$$\Delta G^{\mathrm{ex}}_{\mathrm{La(Ga-40wt.\%In)}} = -217.1 + 66.5\cdot 10^{-3}\mathrm{T} \pm 2.9\ \ \mathrm{kJ/mol} \quad (49)$$

$$\Delta G^{\mathrm{ex}}_{\mathrm{La(Ga-70wt.\%)}} = -201.2 + 55.0\cdot 10^{-3}\mathrm{T} \pm 3.2\ \ \mathrm{kJ/mol} \quad (50)$$

$$\Delta G^{\mathrm{ex}}_{\mathrm{La(In)}} = -188.1 + 59.3\cdot 10^{-3}\mathrm{T}\ \ \mathrm{kJ/mol} \quad (51)$$

$$\Delta G^{\mathrm{ex}}_{\mathrm{U(Ga)}} = -95.1 + 26.4\cdot 10^{-3}\mathrm{T}\ \ \mathrm{kJ/mol} \quad (52)$$

$$\Delta G^{\mathrm{ex}}_{\mathrm{U(Ga-20wt.\%In)}} = -143.3 + 56.8\cdot 10^{-3}\mathrm{T} \pm 3.9\ \ \mathrm{kJ/mol} \quad (53)$$

$$\Delta G^{\mathrm{ex}}_{\mathrm{U(Ga-40wt.\%In)}} = -90.9 + 46.3\cdot 10^{-3}\mathrm{T} \pm 3.8\ \ \mathrm{kJ/mol} \quad (54)$$

$$\Delta G^{\mathrm{ex}}_{\mathrm{U(Ga-70wt.\%In)}} = -73.8 + 40.5\cdot 10^{-3}\mathrm{T} \pm 3.8\ \ \mathrm{kJ/mol} \quad (55)$$

$$\Delta G^{\mathrm{ex}}_{\mathrm{U(In)}} = -38.9 + 44.7\cdot 10^{-3}\mathrm{T}\ \ \mathrm{kJ/mol} \quad (56)$$

Using the temperature dependencies of the apparent standard potentials of lanthanum (35)–(39) and uranium (40)–(44) alloys, the following expressions for separation factor of uranium and lanthanum were obtained:

$$\log\theta_{\mathrm{La\text{-}U(Ga)}} = 2.33 + \frac{1935}{\mathrm{T}} \quad (57)$$

$$\log\theta_{\mathrm{La\text{-}U(Ga-20wt.\%In)}} = -2.85 + \frac{6006}{\mathrm{T}} \pm 0.02 \quad (58)$$

$$\log\theta_{\mathrm{La\text{-}U(Ga-40wt.\%In)}} = -3.97 + \frac{6421}{\mathrm{T}} \pm 0.02 \quad (59)$$

$$\log\theta_{\mathrm{La\text{-}U(Ga-70wt.\%In)}} = -5.25 + \frac{6818}{\mathrm{T}} \pm 0.02 \quad (60)$$

$$\log\theta_{\mathrm{La-U(In)}} = -0.20 + \frac{2419}{\mathrm{T}} \quad (61)$$

The results obtained show the shift of the partial enthalpy change of mixing toward more positive values with increasing concentration of indium in the binary alloys. A three-dimensional $\log\Theta_{La/U} - C_{(Ga-In)} - 1/T$graph showing the relationship between La/U separation factor, In concentration in Ga-In solvent alloy, and temperature for molten Me-(Ga-In)/3LiCl-2KCl system is presented in **Figure 8** and is described by the following equation:

$$\log\Theta_{U/La} = \left(1935 + 184 \cdot C - 2 \cdot C^2\right)/T + 2.33 - 0.246 \cdot C + 0.002 \cdot C^2 \quad (62)$$

where C is the concentration of In in Ga-In alloy (wt.%).

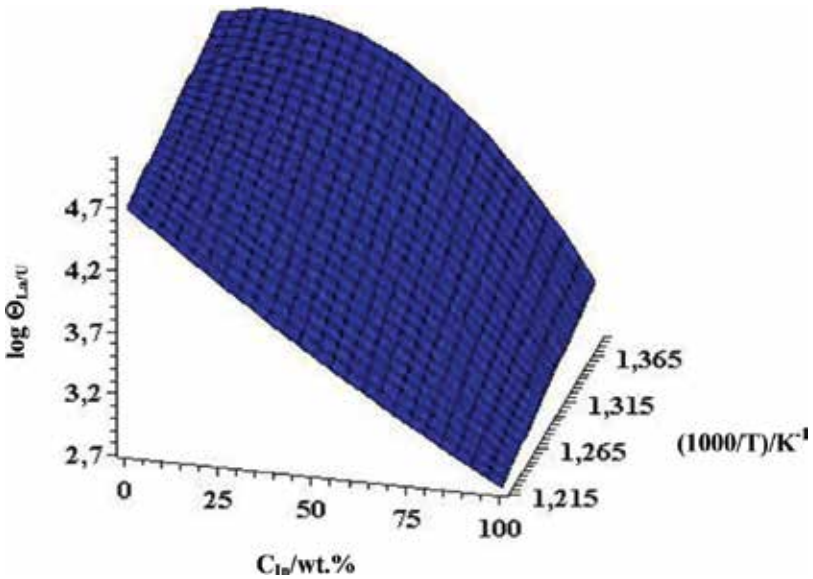

Figure 8. Three-dimensional $\log\Theta_{U/La} - C_{(Ga-In)} - 1/T$ graph for U/La couple.

4. Conclusions

The basic thermodynamic properties of lanthanum, neodymium, and uranium in liquid Ga-In and Ga-Al alloys between 723 and 823 K were determined. Low values of the activity coefficients showed strong interaction between lanthanides and the liquid alloys. The values of uranium and lanthanide separation factors showed that the alloys investigated here have considerable advantage compared to liquid cadmium. Analysis of the data obtained showed that Ga-In and Ga-Al alloys are the prospective media for application in partitioning technologies of spent nuclear fuels and nuclear waste treatment.

Acknowledgements

The reported study was funded by RFBR according to the research project No. 17-03-00694.

Author details

Valeri Smolenski[1,2*], Alena Novoselova[1,2], Alexander Bychkov[3], Vladimir Volkovich[4], Yana Luk'yanova[5] and Alexander Osipenko[5]

*Address all correspondence to: smolenski.valeri@gmail.com

1 Institute of High-Temperature Electrochemistry UB RAS, Ekaterinburg, Russia

2 College of Materials Science and Chemical Engineering, Harbin Engineering University, Harbin, P.R. China

3 National Research Nuclear University - MEPhI, Moscow, Russia

4 Department of Rare Metals and Nanomaterials, Institute of Physics and Technology, Ural Federal University, Ekaterinburg, Russia

5 JSC "State Scientific Centre-Research Institute of Atomic Reactors", Dimitrovgrad, Russia

References

[1] Koyama T, Iizuka M, Tanaka H, Tokiwai M, Shoji Y, Fujita R, Kobayashi T. An experimental study of molten salt electrorefining of uranium using solid iron cathode and liquid cadmium cathode for development of pyrometallurgical reprocessing. Journal of Nuclear Science and Technologies. 1997;**34**:384-393. DOI: 10.1080/18811248.1997.9733678

[2] Sakamura Y, Hijikata T, Kinoshita K, Inoue T, Storvick TS, Krueger CL, Roy JJ, Grimmett DL, Fusselman SP, Gay RL. Measurement of standard potentials of actinides (U, Np, Pu, Am) in LiCl-KCl eutectic salt and separation of actinides from rare earths by electrorefining. Journal of Alloys and Compounds. 1998;**271–273**:592-596. DOI: 10.1016/S0925-8388(98)00166-2

[3] Sakamura Y, Inoue T, Shirai O, Iwai T, Arai Y, Suzuki Y. Studies on pyrochemical reprocessing for metallic and nitride fuels; behavior of transuranium elements in LiCl–KCl/liquid metal systems. In: Proceedings of the International Conference on Future Nuclear Systems GLOBAL'99; 29 August-2 September; Wyoming; 1999

[4] Kinoshita K, Kurata M, Inoue T. Estimation of material balance in pyrometallurgical partitioning process of trans-uranic elements from high-level liquid waste. Journal of Nuclear Science and Technology. 2000;**37**:75-83. DOI: 10.1080/18811248.2000.9714869

[5] Lebedev VA. Selectivity of Liquid Metal Electrodes in Molten Halide. Chelyabinsk: Metallurgiya; 1993. 342 p

[6] Smolenski V, Novoselova A, Osipenko A, Maershin A. Thermodynamics and separation factor of uranium from lanthanum in liquid eutectic gallium-indium alloy/molten salt system. Electrochimica Acta. 2014;**145**:81-85. DOI: 10.1016/j.electacta.2014.08.081

[7] Smolenski V, Novoselova A, Osipenko A, Kormilitsyn M, Luk'yanova Y. Thermodynamics of separation of uranium from neodymium between the gallium-indium liquid alloy and the LiCl-KCl molten salt phases. Electrochimica Acta. 2014;**133**:354-358. DOI: 10.1016/j.electacta.2014.04.042

[8] Kurata M, Uozumi K, Kato T, Iizuka M. Thermodynamic evaluation of liquid Cd cathode containing U and Pu. Journal of Nuclear Science and Technology. 2009;**46**:1070-1075. DOI: 10.1080/18811248.2009.9711617

[9] Roy JJ, Grantham LF, Grimmett DL, Fusselman SP, Krueger CL, Storvick TS, lnoue T, Sakamura Y, Takahashi N. Thermodynamic properties of U, Np, Pu, and Am in molten LiCl-KCI eutectic and liquid cadmium. Journal of the Electrochemical Society. 1996;**143**:2487-2492. DOI: 10.1149/1.1837035

[10] De Cordoba G, Laplace A, Conocar O, Lacquement G, Caravaca C. Determination of the activity coefficients of neodymium in liquid aluminum by potentiometric methords. Electrochimica Acta. 2008;**54**:280-288. DOI: 10.1016/j.electacta.2008.08.002

[11] Serp J, Lefebvre P, Malmbeck R, Rebizant J, Vallet P, Glatz J-P. Separation of plutonium from lanthanum by electrolysis in LiCl-KCl onto molten bismuth electrode. Journal of Nuclear Materials. 2005;**340**:266-270. DOI: 10.1016/j.jnucmat.2004.12.004

[12] Smirnov MV. Electrode Potentials in Molten Chlorides. Moscow: Nauka; 1973. 267 p

[13] Smolenski V, Novoselova A, Mushnikov P, Osipenko A. Study of the electrochemical behavior of U(III) ions on liquid cd electrode and preparation of the U–Cd intermetallic compound in fused 3LiCl–2KCl eutectic. Journal of Radioanalitical and Nuclear Chemistry. 2017;**311**:127-133. DOI: 10.1007/s10967-016-4932-0

[14] Smolenski V, Novoselova A, Volkovich V, Luk'yanova Y, Osipenko A, Bychkov A, Griffiths TR. The effect of Al concentration on thermodynamic properties of Nd and U in Ga–Al-based alloys and the separation factor of Nd/U couple in a "molten salt-liquid metal system". Journal of Radioanalitical and Nuclear Chemistry. 2017;**311**:687-693. DOI: 10.1007/s10967-016-5053-5

[15] Volkovich VA, Maltsev DS, Yamshchikov LF, Chukin AV, Smolenski VV, Novoselova AV, Osipenko AG. Thermodynamic properties of uranium in gallium-aluminum based alloys. Journal of Nuclear Materials. 2015;**465**:153-160. DOI: 10.1016/j.jnucmat.2015.05.022

Chapter 7

Chemical Thermodynamics of Uranium in the Soil Environment

Michael Thomas Aide

Additional information is available at the end of the chapter

http://dx.doi.org/10.5772/intechopen.72107

Abstract

Uranium is present in the soil environment because of human activity, including the usage of U-bearing phosphorus fertilizers. In oxic and many suboxic soil environments, U(VI) is the dominant uranium valence species. With pH, pe (Eh), the partial pressure of CO_2, the mineralogy of the adsorbing surfaces and the uranium concentration as the key master variables, U(VI) will predictably participate in hydrolysis, ion-pairing, complexation, ion-exchange, mineral precipitation and adsorption reactions. An extensive listing of thermochemical data is currently available for detailed simulations to assist with model setup, data interpretation and system understanding. In this chapter, simulations of U(VI) hydrolysis with variable pCO_2 activities, U(IV) and U(VI) precipitation, U(VI) reduction and U(VI) complexation with carbonate and phosphate assemblages illustrate the usefulness and applicability of simulations in data analysis and experimental design.

Keywords: uranium hydrolysis, uranium complexation, uranium adsorption, simulation, soil

1. Properties, sources, characteristics of soil uranium

Uranium is the third element in the actinide series having an atomic number of 92 and an electronic configuration of [Rn] $5f^3 6d^1 7s^2$. The 5f orbitals are less effective in penetrating the inner core electrons than the 4f orbitals (lanthanide series), thus permitting more favored covalent bonding character [1]. Uranium(IV) and uranium(VI) have ionic radii of 89 and 73 pm, respectively. The two, more abundant, long-lived isotopes of uranium are $^{235}U_{92}$ and $^{238}U_{92}$. The naturally occurring mass abundances of uranium isotopes are ^{234}U (0.0057%), ^{235}U (0.71%) and ^{238}U (99.284%). ^{235}U is fissile, whereas ^{238}U in a breeder reactor will yield fissile ^{239}Pu [2].

Uranium decay is an isotope function, with (i) $^{238}U92$ decaying by α-emission to $^{234}Th_{90}$ (half-life of 4.45×10^9 years) and then by two successive β-emissions (half-life of 24.1 days and half-life of 1.18 minutes) to yield ^{234}U. ^{234}U will undergo α-emission (half-life of 2.45×10^5) to yield $^{230}Th_{90}$, whereas ^{235}U decaying by α-emission to yield ^{231}Th (half-life of 7.04×10^8 years) and later in the decay sequence to yield ^{227}Th [2].

2. Introduction to soil uranium

The Earth's crustal uranium abundance is centered near 2.3 mg U/kg [1]. Soil parent materials vary substantially in their uranium concentrations, with granites (4.4 mg U/kg) and shales (3.8 mg U/kg) having greater abundances than basalts (0.8 mg U/kg) and K-feldspars (1.5 mg U/kg) [3]. The phyllosilicates, muscovite and biotite have U concentrations centering near 20 mg U/kg, and some zircon minerals may have up to 2500 mg U/kg [3]. Aide et al. [4] documented total uranium concentrations by soil horizon depth in numerous southeastern Missouri soils, noting that the uranium concentrations varied from 0.58 to 2.89 mg U/kg, with course-textured soils generally having smaller U concentrations. In their study, uranium in individual soil pedons was well correlated with Fe-oxyhydroxide concentrations. Birke et al. [5] reported that the amount of uranium in river waters in Germany varied from 0.007 to 43.7 μg U/L, with a median of 0.33 μg U/L. Mendez-Garcia et al. [6] observed that high uranium concentrations in sediment in the Rio Grande Basin in Mexico were of natural occurrence.

Common uranium-bearing minerals include: uraninite [UO_2], pitchblende [U_3O_8], coffinite [$U(SiO_4)_{1-x}(OH)_{4x}$], brannerite [UTi_2O_6], davidite [(rare earth elements) (Y,U) (Ti,Fe^{3+}) 20 O_{38}] and thucholite [uranium-bearing pyrobitumen]. Less abundant uranium-bearing minerals include: autunite [$Ca(UO_2)_2(PO4)_2 \bullet 8–12\ H_2O$], carnotite [$K_2(UO_2)_2(VO_4)_2 \bullet 1–3\ H_2O$], seleeite [$Mg(UO_2)_2(PO_4)_2 \bullet 10\ H_2O$], torbernite [$Cu(UO_2)_2(PO_4)_2 \bullet 12\ H_2O$], tyuyamunite [$Ca(UO_2)_2(VO_4)_2 \bullet 5–8\ H_2O$], uranocircite [$Ba(UO_2)_2(PO_4)_2 \bullet 8–10\ H_2O$], uranophane [$Ca(UO_2)_2(HSiO_4)_2 \bullet 5\ H_2O$], zeunerite [$Cu(UO_2)_2(AsO_4)_2 \bullet 8–10\ H_2O$], rutherfordine [$UO_2CO_3$] and schoepite [$(UO_2)_8O_2(OH)_2 \bullet 12H_2O$]. Uranium(V) species and associated minerals are comparatively rare because of disproportionation into U(IV) and U(VI) species [1].

Soils may become uranium impacted because of nuclear fuel production, nuclear weapons production, depleted uranium in munitions, coal combustion and most importantly by phosphorus fertilizer applications [7–19]. Stojanovic et al. [17] observed that maize and sunflower plants may be very useful for uranium phytoremediation, with the root mass acquiring much greater uranium accumulations than culms, leaves and grain. Stojanovic et al. [18] documented previous research showing that the use of phosphorus fertilizers may contribute 73% of the total anthropogenic uranium to the global soil resource. Echevarria et al. [20] observed that low pH levels favored increased uranium plant availability. Laroche et al. [21] in a hydroponic study observed that phosphorus reduced uranyl activity, especially at higher pH intervals.

Plant uptake of U has been investigated for phytoremediation of impacted soils [7, 13–15, 22–34]. Sunflower (*Helianthus annuus*) has been shown to substantially phytoaccumulate U(VI)

[33]. Sheppard et al. [30] noted that leafy vegetables could accumulate U(VI) to a greater extent than common grain crops. Chopping and Shambhag [35] showed U(VI) binding by soil organic matter, particularly if the soil organic materials acquired a negative charge density at or above pH 7. Organic complexes of U may be replaced by other cations, especially divalent and trivalent cations [36].

Phyllosilicates (clay minerals) typically manifest a net negative charge density because of isomorphic substitution and unsatisfied edge charges [36–38]. Al-, Mn- and Fe-oxyhydroxides have variable charged surfaces (amphoteric) that acquire a positive charge density when the pH is more acidic than the mineral's point of zero net charge density [39, 40]. Uranyl ions, along with its hydroxyl monomers and hydroxyl polymers, will participate in adsorption reactions with phyllosilicates and Mn- and Fe-oxyhydroxides [41–49]. The transport of U-bearing colloids by wind and water erosion is an important source of U transport from impacted sites.

There lies great interest in understanding the U transport in natural systems such as soil profiles, sediments and aquifers [4, 9, 10, 19, 40, 50–52]. Johnson et al. [51] investigated depleted uranium soil sites in Nevada (USA), observing that uranium retention is a function of (1) soil type, (2) soil binding site concentrations, (3) the presence of phyllosilicates and their associated Fe-oxyhydroxides, (4) the contaminant concentration, (5) the presence of competing ions and (6) the contaminant speciation based on pH and Eh. They noted that the estimated distribution coefficients (Kd = concentration of the sorbed contaminant/the contaminant in the aqueous phase) increased with soil reaction from pH 7 to pH 11. Roh et al. [16] investigated two U-impacted sites at Oak Ridge, TN using sequential leaching and demonstrated that soil U was associated substantially with carbonates (45%) and Fe-oxyhydroxides (40%).

3. Uranium hydrolysis

Hydrolysis constants for U(IV) are presented in **Table 1**.

The solubility of U(IV) may be estimated from thermochemical data, with the assumption that UO_2 is the crystalline phase, as: $UO_2 + 2H_2O + OH^- = U(OH)_5^-$.

($\log Ks_{1,5} = -3.77$).

$U^{4+} + H_2O = U(OH)^{3+} + H^+$	$\log K_{1,1} = -0.65$
$U^{4+} + 2H_2O = U(OH)_2^{2+} + 2H^+$	$\log K_{1,2} = -0.2.6$
$U^{4+} + 3H_2O = U(OH)_3^+ + 3H^+$	$\log K_{1,3} = -5.8$
$U^{4+} + 4H_2O = U(OH)_4 + 4H^+$	$\log K_{1,4} = -10.3$
$U^{4+} + 5H_2O = U(OH)_5^- + 5H^+$	$\log K_{1,5} = -16.0$
$6U^{4+} + 15H_2O = U_6(OH)_{15}^{9+} + 15H^+$	$\log K_{6,15} = -17.2$

Table 1. Hydrolysis constants for U(IV) (Baes and Mesmer [53]).

	Baes and Mesmer [53]	Davis [54]
$UO_2^{2+} + H_2O = UO_2(OH)^+ + H^+$	$\log K_{1,1} = -5.8$	$= -5.20$
$UO_2^{2+} + 2H_2O = UO_2(OH)_2 + 2H^+$	—	$= -11.50$
$UO_2^{2+} + 3H_2O = UO_2(OH)_3^- + 3H^+$	—	$= -20.00$
$UO_2^{2+} + 4H_2O = UO_2(OH)_4^{2-} + 4H^+$	—	$= -33.00$
$2UO_2^{2+} + 1H_2O = (UO_2)_2(OH)_1^{3+} + H^+$	—	$= -2.70$
$2UO_2^{2+} + 2H_2O = (UO_2)_2(OH)_2^{2+} + 2H^+$	$\log K_{2,2} = -5.62$	$= -5.62$
$3UO_2^{2+} + 5H_2O = (UO_2)_3(OH)_5^+ + 5H^+$	$\log K_{3,5} = -15.63$	$= -15.55$

Table 2. Hydrolysis constants for U(VI) [53, 54].

The uranyl ion (UO_2^{2+}) is an oxycation, given that the high charge polarization of U^{6+} prevents this aqueous species from being stable. Hydrolysis constants for U(VI) are presented in **Table 2**.

In low ionic strength media, the U(VI) polymers are not thermodynamically favored, with the exception of $(UO_2)_3(OH)_5^+$ [41, 42, 44, 46, 49, 54–58].

4. Simulation of uranium hydrolysis

Using the MinteqA2 software [59], U(VI) speciation may be estimated from thermochemical data for pH intervals from pH 4 to pH 8. Setting the total U(VI) concentration at 10^{-8} mole/liter, the pCO_2 pressure at 0 and then again at 0.02 bar (2 kPa) were the primary model vari able inputs. Establishing a constant ionic strength with 0.01 mole $NaNO_3$/liter, activity coefficients were estimated using the Debye-Huckel equation. In the CO_2 closed system, UO_2^{2+} is the dominant species in very acidic media, whereas $UO_2(OH)^+$ is the dominant species from pH 6 to pH 8 (**Table 3**). The ion pair $UO_2NO_3^+$ is an important secondary species, particularly in acidic media. In the CO_2 open system, UO_2^{2+} is the dominant species in very acidic media; however, the UO_2CO_3, $UO_2(CO_3)_2^{2-}$ and $UO_2(CO_3)_3^{4-}$ are U(VI) species increasingly dominant upon transition from acidic media to neutral and then to alkaline media (**Table 3**). Importantly, the uranyl carbonate complexes are stable at Eh conditions that would promote U(VI) reduction in CO_2 closed systems. This MinteqA2 simulation of dilute U(VI) speciation closely corresponds with the analytical data and its MinteqA2 simulation as presented by Langmuir [38] and also the data analysis from Waite et al. [58].

Repeating the simulation at 10^{-3} mol U/L, with allowance for mineral precipitation yielded different U species distributions across the pH intervals (**Table 4**). At pH 4, the UO_2^{2+} species is increasingly converted by polymerization into the $(UO_2)_2(OH)_2^{2+}$ species. At pH 5, the UO_2^{2+} and UO_2CO_3 species similarly transitioned into the $(UO_2)_3(OH)_5^+$ and the $(UO_2)_2(OH)_2^{2+}$ species. The pH 7 and 8 simulations witnessed the expanding abundances of $UO_2(CO_3)_2^{2-}$. Rutherfordine (UO_2CO_3) was indicated to have precipitated at pH 4–7, whereas calcite ($CaCO_3$) precipitated at pH 8.

Species	–log (activity)				
	pH 4	pH 5	pH 6	pH 7	pH 8
UO_2	8.21 (96.8%)	9.5 (44.8%)	10.3	13.6	19.2
$UO_2(OH)$	10.1	9.4 (4.1%)	10.2	12.5	17.1
$(UO_2)_2(OH)_2$	14.0	12.7	14.2	18.8	27.9
$(UO_2)_3(OH)_5$	20.2	16.2	16.6	21.4	33.1
UO_2NO_3	10.0 (1.2%)	10.3	12.1	15.4	20.9
UO_2CO_3	9.9 (1.1%)	8.3 (50.3%)	8.1 (83.8%)	9.4 (4.3%)	
$UO_2(CO_3)_2$	14.9	11.2	9.0 (14.8%)	8.3 (77.8%)	9.9 (2.5%)
$UO_2(CO_3)_3$	22.2	16.5	12.3	9.6 (17.9%)	9.1 (97.5%)

Total U concentration was 10^{-8} mole/L.

Activity coefficients were determined by the Debye-Huckel equation.

The presence of CO_2(g) at 2×10^{-2} bar (2 kPa) and an ionic strength standardized by 0.01 *M* $NaNO_3$. Calcium concentrations were 0.001 mol/L. Within a pH column, ( ) indicates the percentage of the U species.

Table 3. The MinteqA2 simulation of U(VI) speciation.

Species	–log (activity)				
	pH 4	pH 5	pH 6	pH 7	pH 8
UO_2	2.61 (38.1%)	4.6 (14.5%)	6.6	8.6	13.6
$UO_2(OH)$	4.51	5.5 (1.3%)	6.5	7.5	11.7
$(UO_2)_2(OH)_2$	2.79 (49.8%)	4.8 (19%)	6.8	8.8	17.1
$(UO_2)_3(OH)_5$	3.41 (11.1%)	4.4 (48.6%)	5.4 (19.8%)	6.4	16.9
UO_2NO_3	4.39	6.4	8.4	10.4	15.6
UO_2CO_3	4.36	4.4(16.4%)	4.4 (66.6%)	4.4 (4%)	7.5
$UO_2(CO_3)_2$	9.31	7.3	5.3 (11.8%)	3.3 (75.8%)	4.5
$UO_2(CO_3)_3$	16.6	12.6	8.6	4.6 (20.0%)	3.7 (99.5%)

Total U concentration was 10^{-3} mole/L, which was allowed to equilibrate and allow precipitation.

Calcium concentrations were standardized at 10^{-3} mole/L. The presence of CO_2 (g) at 2×10^{-2} bar (2×10^3 pascal) and an ionic strength standardized by 0.01 *M* $NaNO_3$. Within a pH column, ( ) indicates the percentage of the U species. Activity coefficients were determined by the Debye-Huckel equation. Rutherfordine (UO_2CO_3) was predicted to precipitate from pH 4 to pH 7, whereas calcite was predicted to precipitate at pH 8.

Table 4. The MinteqA2 simulation of U(VI) solubility by species in the presence of CO_2 (g).

5. Uranium oxidation and reduction

The reduction of U(VI) to U(IV) may be presented as [53]:

$$UO_2^{2+} + 4H^+ + 2e^- = U^4 + 2H_2O \quad E^0 = 0.329\text{volts} \tag{1}$$

At Eh values less than 0.2 volts, U(VI) reduction to uraninite (UO_2) is favored. Stewart et al. [60] observed that U(VI) reduction to U(IV) is inhibited in the presence of ferrihydrite. Yajima et al. [61] also observed that U(VI) reduction to U(IV) limited mobility. Goldhaber et al. [62] observed that coffinite formed via reduction processes in sedimentary rocks. Fendorf et al. [63] reviewed the biotic and abiotic pathways for U(VI) reduction in anaerobic soils, and they noted that U(IV) has more limited mobility and binds more preferentially to substrates than U(VI). Uranyl reduction is facilitated by bacterially mediated reactions [64]; however, non-crystalline ferric oxides and nitrate may be effective terminal electron acceptors. Similarly, Burgos et al. [63] observed that soil humic acid partially inhibits U(VI) reduction.

6. Simulation of uranium reduction

At a pe of 5 (296 mv), indicative of suboxic soil redox conditions, and at a total U concentration of 10^{-8} mol/L, the MinteqA2 simulation of U(VI) reduction to U(IV) indicates that U(IV) would

Species	–log (activity)				
	pH 4	pH 5	pH 6	pH 7	pH 8
U(VI) Speciation					
UO_2	8.2 (98.6%)	8.5 (44.8%)	10.3	13.6	19.2
$UO_2(OH)$	10.1	9.4 (4.1%)	10.2	12.5	17.1
$(UO_2)_2(OH)_2$	14.0	12.7	14.2	18.8	27.9
$(UO_2)_3(OH)_5$	20.2	16.2	16.6	21.4	33.1
UO_2NO_3	10.0 (1.2%)	10.3	12.0	15.4	21.0
UO_2CO_3	10.0 (1.1%)	8.3 (50.5%)	8.1 (83.8%)	9.4 (4.3%)	12.9
$UO_2(CO_3)_2$	14.9	11.3	9.0 (14.8%)	8.3 (77.8%)	9.9 (2.5%)
$UO_2(CO_3)_3$	22.2	16.5	12.3	9.6 (17.9%)	9.1 (97.5%)
U(IV) Speciation					
U^{4+}	25.0	29.3	35.1	42.4	52.0
U(OH)	21.7	25.0	29.8	36.0	44.6
$U(OH)_2$	19.3 (1.6%)	21.6	25.4	30.7	44.6
$U(OH)_3$	17.9 (24.1%)	19.3 (1.1%)	22.0	26.3	32.9
$U(OH)_4$	17.1 (58.7%)	17.8 (26.9%)	19.6 (3.6%)	22.9	28.5
$U(OH)_5$	18.1 (15.7%)	17.4 (72.0%)	18.2 (96.4%)	20.5 (99.6%)	25.1 (100%)

Total U concentration was 10^{-8} mole/L, which was allowed to equilibrate and allow reduction at a pe of 5 (296 mv). Activity coefficients were determined by the Debye-Huckel equation.

Calcium concentrations were standardized at 10^{-3} mole/L. The presence of CO_2 (g) at 2×10^{-2} bar (2×10^3 pascal) and an ionic strength standardized by 0.01 *M* $NaNO_3$. Within a pH column, ( ) indicates the percentage of the U species.

Table 5. The MinteqA2 simulation of U(VI) reduction to U(IV) in the presence of CO_2 (g) at 2×10^{-2} bar (2 kilopascal) and an ionic strength standardized by 0.01 *M* $NaNO_3$.

U(VI) Speciation	–log (activity)	U(IV) Speciation	–log (activity)
UO_2	19.9	U^{4+}	28.7
$UO_2(OH)$	19.8	U(OH)	23.3
$(UO_2)_2(OH)_2$	33.3	$U(OH)_2$	18.9
$(UO_2)_3(OH)_5$	45.2	$U(OH)_3$	15.6
UO_2NO_3	21.6	$U(OH)_4$	13.2 (3.6%)
UO_2CO_3	17.6 (83.7%)	$U(OH)_5$	11.8 (96.4%)
$UO_2(CO_3)_2$	18.6 (14.8%)		
$UO_2(CO_3)_3$	21.8		

Total U concentration was 10^{-3} mole/L, which was allowed to equilibrate and allow reduction at a pe of −3 (−177 mv). Activity coefficients were determined by the Debye-Huckel equation. Calcium and sulfate were present initially at 0.001 mole/L. Uraninite was precipitated and established the U equilibria (saturation index 0.00). No carbonate, sulfate or sulfide minerals were documented to precipitate. Calcium concentrations were standardized at 10^{-3} mole/L. The presence of CO_2 (g) at 2×10^{-2} bar (2×10^3 pascal) and an ionic strength standardized by 0.01 *M* $NaNO_3$. Within a column, ( ) indicates the percentage of the U species.

Table 6. The MinteqA2 simulation of U(VI) reduction to U(IV) in the presence of CO_2 (g) at pH 6 at a pe of −3 (−177 mv).

be undetectable by inductively coupled plasma emission spectroscopy-mass spectroscopy or other comparable analytical technologies (**Table 5**). At pH 4, the dominant U(IV) species was $U(OH)_4$, whereas at pH 5–8, the dominant species was $U(OH)_5^-$. The dominant U(VI) species were UO_2 (pH 4), UO_2 and UO_2CO_3 (pH 5), UO_2CO_3 (pH 6), $UO_2(CO_3)_2$ (pH 7) and $UO_2(CO_3)_3$ (pH 8).

At a pe of −3 (−177 mv), indicative of anoxic soil redox conditions, and at a total U concentration of 10^{-3} mole/L at pH 6, the simulation of U(VI) reduction to U(IV) indicates that the dominant U(IV) species was $U(OH)_5^-$ (**Table 6**). The dominant U(VI) species were UO_2CO_3 (83.7%) and $UO_2(CO_3)_2$ (14.8%). The MinteqA2 predicted that uraninite(UO_2) formed as a solid phase.

7. Uranium complexation with an emphasis on phosphorus

Uranium complexation pairs a central cation (coordination center) with a surrounding array of molecules and ions. Phosphorus interactions with U(VI) have been studied to assess whether phosphorus may reduce the availability and mobility of U(VI) [12, 65–67]. Stojanovic et al. [18] reported that phosphorus may readily form uranyl phosphates and subsequently precipitate autunite. They noted that at pH levels greater than 6.0, the dominant U(VI)-phosphorus species was the plant-available UO_2PO_4 species, whereas at more acidic soil reactions, UO_2HPO_4 and $UO_2H_2PO_4^+$ were more abundant and are not considered as plant-available U-phosphate species. Grabias et al. [65] studied uranyl acetate immobilization in ferruginous soils amended with phosphates. In acidic pH ranges, a strong U(VI) sorption was observed in the presence of phosphate, supporting their premise that adsorption was promoted by the formation of $UO_2(H_2PO_4)(H_3PO_4)^+$, $UO_2(H_2PO_4)_2$ and $(UO_2)_3(PO_4)_3\ 4H_2O$.

Mehta et al. [67] demonstrated that U(VI) flux in soil columns was substantially reduced when phosphate was present. Sequential extractions demonstrated that the U(VI) could be readily extracted by ion-exchange and dilute acid treatments. Laser-induced florescence spectroscopy inferred adsorption to be the dominant retention mechanism.

Sandino and Bruno [68] determined the solubility of $(UO_2)_3(PO_4)_2\ 4H_2O$ (s) and the formation of U(VI) phosphate complexes over the pH range of pH 4–9. In their study, UO_2HPO_4 and $UO_2PO_4^-$ were the dominant U species. Minimum U(VI) solubility for the $(UO_2)_3(PO_4)_2\ 4H_2O$ (s) system occurred near pH 6, whereas the minimum U(VI) solubility for amorphous (non-crystalline) and crystalline schoepite occurred near the pH levels of pH 7.4 and 8.4, respectively. Thermodynamic data for U(VI) with respect to phosphate and carbonate from the literature are well-documented by Sandino and Bruno [68].

Lenhart et al. [69] described uranium(VI) complexation with citric acid, humic acid and fulvic acid in acidic media (pH 4.0 and 5.0). Using Schubert's ion-exchange method, the U(VI)-citric acid complex was determined to be 1:1 uranyl-citrate complex ($\beta_{1,1} = 6.69 \pm 0.3$ at I = 0.10). Humic and fulvic acids were demonstrated to strongly bind to U(VI), with humic acid forming a slightly stronger binding complex. The U(VI)-humic acid and U(VI)-fulvic acid complexes were determined to be non-integral (1 U(VI) with between 1 and 2 humic or fulvic acids), suggesting that a 1:1 stoichiometry involving a limited number of high-affinity sites.

Ivanov et al. [70] observed uranyl sorption on bentonite in the presence of humic acid with trace levels of uranium(VI). Uranyl sorption on bentonite was shown to be strongly pH dependent. In the absence of humic acid, U(VI) sorption exhibited a sorption edge between pH 3.2 and pH 4.2. In the presence of humic acid, U(VI) sorption slightly increased at low pH and curtails at moderate pH. Soluble uranyl carbonate species inhibited U(VI) sorption at alkaline pH levels. At pH intervals from pH 3 to pH 4, UO_2HA was predicted ($[U] = 8.4 \times 10^{-11}$ and $pCO_2 = 10^{-3.5}$ atm, HA = humic acid). From pH 5 to pH 7, $UO_2(OH)HA$ was predicted to be the dominant species. Tinnacher et al. [71] studied the reaction kinetics of tritium-labeled fulvic acid on uranium(VI) sorption onto silica, demonstrating that metal sorption rates are a complex function of metal and organic ligand concentrations and the nature and abundance of mineral surface sites.

$2UO_2^{2+} + 3H_2O + H_2CO_3 = (UO_2)_2CO_3(OH)_3^- + 5H^+$	log K = −17.54
$UO_2^{2+} + H_2CO_3 = UO_2CO_3 + 2H^+$	log K = −7.01
$UO_2^{2+} + 2H_2CO_3 = UO_2(CO_3)_2^{2-} + 4H^+$	log K = −16.43
$UO_2^{2+} + 3H_2CO_3 = UO_2(CO_3)_3^{4-} + 6H^+$	log K = −28.45
$UO_2^{2+} + NO_3^- = UO_2NO_3^+$	log K = 0.30
$H^+ + CO_3^{2-} = HCO_3^-$	log K = −6.35
$2H^+ + CO_3^{2-} = H_2CO_3$	log K = −16.68

Table 7. Formation constants for selected aqueous species (Davis [44]).

$UO_2^{2+} + 2H_2O = UO_2(OH)_2 + 2H^+$	log K = −5.4
$UO_2^{2+} + CO_3^{2-} = UO_2CO_3$	log K = 14.11
$2UO_2^{2+} + Ca^{2+} + 2PO_4^{3-} = Ca(UO_2)_2(PO_4)_2$	log K = 48.61
$2UO_2^{2+} + Fe^{2+} + 2PO_4^{3-} = Fe(UO_2)_2(PO_4)_2$	log K = 46.00
$UO_2^{2+} + H^+ + PO_4^{3-} = H(UO_2)PO_4$	log K = 25.00

Table 8. Precipitation reactions involving U(VI) (Chen and Yiacoumi [40]).

Reaction	log β
$UO_2^{2+} + H_3PO_4 = UO_2H_3PO_4^{2+}$	0.76 ± 0.15
$UO_2^{2+} + H_3PO_4 = UO_2H_2PO_4^{+} + H^+$	1.12 ± 0.07
$UO_2^{2+} + 2H_3PO_4 = UO_2(H_3PO_4)H_2PO_4^{+} + H^+$	1.69 ± 0.15
$UO_2^{2+} + 2H_3PO_4 = UO_2(H_2PO_4)_2 + H^+$	0.87 ± 0.05
H_3PO_4 Ka1, Ka2 and Ka3 constants are (−2.14 ± 0.03), (−7.21 ± 0.02) and (−12.35 ± 0.03), respectively.	

Table 9. Experimental equilibrium data for the U(VI)-H_3PO_4 at I = 0 (Grenthe et al. [55]).

Sandino and Bruno [68] reported the oxalate and sulfate complexation reactions involving the uranyl cation: (1) UO_2^{2+} + Oxalate^{2-} = UO_2Oxalate, log β = 6.02 and (2) UO_2^{2+} + Sulfate^{2-} = UO_2Sulfate, log β = 1.92. Tandy et al. [72] reported that citrate and malate from root exudates supported greater uranium concentrations in the adjacent soil solution. Sandino and Bruno [68] provided phosphate complexation reactions involving the uranyl cation: (1) UO_2^{2+} + $HPO_4^{2-} = UO_2HPO_4$, log β = 7.28 ± 0.10 and (2) $UO_2^{2+} + PO_4^{3-} = UO_2PO_4^{1-}$, log β = 13.25 ± 0.09. Additional equilibrium constants are presented in **Tables 7–9**.

8. Simulation of uranium complexation with H_3PO_4

The MinteqA2 simulation of U(VI) at 10^{-3} mol U/L demonstrated that the dominant U(VI)-phosphate species were $UO_2(HPO_4)_2$ at pH 4 and 6, whereas at pH 8, the dominant species were $UO_2(CO_3)_3^{4-}$ (67.9%) and $UO_2(HPO_4)_2$ (30.6%). Rutherfordine and $(UO_2)_3(PO_4)_2$ were formed as solid phases (**Table 10**).

Species	−log (activity)		
	pH 4	pH 6	pH 8
UO_2	5.3 (3.1%)	7.3	14.4
$UO_2(OH)$	7.2	7.2	12.3
$(UO_2)_2(OH)_2$	8.2	8.2	18.4
$(UO_2)_3(OH)_5$	11.5	7.5	18.9

Species	–log (activity)		
	pH 4	pH 6	pH 8
UO_2NO_3	7.1	9.0	16.1
UO_2HPO_4	6.4	7.4	11.0
$UO_2(HPO_4)_2$	3.8 (98.4%)	3.8 (96.0%)	3.8 (30.6%)
$UO_2H_2PO_4$	7.2	10.2	15.8
$UO_2(H_2PO_4)_2$	10.1	14.1	18.1
$UO_2(H_2PO_4)_3$	13.3	18.3	20.7
UO_2PO_4	8.8	7.8	9.4
UO_2CO_3	7.1	5.1 (3.3%)	8.2
$UO_2(CO_3)_2$	12.0	6.0	5.1 (1.5%)
$UO_2(CO_3)_3$	19.3	9.3	4.4 (67.9%)

Total U concentration was 10^{-3} mole/L, which was allowed to equilibrate and allow precipitation of rutherfordine and $(UO_2)_3(PO_4)_2$.

Activity coefficients were determined by the Debye-Huckel equation.

Calcium and H_3PO_4 concentrations were initially standardized at 10^{-3} mole/L. The presence of CO_2 (g) at 2×10^{-2} bar (2 kPa) and an ionic strength standardized by 0.01 *M* $NaNO_3$. Within a pH column, ( ) indicates the percentage of the U species.

Table 10. The MinteqA2 simulation of U(VI) species in the presence of CO_2 (g) and H_3PO_4.

9. Uranium solubility and precipitation

The solubility of U(VI) may be estimated from thermochemical data with the assumption that $UO_2(OH)_2$ is the crystalline phase [53] as:

$$UO_2(OH)_2 + 2H^+ = UO_2^{2+} + 2H_2O \qquad \text{Log } K_{s1,0} = 5.6. \tag{2}$$

Hsi and Langmuir [56] investigated the adsorption of U(VI) onto noncrystalline $Fe(OH)_3$ and goethite (α-FeOOH) in batch 0.1 mole $NaNO_3$/liter suspensions prepared with different total carbonate concentrations and pH intervals. Hsi and Langmuir documented that the optimum adsorption pH was near pH 6.3–6.5 for noncrystalline $Fe(OH)_3$ and in alkaline media, U(VI)-carbonate complexes effectively reduced U(VI) adsorption. The effect of carbonate in the goethite suspensions broadened the pH of maximum U(VI) adsorption from pH 5.7 to pH 8.0, a feature attributed to the lack of U(VI)-carbonate complex desorption. Waite et al. [58] investigated U(VI) adsorption onto hydrous ferric oxides, noting that the maximum U(VI) adsorption occurred from pH 5 to pH 9; however, in the presence of carbonate, the U(VI) adsorption in the pH interval from pH 8 to pH 9 was limited. In general, U(VI) adsorption into Fe-oxyhydroxides is greater than phyllosilicate minerals.

Typically, the pH range of minimal U(VI) mineral solubility coincides with the pH range for optimal U(VI) adsorption. U(IV) complexes are frequently less soluble and less mobile than U(VI) complexes [73]. Duquene et al. [23] noted that U(VI) reduction to less soluble U(IV), by either biotic or abiotic processes, influenced uranium mobility. Stojanovic et al. [17] confirmed that soil temperature, pH, oxidation–reduction potentials and the presence of complexing agents were important factors influencing uranium bioavailability and plant uptake. Shahandeh and Hossner [33] employed a selective sequential extraction protocol to show that U(VI) partitioned into exchangeable, carbonate, manganese, iron, organic and residual fractions. In soils where the carbonate fraction was expected to be important, appreciable plant uptake of U(VI) into the roots and culms of a wide variety of plants was demonstrated. In soils having U(VI) partitioning into iron, manganese and organic fractions, the U(VI) plant uptake was substantially smaller.

Sandino and Bruno [68] provided the solubility estimate for $(UO_2)_3(PO_4)_2\ 4H_2O(s) = 3UO_2^{2+} + 2PO_4^{3-} + 4H_2O$ as log Kso ± 2σ = 48.48 ± 0.16.

10. Uranium adsorption

In a review, Langmuir [38] reported solution U(VI) speciation data from pH 7 groundwater at Yucca Mountain (Nevada, USA) with a total U(VI) concentration of 10^{-8} mol/L. The U(VI) percentage speciation was: (1) UO_2CO_3 at 7.9%, (2) $UO_2(CO_3)_2$ at 83.1%, (3) $UO_2(CO_3)_3$ at 7.8%, (4) UO_2F at 0.007%, (5) $UO_2(OH)_2$ at 0.06% and (6) UO_2PO_4 at 0.8%. Pabalan and Turner [57] used a double layer model for simulating U(VI) adsorption on a smectite (montmorillonite). Their surface complexation constants were (1) > AlO^- of −9.73, (2) > $Al(OH)_2^+$ of 8.33, (3) > SiO^- of −7.20, (4) AlO-UO_2^+ of 2.70, (5) > SiO-UO_2^+ of 2.60, (6) AlO-$(UO_2)_3(OH)_5$ of −14.95 and (7) SiO-$(UO_2)_3(OH)_5$ of −15.29.

Uranium(VI) may be adsorbed onto Fe-oxyhydroxides which may subsequently pursue distinctive pathways: (1) U(VI) undergoes reduction to U(IV) by mobile Fe^{2+} or H_2S or (2) desorbed, especially in alkaline solutions at elevated pH levels. Surface properties of soil mineral phases have altered chemical's reactivity because of the presence of small quantities of noncrystalline Fe- and Al-oxyhydroxides. Thus, these alterations of chemical affinity may be attributed to differences in surface area, abundance and composition of Al-OH, Fe-OH and Si-OH groups, and other features that impact the structure of adsorption surfaces (**Table 11** and **12**).

	Log K for ≡Al	**Log K for ≡Si**
$SOH + H^+ = SOH_2^+$	12.3	−0.95
$SOH = SO^- + H^+$	−13.6	−6.95
$SOH + UO_2^{2+} = SO\text{-}UO_2^+ + H^+$	7.1	0.15
$SOH + (UO_2)_3(OH)_5^+ = SO\text{-}(UO_2)_3(OH)_5 + H^+$	−15.8	−16.80

S is the surface site representing Al and Si.

Table 11. Adsorption site reactions and surface protonation/deprotonation reactions (McKinley et al. [46]).

$S(OH)_2 + UO_2^{2+} = SO_2HUO_2^{2+} + H^+$
$S(OH)_2 + UO_2^{2+} = SO_2UO_2^{2+} + 2H^+$
$S(OH)_2 + UO_2^{2+} + H_2CO_3 = SO_2UO_2H_2CO_3 + 2H^+$
$S(OH)_2 + UO_2^{2+} + H_2CO_3 = SO_2UO_2HCO_3^- + 3H^+$
$S(OH)_2 + UO_2^{2+} + H_2CO_3 = SO_2UO_2CO_3^{2-} + 4H^+$
$S(OH)_2 + UO_2^{2+} + 2H_2CO_3 = SO_2UO_2H_2CO_3HCO_3^- + 3H^+$
$S(OH)_2 + UO_2^{2+} + 2H_2CO_3 = SO_2UO_2(H_2CO_3)_2^{2-} + 4H^+$
$S(OH)_2 + UO_2^{2+} + 2H_2CO_3 = SO_2UO_2CO_3HCO_3^- + 5H^+$
$S(OH)_2 \pm UO_2^{2+} + 2H_2CO_3 = SO_2UO_2(CO_3)_2^{4-} \pm 6H^+$
where $S(OH)_2$ is the surface site.

Table 12. Surface reactions on surface adsorption modeling (Herbelin and Westall [74]).

Davis et al. [44] used the generalized composite model with variations of defining equilibria to model adsorption scenarios of UO_2^{2+} onto mixed mineralogy samples from the Koongarra W2 (Australia) U-impacted samples. The UO_2^{2+} initial equilibration concentration was 3.9×10^{-6} mole U/L with variable CO_2 partial pressures. Given the different model equilibrium constraints, in general, the adsorption species dominance was (1) SO_2UO_2 (pH 5.2–5.6), (2) $SO_2UO_2CO_3^{2-}$ (pH 8.3–8.5), (3) $SO_2UO_2CO_3HCO_3^{3-}$ (pH 7.5–8.7), (4) $SO_2UO_2HCO_3^{1-}$ (pH 6.5–7.8), (5) $SO_2UO_2(HCO_3)^{3-}$ (pH ≈ 8) and (6) SO_2HUO_2 (pH ≈ 6), where S is the surface site.

Waite et al. [58] investigated U(VI) adsorption onto ferrihydrite as a function of U(VI) concentration and the partial pressure of CO_2. Using the diffuse double layer model with two site surface complexes (weak and strong ≡FeOH), they hypothesized that UO_2 and at higher pH levels, $UO_2(CO_3)$ formed inner sphere mononuclear, bidentate complexes involving the Fe octahedron edge and the uranyl ion. The U-interacting surface reactions without CO_2 participation were $[\equiv Fe(OH)_2] + UO_2^{2+} = [FeO_2]UO_2 + 2H^+$ with log K = −2.57 for the strong site and log K = −6.28 for the weak site. The U-interacting surface reactions with CO_2 participation were $[\equiv Fe(OH)_2] + UO_2^{2+} + CO_2 = [FeO_2]UO_2CO_3^{2-} + 2H^+$ with log K = 3.67 for the strong site and log K = −0.42 for the weak site.

McKinley et al. [46] observed U(VI) hydrolysis and adsorption onto smectite (SWy-1) at three ionic strengths over a pH range of 4.0–8.5. At low ionic strength, U(VI) adsorption decreased from pH 4 to pH 7, whereas at higher ionic strengths, U(VI) adsorption increased with increasing pH, an attribute attributed to uranyl hydrolysis and cation exchange involving the background electrolyte. Aluminol surface sites were dominant with adsorption of UO_2^{2+}, whereas $(UO_2)_3(OH)_5^+$ was important in alkaline pH on SiOH edge sites. Turner et al. [49] employed a composite model based on gibbsite (α-$Al(OH)_3$) and silica (α-SiO_2) equilibrations under similar experimental conditions to investigate U(VI) adsorption onto ferruginous beidellite (smectite family) over a pH range from 4.0 to 10.0. The adsorption envelopes for both Al (gibbsite) and Si (silica) began near pH 4 and declined near pH 5.5. With the U(VI) concentration established at UO_2 at 10^{-7} mol U/L, the model predicted the U aqueous species to be

UO_2, $UO_2(OH)^+$, $UO_2(OH)_2$ and $UO_2(OH)_3^-$. At UO_2 at 10^{-5} mol U/L, the model predicted the U aqueous species to be the same U species at 10^{-7} mol U/L with the addition of $(UO_2)_2(OH)_2^{2+}$, $(UO_2)_3(OH)_5^+$, $(UO_2)_4(OH)_7^+$ and $(UO_2)_3(OH)_7^{1-}$. The sorption site species were proposed as $SiO(UO_2)_3(OH)_5$ and $SiO(UO_2)^+$ at Si sites and $AlO(UO_2)_3(OH)_5$ and $AlO(UO_2)^+$ at Al sites.

Gao et al. [75] investigated U(VI) sorption on kaolinite using batch experiments to observe the effects of pH, U(VI) concentration and the presence of oxyanions. The sorption of U(VI) on kaolinite increased with pH increases from pH 4.0 to pH 6.5, thereafter, a sorption plateau was indicated. The presence of phosphate increased U(VI) sorption, especially in the pH range from pH 3.0 to pH 6.0, whereas sulfate had no measurable influence. UO_2HPO_4 is predicted as the major U(VI)-phosphate species from pH 4.0 to pH 6.0, thus, the sorption promotion effect of phosphate was attributed to [$\equiv SOH + UO_2^{2+} + HPO_4^{2-} = \equiv SOUO_2HPO_4^- + H^+$].

Barnett et al. [41] observed that U(VI) adsorption on naturally occurring media of mixed mineralogy was nonlinear, suggesting that preferential and finite binding sites exist. Adsorption increased strongly with pH transition from pH 4.5 to pH 5.5 and decreased sharply from pH 7.5 to pH 8.5. The reduced adsorption was associated with carbonate-U(VI) complexes. Hummel et al. [76] provided an excellent companion thermochemical database. The MinteqA2 is able to perform adsorption simulations using: (1) Langmuir, (2), ion-exchange, (3) triple layer, (4) Freundlich, (5) constant capacitance and (6) diffuse layer [59].

Author details

Michael Thomas Aide

Address all correspondence to: mtaide@semo.edu

Department of Agriculture, Southeast Missouri State University, Cape Girardeau, Missouri, USA

References

[1] Greenwood NN, Earnshaw A. Chemistry of the Elements. New York: Pergamon Press; 1984

[2] Keller C. Radiochemistry. Ellis Horwood Series in Physical Chemistry. Chichester, UK: Ellis Horwood Limited; 1988

[3] Wanty RB, Nordstrom DK. Natural radionuclides. In: Alley WM, editor. Regional Ground-Water Quality. New York: Van Nostrand Reinhold; 1995

[4] Aide MT, Beighley D, Dunn D. Soil profile thorium and uranium concentration distribution in southeastern Missouri soils. In: Jamison R, editor. Thorium, Chemical Properties, Uses, and Environmental Effects. NY: NOVA Publishers; 2014

[5] Birke M, Rauch U, Lorenz H. Uranium in stream and mineral water of the Federal Republic of Germany. Environmental Geochemistry and Health. 2009;**31**:693-706

[6] Mendez-Garcia CG, Luna-Porres MY, Montero-Cabrera ME, Renteria-Villalobos M, Perez-Cazares B, Garcia-Tenorio R. Arsenic, lead, and uranium concentrations on sediments deposited in reservoirs in the Rio Grande Basin, USA-Mexico border. Journal of Soils and Sediments. 2016;**16**:1970-1985

[7] Bleise A, Danesi PR, Burkart W. Properties, use and health effects of depleted uranium (DU): A general overview. Journal of Environmental Radioactivity. 2003;**64**:93-112

[8] Dowdall M, Gwynn JP, Gabrielsen GW, Lind B. Assessment of elevated radionuclide levels in soils associated with an avian colony in a high arctic environment. Soil and Sediment Contamination. 2005;**14**:1-11

[9] Graham MC, Oliver IW, MacKenzie AB, Ellam RM, Farmer JG. Mechanisms controlling lateral and vertical pore-water migration of depleated uranium (DU) at two UK weapons testing sites. Science of the Total Environment. 2011;**409**:1854-1866

[10] Hamby DM, Tynybekov AK. Uranium, thorium, and potassium in soils along the shore of Lake Issyk-Kyol in the Kyrghyz Republic. Environmental Monitoring and Assessment. 2002;**73**:101-108

[11] Handley-Sidhu S, Keith-Roach MJ, Lloyd JR, Vaughan DJ. A review of the environmental corrosion, fate and bioavailability of munitions grade depleted uranium. Science of the Total Environment. 2010;**408**:5690-5700

[12] Kratz S, Schung E. Rock phosphate and P-fertilizers as sources of P contamination in agriculture soils. In: Merkel BJ, Hasche-Berger A, editors. Uranium in the Environment. Berlin: Springer; 2006. pp. 57-68

[13] Morton LS, Evans CV, Estes GO. Natural uranium and thorium distributions in podzolized soils and native blueberry. Journal of Environmental Quality. 2002;**31**:155-162

[14] Raju KK, Raju AN. Biogeochemical investigation in south eastern Andhra Pradesh: The distribution of rare earths, thorium and uranium in plants and soils. Environmental Geology. 2000;**39**:1102-1106

[15] Rivas MDC. Interactions between soil uranium contamination and fertilization with N, P, and S on the uranium content and uptake of corn, sunflower, and bean and soil microbiological parameters. In: Landbauforschung Volkenrode Sonderheft 287. Germany: Braunschweig; 2005

[16] Roh Y, Lee SR, Choi SK, Elless MP, Lee SY. Physicochemical and mineralogical characterization of uranium-contaminated soils. Soil and Sediment Contamination. 2000;**9**:463-486

[17] Stojanovic MD, Stevanovic DR, Milojkovic JV, Grubisic MS, Iies DA. Phytotoxic effect of uranium on the growing up and development the plant of corn. Water, Air, and Soil Pollution. 2010;**209**:401-410

[18] Stojanovic M, Stevanovic D, Milojkovic J, Mihajlovic ML, Lopicic Z, Sostaric T. Influence of soil type and physical-chemical properties on uranium sorption and bioavailability. Water, Air, and Soil Pollution. 2012;**223**:135-144

[19] Varinlioglu A, Kose A. Determination of natural and artificial radionuclide levels in soils of western and southern coastal area of Turkey. Water, Air, Soil Pollution. 2005; **164**:401-407

[20] Echevarria G, Sheppard IM, Morel JL. Effect of pH on the sorption of uranium in soils. Journal of Environmental Radioactivity. 2001;**53**:257-264

[21] Laroche L, Henner P, Camilleri V, Morello M, Garnier-Laplace L. Root uptake of uranium by a higher plant model (*Phaseolus vulgaris*) – Bioavailability from soil solution. Radioprotection. 2005;(40):33-39

[22] Bhattacharyya P, Datta SC, Dureja P. Interrelationship pf pH, organic acids, and phosphorus concentration in soil solution of rhizosphere and non-rhizosphere of wheat and rice crops. Communications in Soil Science and Plant Analysis. 2003;**34**:231-245

[23] Daquene L, Vandenhove H, Tack F, Van der Avoot E, Wannijn J, Van Hees M. Phytoavailability of uranium: Influence of plant species and soil characteristics. In: Merkel BJ, Hasche-Berger A, editors. Uranium in the Environment. Berlin: Springer; 2006

[24] Daquene L, Van Hees M, Baeten E, Wannijn J, Vandenhove H. Effect of biodegradable amendments on uranium solubility in contaminated soils. Science of the Total Environment. 2008;**391**:26-33

[25] Daquene L, Vandenhove H, Tack F, Meers E, Baeten J, Wannijn J. Enhanced phytoextraction of uranium and selected heavy metals by Indian mustard grass and ryegrass using biodegradable soil amendments. Science of the Total Environment. 2009;**407**:1495-1505

[26] Entry JA, Vance NC, Hamilton MA, Zabowski D, Watrud LS, Adriano DC. Phytoremediation of soil contaminated with low concentrations of radionuclides. Water, Air, and Soil Pollution. 1996;**88**:167-176

[27] Huang FYC, Brady PV, Lindgren ER, Guerra P. Biodegradation of uranium-citrate complexes: Implications for extraction of uranium from soils. Environmental Science & Technology. 1998;**32**:379-382

[28] Huang JW, Blaylock MJ, Kapulnik Y, Demsley BBD. Phytoremediation of uranium-contaminated soils: Role of organic acids in triggering uranium hyperaccumulation in plants. Environmental Science & Technology. 1998;**32**:2004-2008

[29] Sevostianova E, Lindermann WC, Ulery AL, Remmenga MD. Plant uptake of depleted uranium from manure-amended and citrate treated soil. International Journal of Phytoremediation. 2010;**12**:550-561

[30] Sheppard MI, Sheppard SC, Thibault. Uptake by plants and migration of uranium and chromium in field lysimeters. Journal of Environmental Quality. 1984;**13**:357-361

[31] Ebbs SD, Brady DJ, Kochian LV. Role of uranium speciation in the uptake and translocation of uranium by plants. Journal of Experimental Botany. 1998;**49**:1183-1190

[32] Ebbs SD, Norvell WA, Kochian LV. The effect of acidification and chelating agents on the solubilization of uranium from contaminated soil. Journal of Environmental Quality. 1998;**27**:1486-1494

[33] Shahandeh H, Hossner LR. Role of soil properties in phytoaccumulation of uranium. Water, Air, and Soil Pollution. 2002;**141**:165-180

[34] Kumar A, Singhal RK, Preetha J, Rupali K, Narayanan U, Suresh S, Mishra MK, Ranade AK. Impact of tropical ecosystem on the migrational behavior of K-40, Cs-137, Th-232 and U-238 in perennial plants. Water, Air, and Soil Pollution. 2008;**192**:293-302

[35] Chopping PM, Shanbhag GR. Binding of uranyl to humic acid. Journal of Inorganic and Nuclear Chemistry. 1981;**43**:3369-3374

[36] Essington M. Soil and Water Chemistry: An Integrative Approach. Boca Raton, FL: CRC Press; 2004

[37] Moon JW, Roh Y, Phelps TJ, Phillips DH, Watson DB, Kim YJ, Brooks SC. Physiochemical and mineralogical characterization of soil-saprolite cores from a research site, Tennessee. Journal of Environmental Quality. 2006;**35**:1731-1741

[38] Langmuir D. Aqueous environmental geochemistry. Upper Saddle River, New Jersey: Prentiss-Hall; 1997

[39] Sato T, Murakami T, Yanase N, Isobe H, Payne TE, Airy P. Iron nodules scavenging uranium from ground water. Environmental Science & Technology. 1997;**31**:2854-2858

[40] Chen JP, Yiacoumi S. Modeling of depleted uranium transport in subsurface systems. Water, Air and Soil Polution. 2002;**140**:173-201

[41] Barnett MO, Jardine PM, Brooks SC, Selim HM. Adsorption and transport of uranium (VI) in subsurface media. Soil Science Society of America. 2000;**64**:908-917

[42] Barnett MO, Jardine PM, Brooks SC. Uranium(VI) adsorption to heterogeneous subsurface media: Application of a surface complexation model. Environmental Science & Technology. 2002;**36**:937-942

[43] Cygan RT. Molecular models of radionuclide interaction with soil minerals. In: Zhang P-C, Brady PV, editors. Geochemistry of Soil Radionuclides. Soil Science Society America Special Publication 59. Madison, WI: Soil Science Society America; 2002

[44] Davis JA, Payne TE, Waite TD. Simulating the pH and pCO_2 dependence of uranium(VI) adsorption by a weathered schist with surface complexation models. In: Zhang P-C, Brady PV, editors. Geochemistry of Soil Radionuclides. Soil Science Society America Special Publication 59. Madison, WI: Soil Science Society America; 2002

[45] Honeyman BD, Ranville JF. Colloid properties and their effects on radionuclide transport through soils and groundwaters. In: Zhang P-C, Brady PV, editors. Geochemistry

of Soil Radionuclides. Soil Science Society America Special Publication 59. Madison, WI: Soil Science Society America; 2002

[46] McKinley JP, Zachara JM, Smith SC, Turner GD. The influence of uranyl hydrolysis and multiple site-binding reactions on the adsorption of U(VI) to montmorillonite. Clays and Clay Minerals. 1995;**43**:586-598

[47] Runde W. Geochemical interactions of actinides in the environment. In: Zhang P-C, Brady PV, editors. Geochemistry of Soil Radionuclides. Soil Science Society America Special Publication 59. Madison, WI: Soil Science Society America; 2002

[48] Runde W, Neu MP, Conradson SD, Li D, Lin M, Smith DM, Van-Pelt CE, Xu Y. Geochemical speciation of radionuclides in soil and solution. In: Zhang P-C, Brady PV, editors. Geochemistry of Soil Radionuclides. Soil Science Society America Special Publication 59. Madison, WI: Soil Science Society America; 2002

[49] Turner GD, Zachara JM, McKinley JP, Smith SC. Surface charge properties and UO_2^{2+} adsorption on a subsurface smectite. Geochimica et Cosmochimica Acta. 1996;**60**: 3399-3414

[50] Bidoglio G, De Plano A, Righetto L. Interaction and transport of plutonium-humic acid particles in groundwater environments. Materials Research Society Symposium Proceedings. 1989;**127**:823-830

[51] Johnson WH, Buck BJ, Brogonia H, Brock AL. Variations in depleted uranium sorption and solubility with depth in arid soils. Soil and Sediment Contamination. 2004;**13**:533-544

[52] Martinez-Aguirre A, Perianez R. Sedimentary speciation of U and Th isotopes in a marsh area at the southwest of Spain. Journal of Radioanalytical and Nuclear Chemistry. 2001;**247**:45-52

[53] Baes CF, Mesmer RE. The Hydrolysis of Cations. N.Y: Wiley-Interscience; 1976

[54] Davis JA. Surface complex modeling of uranium(VI) adsorption on natural mineral assemblages. In: NUREG/CR-6708. Washington DC: U.S. Nuclear Regulatory Commission; 2001

[55] Grenthe I, Fuger J, Lemire R, Muller AB, Nguyen-Trung C, Wanner H. Chemical Thermodynamics of Uranium. France: OECD Nuclear Energy Agency (NEA); 1992

[56] Hsi C-KD, Langmuir D. Adsorption of uranyl onto ferric oxyhydroxides: Application of the surface complexation site binding model. Geochimica et Cosmochimica Acta. 1985;**49**:1931-1941

[57] Pabalan RT, Turner DR. Uranium(6+) sorption on montmorillonite: Experimental and surface complexation modeling study. Aqueous Geochemical. 1997;**2**:203-226

[58] Waite TO, Davis JA, Payne TE, Waychunas GA, Xu N. Uranium (VI) adsorption to ferrihydrate: Application of a surface complexation model. Geochimica et Cosmochimica Acta. 1994;**58**:5465-5478

[59] Allison JD, Brown DS, Novo-Gradac KL. Minteqa2/Prodefa2, a Geochemical Assessment Model for Environmental Systems: Version 3.0. Athens, GA: Environmental Research Laboratory, Office of Research and Development, USEPA; 1991

[60] Stewart BD, Neiss J, Fendorf S. Quantifying constraints imposed by calcium and iron on bacterial reduction of uranium(VI). Journal of Environmental Quality. 2007;**36**:363-372

[61] Yajima T, Kawamura Y, Ueta S. Uranium(IV) solubility and hydrolysis constants under reduced conditions. Materials Research Society Symposium Proceedings. 1995;**333**: 1137-1142

[62] Goldhaber MB, Hemingway BS, Mohagheghi A, Reynolds RL, Northrop HR. Origin of coffinitein sedimentary rocks by a sequential adsorption reduction mechanism. Bulletin de Mineralogie. 1987;**110**:131-141

[63] Fendorf S, Hansel CM, Wielinga. Operative pathways of chromate and uranyl reduction within soils and sediments. In: Zhang P-C, Brady PV, editors. Geochemistry of Soil Radionuclides. Soil Science Society America Special Publication 59. Madison, WI: Soil Science Society America; 2002

[64] Burgos WD, Senko JM, Dempsey BA, Roden EE, Stone JJ, Kemner KM, Kelly SD. Soil humic acid decreases biological uranium(VI) reduction by *Shewanella putrefaciens* CN32. Environmental Engineering Science. 2007;**24**:755-761

[65] Grabias E, Gladysz-Plaska A, Ksiazek A, Majdan M. Efficient uranium immobilization on red clay with phosphates. Environmental Chemistry Letters. 2014;**12**:297-301

[66] Jerden LJ, Sinha KA. Phosphate based immobilization of uranium in an oxidizing bedrock aquifer. Applied Geochemistry. 2003;**18**:823-843

[67] Mehta VS, Giammar DE, Maillot F, Catalano JG, Wang Z. Transport of U(VI) through sediments amended with phosphate to induce in situ uranium immobilization. Water Research. 2015;**69**:307-317

[68] Sandino A, Bruno J. The solubility of $(UO_2)_3(PO_4)_2$ $4H_2O$ (s) and the formation of U(VI) phosphate complexes: Their influence in uranium speciation in natural waters. Geochimica et Cosmochimica Acta. 1992;**56**:4135-4145

[69] Lenhart JJ, Cabaniss SE, MacCarthy P, Honeyman BD. Uranium(VI) complexation with citric, humic and fulvic acids. Radiochimica Acta. 2000;**88**:345-353

[70] Ivanov P, Griffiths T, Bryan ND, Borrhikov G, Dmitriev S. The effect of humic acid on uranyl sorption onto bentonite at trace uranium levels. Journal of Environmental Monitoring. 2012;**14**:2968-2975

[71] Tinnacher RM, Nico PS, Davis JA, Honeyman BD. Effects of fulvic acid on uranium(VI) sorption kinetics. Environmental Science & Technology. 2013;**47**:6214-6222

[72] Tandy S, Brittain SR, Grail BM, Mcleod CW, Paterson A, AD T. Fine scale measurement and mapping of uranium in soil solution in soil and plant-soil microcosms, with special reference to depleted uranium. Plant and Soil. 2013;**368**:471-482

[73] Phillips DH, Watson DB, Roh Y, Mehlhorn TL, Moon JW, Jardine PM. Distribution of uranium in weathered fractured saprolite/shale and ground water. Journal of Environmental Quality. 2006;**35**:1715-1730

[74] Herbelin AL, Westall JA. FITEQL: A computer program for the determination of chemical equilibrium constants from experimental data. Version 4.0 Rep.99-01. Oregon State Univ., Corvallis; 1999

[75] Gao L, Yang Z, Shi K, Wang X, Guo Z, Wu W. U(VI) sorption on kaolinite: Effects of pH, U(VI) concentration and oxyanions. Journal of Radioanalytical and Nuclear Chemistry. 2010;**284**:519-526

[76] Hummel W, Berner U, Curti E, Pearson FJ, Thoenen T. Nagra/PSI Chemical Thermodynamic Data Base 01/01. USA: Universal Publishers/uPUBLISH.com; 2002

Edited by Nasser S. Awwad

This edited volume *Uranium: Safety, Resources, Separation, and Thermodynamic Calculation* is a collection of reviewed and relevant research chapters, offering a comprehensive overview of recent developments in the study of uranium.

This publication aims at providing a thorough overview of the latest research efforts by international authors on uranium studies and opens new possible research paths for further novel developments.

Published in London, UK

IntechOpen

ISBN 978-1-83881-387-1